REPORT DOCUMENTATION PAGE

Form Approved
OMB No. 0704-0188

1. REPORT DATE *(DD-MM-YYYY)*	2. REPORT TYPE	3. DATES COVERED *(From - To)*
07-22-2004	Final Report	Feb 2001 - Feb 2004

4. TITLE AND SUBTITLE
Development of an Eddy Collision Model of Turbulence

5a. CONTRACT NUMBER
N00014-01-1-0483

5b. GRANT NUMBER

5c. PROGRAM ELEMENT NUMBER

6. AUTHOR(S)
Blair Perot

5d. PROJECT NUMBER

5e. TASK NUMBER

5f. WORK UNIT NUMBER

7. PERFORMING ORGANIZATION NAME(S) AND ADDRESS(ES)
University of Massachusetts
Amherst, MA 01003

8. PERFORMING ORGANIZATION REPORT NUMBER

9. SPONSORING/MONITORING AGENCY NAME(S) AND ADDRESS(ES)
Office of Naval Research

10. SPONSOR/MONITOR'S ACRONYM(S)
ONR

11. SPONSOR/MONITOR'S REPORT NUMBER(S)

12. DISTRIBUTION/AVAILABILITY STATEMENT
Approved for Public Release

13. SUPPLEMENTARY NOTES

20040809 027

14. ABSTRACT

Simple fluids such as gasses and liquids are the result of collisions between molecules. More complex fluids, such as granular flows and colloidal suspensions (non-Newtonian fluids), result from the more complex collision (or interaction) behaviors of their constituent particles. In this project we have demonstrated that collision rules can be constructed for large chunks of fluid material (eddies) such that the resulting collective system behaves like the mean (RANS) flow of a turbulent fluid. These collision rules are, in essence, a turbulence model. This project has demonstrated its three primary objectives. First, it has shown that modeling turbulent flow as a collection of colliding (interacting) objects (eddies) is a theoretically viable approach. Second, the project has shown that modeling turbulence in this way can be made computationally efficient and comparable to classic Reynolds stress transport (RST) models. Finally, the collisional approach to turbulence modeling has lead to some insights into turbulence and turbulence modeling that would probably not have been achieved via the traditional RST approach.

15. SUBJECT TERMS

16. SECURITY CLASSIFICATION OF:			17. LIMITATION OF ABSTRACT	18. NUMBER OF PAGES	19a. NAME OF RESPONSIBLE PERSON
a. REPORT	b. ABSTRACT	c. THIS PAGE		93	Blair Perot
					19b. TELEPHONE NUMBER *(Include area code)* 413-545-3925

Final Report: Development of an Eddy Collision Model of Turbulence

Principal Investigator: Blair Perot
Contract Number: N00014-01-1-0483
Dates: Feb. 2001 – Feb. 2004

Graduate Students: Chris Chartrand, Sadbhaw Natu, Wei Liu, Sidhartha Katoly

Summary

Simple fluids such as gasses and liquids are the result of collisions between molecules. More complex fluids, such as granular flows and colloidal suspensions (non-Newtonian fluids), result from the more complex collision (or interaction) behaviors of their constituent particles. In this project we have demonstrated that collision rules can be constructed for large chunks of fluid material (eddies) such that the resulting collective system behaves like the mean (RANS) flow of a turbulent fluid. These collision rules are, in essence, a turbulence model.

The project has demonstrated its three primary objectives. First, it has shown that modeling turbulent flow as a collection of colliding (interacting) objects (eddies) is a theoretically viable approach. Second, the project has shown that modeling turbulence in this way can be made computationally efficient and comparable to classic Reynolds stress transport (RST) models. Finally, the collisional approach to turbulence modeling has lead to some insights into turbulence and turbulence modeling that would probably not have been achieved via the traditional RST approach.

The prediction (or modeling) of turbulent fluid flow is arguably the greatest bottleneck in the Navy's ability to rapidly design innovative devices and respond to environmental threats[73]. While this research does not address a specific Navy operational issue, it has an extremely broad impact on Navy operations and the Navy's ability to successfully execute its mission.

Motivation: Why a collision model.

The collision model is inspired by the strong analogy between granular flows and turbulent fluid flow. An example of a granular flow might be Cheerios in a factory being piped and then poured into boxes. Similarly, turbulent flow can be thought of as a collection of eddies that interact with their local neighbors as they are piped and poured. In both cases, the particles of interest are of roughly the same size as the pipes and mean flow length scales. This causes the resulting flows to be non-Newtonian. The behavior of the two flows is not identical because turbulent eddies have a range of length scales

and Cheerios (or sand grains, or many other granular flows) have a uniform size. In addition, eddies and Cheerios have different interaction behaviors.

The traditional approach to modeling turbulence or non-Newtonian fluids is to hypothesize equations for unknown stress tensors (in turbulence this is the Reynolds stress tensor). Because, the particles making up the flow are roughly the same size as the gradients in the mean flow these particles respond on similar timescales as the mean flow. This means that algebraic models are rarely predictive, and evolution equations for the stress tensor must be hypothesized. In turbulence, these are the Reynolds stress transport (RST) equations. Simpler turbulence models, such as k-ε, are simplifications of the RST equations. Similar transport equations are hypothesized for non-Newtonian flows, and many turbulence modeling concepts (realizability, material frame indifference, tensor consistency) were borrowed directly from the non-Newtonian literature at this transport equation level.

However, it has long been recognized in the non-Newtonian fluid community that transport equation models have serious limitations. An alternative approach is to model the fluid at the particle collision level rather than using a transport equation for the stress. This approach is more versatile, and in many ways, more fundamental. For example, modeling a gas as particles with binary elastic hard sphere collisions gives the Navier-Stokes equations and the perfect gas law when the density is high, as well as the correct gas behavior when the density is low (where Navier-Stokes is not valid).

Numerical solution of collision models.

Once a certain collision behavior has been hypothesized there are three very different ways to solve the particle system numerically and obtain a prediction of the fluid behavior. The most straightforward technique is the 'molecular dynamics' approach where one numerically tracks all the particles in the domain, and performs collisions when they occur. This approach has a computational cost equivalent to large eddy simulation (LES) and is not considered further. The other two approaches note that one does not really care what happens to individual particles but only what happens to particles on average. The quantity of interest then becomes the probability density function that describes the probability that a particle (at a certain place and time) has a certain velocity. The evolution of the probability distribution function, f, obeys the exact equation

$$\frac{\partial f}{\partial t} + v_i \frac{\partial f}{\partial x_i} + a_i \frac{\partial f}{\partial v_i} = \left.\frac{df}{dt}\right|_{collisions} \qquad (1)$$

where a_i is the acceleration due to external forces (like gravity) and the right-hand side describes the average affect of the collisions on the PDF. It is this average collision behavior that we now wish the models to predict.

There are two different ways to solve this PDF equation. One way is to assume the collision model has a Fokker-Planck form (see equations 2 through 4). Then using the equivalence between the Fokker-Planck equation and the Langevin equation (Brownian

motion), it is possible to construct a Lagrangian particle method. This is the approach extensively researched by Pope and coworkers[4,14,18,55]. The Lagrangian particles move like Brownian dust particles. They move with the flow and are randomly perturbed using a prescription given by the model. In this way each particle is independent from all the others, and simply interacts with the average of all the other particles. This is less expensive than tracking and implementing individual collisions ('molecular dynamics' approach) but is still expensive because a large statistical sample of particles is required.

The numerical approach used in this project was to solve the PDF equation using a standard Eularian mesh in physical space, **x**, as well as in velocity space, **v**. Normally, this approach would be rejected outright since 10 mesh points in each direction then requires a million mesh points in total and is too expensive. The resolution to this problem is to use an extremely coarse mesh in the velocity space (3 points in each direction). This means we are solving 27 equations for each point in space. For comparison, a RST model solves 3 velocity, 1 pressure, and 6 stress equations (10 equations) per point in space. However, since the RST equations are highly coupled and nonlinear, and the PDF equations are not, the solution times are very comparable.

A very coarse mesh in velocity space is an idea borrowed from Lattice-Boltzmann methods for solving the Navier-Stokes equations. These methods solve a PDF equation with a very simple collision term that is intended to give Navier-Stokes (Newtonian) fluid behavior. The difference here is that we solve a PDF equation with a much more complex collision term, which results in RANS behavior for the fluid. The coarse mesh is acceptable in both cases because the interest is not in the PDF itself but in its lowest order moments - the mean flow and the stresses. These low order moments can be reasonably extracted from a very coarse approximation of the PDF. Note that the Langevin approach is equivalent to approximating the PDF with a random sample, and a large sample is needed even to approximate the low order moments reasonably well. The Langevin approach is slower because it provides more information (about the higher order moments). Unfortunately, we have little interest, in engineering turbulence models, in the extra information the Langevin solution method provides.

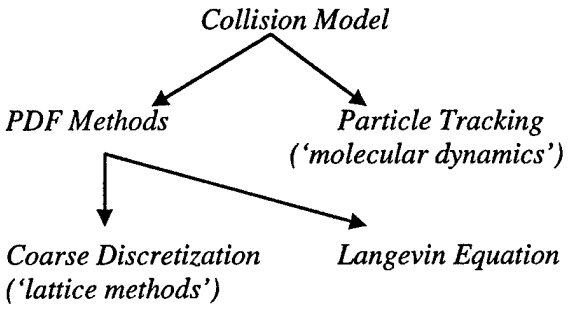

Figure 1 Taxonomy of collision model approaches.

Comparison to Lattice Boltzmann Methods.

While the approach taken in this work is inspired by the success of lattice-Boltzmann numerical methods, the approach is significantly different. This is because the PDF governing molecular interactions (Lattice-Boltmann) has a variance (width) that is much larger than the mean and which is essentially constant (related to the speed of sound). In

contrast, the PDF for turbulence has a variance which is much smaller than the mean (turbulence intensities are measured in percent), and which can vary significantly (in time or space). This is illustrated in Figure 2.

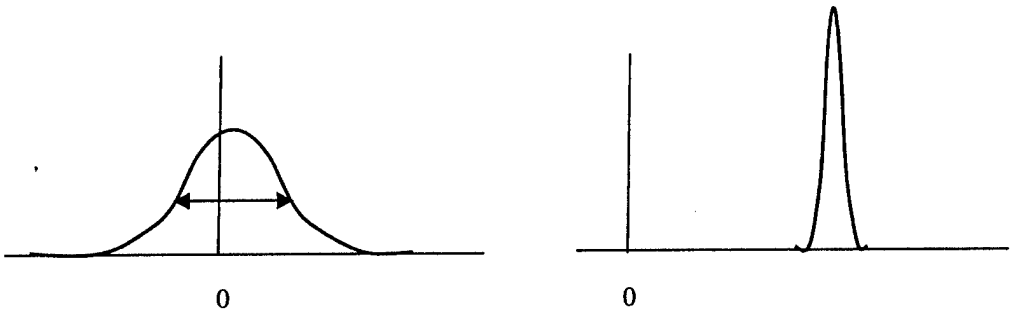

Figure 2. Left: typical PDF for molecules. Right: typical PDF for turbulence.

To capture the turbulence PDF with only three points it was necessary to have a moving adaptive mesh in velocity space. In order to avoid losses due to interpolating one mesh to another as the mesh moves, we implemented a fully conservative scheme in which the mesh moves continuously in time (during the timestep). This uses technology previously developed by the PI for moving meshes in physical space[71]. In actual practice the PDF is three-dimensional. An isosurface of an actual PDF (the 50% value) is shown in Figure 3. This PDF is modeling the behavior of the Le Penven *et al.* return-to-isotropy Case III > 0 experiment. Note the fairly large changes in the shape and size of the distribution even for this simple experiment. It can also be seen in this figure that a spherical PDF corresponds to isotropic turbulence.

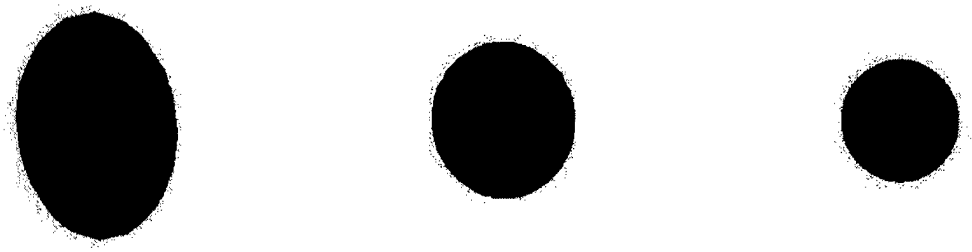

Figure 3. Evolution of the 50% isosurface of the PDF for the return-to-isotropy experiment of Le Penven *et al.* (case III > 0).

Theoretical Analysis.

Lundgren (1967) first derived the exact expression for the collision term in the PDF evolution equation for turbulence. As might be expected, this collision term can not be

expressed solely in terms of the PDF, and practical solution of the PDF evolution equation requires modeling the collision term. In this work we have focused on generalizations of the Fokker-Plank collision term. In its simplest form this collision term has the form,

$$\left.\frac{df}{dt}\right|_{collision} = -\frac{\partial}{\partial v_i}\left[a(v_i - u_i) f\right] + b\frac{\partial^2 f}{\partial v_i^2} \tag{2}$$

where $u_i = \int v_i f dv$ is the mean velocity and a and b are model constants. For turbulence this needs to be generalized. Pope and coworkers use the form,

$$\left.\frac{df}{dt}\right|_{collision} = -\frac{\partial}{\partial v_i}\left[G_{ij} v'_j f\right] + b\frac{\partial^2 f}{\partial v_i^2} + \mu\frac{\partial^2 f}{\partial x_i^2} \tag{3}$$

where $v'_j = v_j - u_j$ is the fluctuating velocity and the first term (the drift term) now has a matrix model parameter G_{ij}, and a viscous term has been added for near wall (low Re number) calculations. The conversion of these Fokker-Planck models to a Langevin equation for numerical solution dictates that the diffusion term (with b) be isotropic and not have a tensor coefficient.

In this project we analyzed the following even more generalized Fokker Plank model.

$$\begin{aligned}\left.\frac{df}{dt}\right|_{collision} = &-\frac{\partial}{\partial v_i}\left[G_{ij} v'_j f\right] + \frac{\partial}{\partial v_i}\left[H_{ij}\frac{\partial f}{\partial v_j}\right] + \frac{\partial}{\partial v_i}\left[(J_{ij} + \mu u_{i,j})\frac{\partial f}{\partial x_j}\right] \\ &+ \frac{\partial}{\partial x_i}\left[\mu\frac{\partial f}{\partial x_i}\right] + \frac{\partial}{\partial v_i}\left[\mu K_{,n}\frac{\partial\left(f v'_i / K\right)}{\partial x_n}\right] + \left.\frac{dv_i}{dt}\right|_{mesh}\frac{\partial f}{\partial v_i}\end{aligned} \tag{4}$$

The last term on the right hand side accounts (exactly) for the mesh motion. The first three terms involve model tensors. Sometimes, these tensors are isotropic and governed by a single parameter. The viscous terms account for low Reynolds number effects and strong inhomogeneity. They do not involve any additional parameters and were derived via analysis and the condition that the model be exact as it approaches a wall (in the laminar sub layer).

Taking the zeroth moment of the collision term (Eqn 4) gives zero, so the zeroth moment of the PDF equation is the mass conservation equation. The first velocity moment of the modeled PDF equation gives the momentum equation,

$$\frac{\partial u_n}{\partial t} + \frac{\partial(u_i u_n + R_{in})}{\partial x_i} - a_n = \frac{\partial}{\partial x_i}\left[\mu u_{n,i}\right] \tag{5}$$

This implies that the acceleration is given by $a_n = -p_{,n} + (\mu u_{i,n})_{,i}$. The viscous contribution to this acceleration is necessary only if the viscosity is not constant.

Taking the moment of the modeled PDF equation with respect to $v'_n v'_m$ gives,

$$\frac{\partial R_{nm}}{\partial t}+\frac{\partial (u_i R_{nm})}{\partial x_i}+\frac{\partial T_{nmi}}{\partial x_i}+(u_{m,j}R_{jn}+u_{n,j}R_{jm})=(G_{mj}R_{jn}+G_{nj}R_{jm})+(H_{nm}+H_{mn}) \\ -(J_{mj}u_{n,j}+J_{nj}u_{m,j})+\frac{\partial}{\partial x_i}\left[\mu\frac{\partial R_{jm}}{\partial x_i}\right]-2\mu K_{,j}\frac{\partial (R_{mn}/K)}{\partial x_j} \tag{6}$$

where $T_{nmi}=\int v'_n v'_m v'_i f d\mathbf{v}$ and $k=\frac{1}{2}R_{ii}$. The tensors G_{ij}, H_{ij}, and J_{ij} describe the model. Complex dissipation and pressure-strain models can be implemented via these tensors. From this analysis it is clear that any Reynolds stress transport model can also be implemented as a generalized Fokker-Planck collision model.

The equation for the total resolved kinetic energy, $E_r=\int\frac{1}{2}v_i v_i f d\mathbf{v}-\frac{1}{2}R_{ii}$, is

$$\frac{\partial E_r}{\partial t}+\frac{\partial}{\partial x_i}\left[u_i E_r+u_k(R_{ik}-\mu u_{i,k})\right]=-(pu_i)_{,i}+u_{n,j}R_{jn}-\mu u_{i,j}(u_{i,j}+u_{j,i})+\frac{\partial}{\partial x_i}\left[\mu\frac{\partial E_r}{\partial x_i}\right] \tag{7}$$

The resolved kinetic energy correctly looses energy as a result of large scale dissipation, and via turbulence production. It is completely specified and does not depend on the model coefficients. The details of these mathematical analyses are presented in Appendix A.

Practical Implementation

When implementing the Fokker-Planck collision model (Eqn. 4) on a coarse mesh, it is attractive to make the change of variables $\hat{f}=\ln(f)$. If f is close to Gaussian (which is expected) then $\hat{f}$ will be close to parabolic. This parabola can be accurately resolved and interpolated by the three points available in our scheme. The evolution equation for $\hat{f}$ as descirbied in Appendix B is,

$$\frac{\partial \hat{f}}{\partial t}+v_i\frac{\partial \hat{f}}{\partial x_i}+(a_i-a_{mesh})\frac{\partial \hat{f}}{\partial v_i}=-G_{ii}-G_{ij}v'_j\frac{\partial \hat{f}}{\partial v_i}+\frac{\partial}{\partial v_i}\left[H_{ij}\frac{\partial \hat{f}}{\partial v_j}\right]+H_{ij}\frac{\partial \hat{f}}{\partial v_i}\frac{\partial \hat{f}}{\partial v_j} \\ +\frac{\partial}{\partial v_i}\left[(J_{ij}+\mu u_{i,j})\frac{\partial \hat{f}}{\partial x_j}\right]+(J_{ij}+\mu u_{i,j})\frac{\partial \hat{f}}{\partial x_j}\frac{\partial \hat{f}}{\partial v_i}+\frac{\partial}{\partial x_i}\left[\mu\frac{\partial \hat{f}}{\partial x_i}\right]+\mu\frac{\partial \hat{f}}{\partial x_i}\frac{\partial \hat{f}}{\partial x_i} \\ +\mu\, k_{,n}\left[\frac{\partial}{\partial x_n}+\frac{\partial \hat{f}}{\partial x_n}\right]\left\{\frac{3}{K}+\frac{v'_i}{K}\frac{\partial \hat{f}}{\partial v_i}\right\} \tag{8}$$

While there are more terms to compute in this version, the equation for $\hat{f}$ is much more accurate to solve numerically. In addition, low order methods and simple difference stencils suffice because $\hat{f}$ is expected to be very close to quadratic.

The models for the tensors G_{ij}, H_{ij}, and J_{ij} require a time scale to be dimensionally correct. For this reason an additional transport equation for the timescale must be included in the model. We have used the standard epsilon transport equation for this purpose since it is very commonly used in RST models as well.

Summary of the Model

As shown in Appendix A, the above PDF equation results in the following turbulence equation.

$$\frac{\partial R_{mn}}{\partial t}+\frac{\partial}{\partial x_i}u_i R_{mn}+\frac{\partial}{\partial x_i}\overline{v'_m v'_n v'_i}+R_{ni}\frac{\partial u_m}{\partial x_i}+R_{mi}\frac{\partial u_n}{\partial x_i}=\left(G_{mj}R_{jn}+G_{nj}R_{jm}\right)$$
$$+\left(H_{mn}+H_{nm}\right)+\frac{\partial}{\partial x_i}\mu\frac{\partial R_{mn}}{\partial x_i}-\left(J_{in}u_{m,i}+J_{im}u_{n,i}\right)-2\mu\frac{\partial K}{\partial x_l}\left(\frac{R_{mn}}{K}\right)_{,l} \quad (9)$$

The triple correlation term, $\frac{\partial}{\partial x_i}\overline{v'_m v'_n v'_i}$, is modeled by $-\frac{\partial}{\partial x_i}\nu_T\frac{\partial R_{mn}}{\partial x_i}$.

The collision model is given by,

$$G_{ij}=C^s_{p2}S_{ij}+C^w_{p2}W_{ij}+\tfrac{1}{2}\left(C^s_{p2}-1\right)\frac{P}{K}\delta_{ij}-\tfrac{1}{2}\frac{\hat{\varepsilon}}{K}C_{p1}\delta_{ij} \quad (10)$$

$$H_{ij}=\tfrac{1}{3}\hat{\varepsilon}C_{p1}\delta_{ij}+\tfrac{2}{3}KC^*_{p2}S_{ij} \quad (11)$$

$$J_{ij}=-\tfrac{2}{3}KC^*_{p2}\delta_{ij} \quad (12)$$

The equivalent Reynolds stress transport equation would be,

$$\frac{\partial R_{mn}}{\partial t}+\frac{\partial}{\partial x_i}u_i R_{mn}-\frac{\partial}{\partial x_i}\nu_T\frac{\partial R_{mn}}{\partial x_i}+\left(u_{m,j}R_{jn}+u_{n,j}R_{jm}\right)=$$
$$\left(C^s_{p2}S_{mj}+C^w_{p2}W_{mj}\right)R_{jn}+\left(C^s_{p2}S_{nj}+C^w_{p2}W_{nj}\right)R_{jm}+\left(C^s_{p2}-1\right)\frac{P}{K}R_{mn}-\frac{\hat{\varepsilon}}{K}C_{p1}R_{mn} \quad (13)$$
$$+\tfrac{2}{3}\hat{\varepsilon}C_{p1}\delta_{mn}+\tfrac{4}{3}KC^*_{p2}S_{mn}+\frac{\partial}{\partial x_i}\nu\frac{\partial R_{mn}}{\partial x_i}-2\mu\frac{\partial K}{\partial x_l}\left(\frac{R_{mn}}{K}\right)_{,l}$$

where $S_{ij}=\frac{1}{2}(u_{i,j}+u_{j,i})$, $\overline{W}_{ij}=\frac{1}{2}(u_{i,j}-u_{j,i})+\varepsilon_{ijk}\Omega_k$, and Ω_k is the rotation rate in a non-inertial frame of reference, and $P=-R_{nm}u_{n,m}$ is the turbulent production rate. The model parameters are given by

$$C_{p1}=1.8\frac{F}{1+F}\frac{\nu_t}{5\nu+\nu_t}\qquad C^*_{p2}=-0.2F^2+.006\frac{P}{\hat{\varepsilon}}$$

$$C^s_{p2}=\frac{\nu_t}{\nu+\nu_t}-.2F\qquad C^w_{p2}=\frac{\nu_t}{\nu+\nu_t}-.4F$$

$$\hat{\varepsilon} = \frac{K\varepsilon}{K + 10\nu\left|\left(\sqrt{K}\right)_{,i}\right|} \qquad \nu_t = .12\frac{F}{\hat{\varepsilon}}$$

where $F = \frac{27}{8}\det(R_{ij}/k)$ is the two-component parameter.

The transport model for the epsilon equation is fairly standard and is given by,

$$\frac{\partial \varepsilon}{\partial t} + u_i \frac{\partial \varepsilon}{\partial x_i} = \frac{\varepsilon}{K}(C_{\varepsilon 1}P - C_{\varepsilon 2}\varepsilon) + \frac{\partial}{\partial x_i}(\nu + C_{\varepsilon 3}\nu_T)\frac{\partial \varepsilon}{\partial x_i} \tag{14}$$

where

$$C_{\varepsilon 1} = 1.43 \qquad C_{\varepsilon 2} = 11/6 \qquad C_{\varepsilon 3} = 0.33 + 0.5\frac{P}{\hat{\varepsilon}}$$

Summary of Results

The PDF collision model (using a coarse moving mesh) was tested on isotropic decaying turbulence at different Reynolds numbers and rotation rates. This flow is affected by the epsilon equation model, but not by the PDF model. However, it is a good test of the PDF numerics, since the exact solutions (for a given epsilon equation model) are known. It was found that spacing the mesh points at 1.61 times the PDF variance was on optimal placement that almost eliminates numerical errors due to the coarse mesh interpolation. The moving mesh algorithm moves the mesh to keep it at this position even as the variance changes in time.

The model was then tested on anisotropic decaying turbulence. Two different experiments (Le Penven et al., and Choi & Lumley) and five different data sets were used to evaluate the performance of the model. This is essentially a test of the models ability to correctly predict slow pressure-strain or return-to-isotropy. Some very interesting results were produced by this study. Whereas all RST models use at least one model constant (and frequently two or more) to model return-to-isotropy, the collisional approach to this problem resulted in a return model that performs well and has no model constants. This is described in detail in Appendix C, which has been submitted for publication.

Next the model was tested in a variety of homogeneous shear flows. They key to predicting these flows correctly is in the modeling of the fast pressure-strain. A detailed study of the fast pressure-stain model parameters was performed. These parameters are often specified as constants, however they can be functions of the Reynolds stress and mean flow gradient tensor invariants. A wide variety of DNS and experimental cases were used to back out the exact values for the fast pressure-strain model parameters in these experiments. Both rapidly strained and slowly strained homogeneous flows were analyzed in this way to obtain the parameter values in both limits. With this data, models for the fast pressure-strain parameters were proposed. This analysis is presented in Appendix D.

Finally, the model was implemented and tested in fully developed channel flow. The issue here is to correctly account for inhomogeneity and low Reynolds number effects. In this situation, the modeling of the dissipation tensor requires close attention. This term dominates near the wall and balances viscous diffusion. A model which accounts for dissipation in inhomogeneous flows was developed. It has been submitted for publication, and is presented in Appendix E. The method of determining the model constants is shown in Appendix F, and the results are in Appendices G and H. This model for the dissipation tensor is exact in regions of strong inhomogeneity and involves no model parameters. The second to last term in Eqn. 4 is due to this model. The fact that the model is exact in this limit is important. It means that the diffusion is exactly balanced at the wall, and therefore that the Reynolds stresses always have the correct asymptotic limits near a wall. This means that elliptic relaxation approaches are not required. In addition, computational stability is significantly enhanced since this is the region where Reynolds stresses are close to becoming unrealizable due to the numerics.

Final Conclusions & Future Work

This project has allowed us to demonstrate that collisional models are a viable alternative to RST models. In one instance, we have even been able to remove a model parameter due to insights gained from this viewpoint. However, it is also clear that this approach, as it stands, has most of the same difficulties and limitations as RST models. In particular:

- The fast pressure-strain model largely dictates the model's performance in flows with mean flow gradients (most flows). There are a large number of constants (a minimum of three), practical difficulty in modeling equilibrium and rapid limits within a single model, and even fundamental problems with assuming that this term can be modeled in terms of the available unknowns (we know in many cases that it can not). These difficulties are common to both RST models and the current collision model.

- The scale (or epsilon) transport equation is the other source of significant error and parameterization (many constants). In the simple form we have so far studied, the collision model in no way address this issue. The same scale transport equation is used as in RST models.

- Finally, although we have used Lattice-Boltzmann discretization ideas, the implementation of these models is not as computationally efficient as an analysis of Lattice-Boltzmann methods might first suggest. The fact that a moving adaptive mesh is required for collisional turbulence simulations means that most of the speed enhancing tricks of Lattice-Boltzmann methods can no longer be applied. The method is therefore computationally also comparable to RST models.

One important distinction between RST models and the collisional modeling approach is that many of these deficiencies can actually be fixed within the collisional framework.

The key is to include more information in the PDF than just the velocity. By assuming that eddies have shape (or more specifically, orientation) as well as velocity, two major problems can be addressed. First, the fast pressure-strain term can now be implemented exactly. Since the production term is already exact, this means that the influence of the mean flow on the turbulence is now captured exactly (up to numerical implementation errors), only nonlinear (turbulence-turbulence) interactions must be modeled. Secondly, eddy shape provides a length scale measure, so a separate scale transport equation is no longer necessary. Including orientation into the collisonal model will increase the cost by an order of magnitude. However, the number of model parameters will also be vastly reduced. If the resulting model is highly predictive then the additional cost may be warranted and will still be far below the cost of the next alternative (large eddy simulation).

Bibliography

1. J. Rotta, "Stastische theorie nichthomegener turbulenz I," Z. für Physik **129**, 547-572 (1951).

2. J. L. Lumley, "Computation modeling of turbulent flows", Adv. Appl. Mech. **18**, 126-176. (1978)

3. S. Sarkar and C. G. Spezial, "A Simple Nonlinear Model for the Return to Isotropy inn Turbulence," Physics of Fluids, Vol. A2, No. 1, pp. 84-93 (1990)

4. D. C. Haworth, and S. B. Pope, "A Generalized Langevin Model for Turbulent Flows," Physics of Fluids, Vol. 29, No. 2, (1986)

5. K. S. Choi and J. L. Lumley, "Turbulence and Chaotic Phenomena in Fluids," *Proceedings of the IUTAM Symposium* (Kyoto, Japan), edited by T. Tatsumi, North-Holland, Amsterdam, p. 267, (1984)

6. T. J. Craft and B. E. Launder, "Computation of Impinging Flows Using Second-Moment Closure," *Proceedings of the Eighth Symposium on Turbulent Shear Flows*, Technical University of Munich, Munich, Germany, pp. 8-5-1 – 8-5-6 (1991).

7. M. Yamamoto and C. Arakawa, "Study on the Pressure-Strain Term in Reynolds Stress models." *Proceedings of the Eighth Symposium on Turbulent Shear Flows*, Technical University of Munich, Munich, Germany, pp. III-17-1 – III-17-2 (1991).

8. C. G. Speziale, S. Sakar and T. B. Gatski, "Modelling the pressure-strain correlation of turbulence: an invariant dynamical systems approach," J. Fluid Mech., Vol. 227, pp 245-272 (1991)

9. P. Degond and M. Lemou, "Toward a Kinetic Model of Turbulent Incompressible Fluids," Université Paul Sabatier, (2000).

10. P. A. Durbin & B. A. Pettersson Reif , *Statistical Theory and Modeling for Turbulent Flows*. Wiley & Sons, 2001.

11. B. E. Launder, "An introduction to single-point closure methodology." In T. B. Gatski, M. Y. Hussaini, and J. L. Lumley, *Simulation and Modeling of Turbulent Flows*, 243-310. New York: Oxford University Press.

12. Tsah-Hsing Shih and J. L. Lumley, "Critical Comparison of Second-Order Closures with Direct Numerical Simulations Homogeneous Turbulence," AIAA Journal, Vol. 31, No. 4, (1993)

13. S. Tavoularis and S. Corrsin, "Experiments in nearly homogeneous turbulent shear flow with a uniform mean temperature gradient. Part1," J. Fluid Mech. **104**, 311-347 (1981).

14. P. K. Yeung and S. B. Pope, "Lagrangian statistics from direct numerical simulations of isotropic turbulence," J. Fluid Mech., **207**, 531-586 (1989)

15. J. Weinstock, "Theory of pressure-strain-rate correlation for Reynolds-stress turbulence closures. Part 1. Off-diagonal element," J. Fluid Mech., **105**, 369-396 (1981)

16. J. Weinstock, "Theory of pressure-strain-rate. Part 2. Diagonal elements," J. Fluid Mech., **116**, 1-29 (1982)

17. T. Sjögren and A. V. Johansson, "Development and calibration of algebraic nonlinear models for terms in the Reynolds stress transport equation," Phys. Fluids **12**, 1554-1572 (2000).

18. S. B. Pope, *Turbulent Flows*, Cambridge University Press, 2000.

19. P. Bradshaw & J. B. Perot, *A Note on the Turbulent Dissipation Rate in the Viscous Wall Region*, Physics of Fluids A, **5** (12), 1993.

20. B. E. Launder, G. J. Reece & W. Rodi, "Progress in the development of a Reynolds stress turbulence closure", J. Fluid Mech. **68**, 537-566 (1975).

21. A. N. Kolmogoroff, "The local structure of turbulence in incompressible viscous fluid for very large Reynolds number," Dokl. Akad. Nauk SSSR, **30**, 301-305 (1941).

22. S. G. Saddoughi and S. V. Veeravalli, "Local isotropy in turbulent boundary layers at high Reynolds number," J. Fluid Mech. **268**, 333 -372 (1994).

23. W. K. George & H. J. Hussein, "Locally axisymmetric turbulence", J. Fluid Mech. **233**, 1-23 (1991).

[24] M. Hallbäck, J. Groth & A. V. Johansson, "A Reynolds stress closures for the dissipation in anisotropic turbulent flows," 7th Symposium on Turbulent Shear Flows, Stanford University, August. (1989).

[25] M. Hallbäck, J. Groth & A. V. Johansson, "An algebraic model for nonisotropic turbulent dissipation rate in Reynolds stress closures," Phys. Fluids, **2** (10, 1859-1866, (1990).

[26] P. A. Durbin and C. G. Speziale, "Local anisotropy in strained turbulence at high Reynolds numbers", ASME J. Fluids Eng. **113**, 707-709 (1991).

[27] J.G. Brasseur, "Comments on the Kolmogorov hypothesis of isotropy in the small scales," *AIAA* Paper 91-0230 (1991).

[28] J. L. Lumly and G. R. Newman, "The return to isotropy of homogeneous turbulence," J. Fluid Mech. **82**, 161-178 (1977).

[29] D. Naot, A. Shavit & M. Wolfstein, "Two-point correlation model and the redistribution of Reynolds stresses," Phys. Fluids **16**, 738-743, (1973).

[30] K. Hanjalic & B. E. Launder, "Contribution towards a Reynolds-stress turbulence closure for low-Reynolds-number turbulence," J. Fluid Mech. **74**, 593-610 (1976).

[31] N. N. Mansour, J. Kim & P. Moin, "Reynolds-stress and dissipation-rate budgets in a turbulent channel flow," J. Fluid Mech. **194**, 15-44 (1988).

[32] M. Hallbäck, A. V. Johansson and A. D. Burden, "Transition and turbulence modeling," Hallbäck, Johansson, Henningson & Alfredsson, eds., Kluwer Academic Publishers, 81-154, (1996).

[33] Y. G. Lai & R. M. C. So, "On near-wall turbulent flow," J. Fluid Mech. **221**, 641-673, (1990).

[34] B. E. Launder and B. L. Li, "On the elimination of wall topography parameters from second moment closure," Phys. Fluids **6**, 537-566 (1994).

[35] C. G. Speziale and T. B. Gatski, "Analysis and modeling of anisotropies in the dissipation rate of turbulence," J. Fluid Mech. **344**, 155-180 (1997).

[36] J. B. Perot "Shear-Free Turbulent Boundary Layers: Physics and Modeling," Ph.D Thesis, Stanford University Tech. Report TF60 (1993).

[37] W. C. Reynolds, "Physical and analytical foundations, concepts, and new directions in turbulence modeling and simulation," In *Turbulence Models and their Applications*. Editions Eyrolles, 61 Bd Saint-Germain Paris 2 (1984).

38. M. Tagawa, Y. Nagano and T. Tsuji, "Turbulence model for dissipation components of Reynolds stresses," In *Eighth Sym. Turbulence Shear Flows*, Munich, Germany 29-3-1 (1991).

39. M. Oberlack, "Non-isotropic dissipation in non-homogeneous turbulence", J. Fluid Mech **350**, 351-374 (1997)

40. J. B. Perot & P. Moin, "Shear-Free Turbulent Boundary Layers, Part 2: New concepts for Reynolds stress transport equation modelling of inhomogeneous flows," J. Fluid Mech. **295**, 229-245 (1995).

41. J. B. Perot and P. Moin, "A Near Wall Model for the Dissipation Tensor," Eleventh Australasian Fluid Mechanics Conference, Hobart, Tasmania, Australia, 13-18 (1992).

42. B. Launder and W. C. Reynolds, "Asymptotic near-wall stress dissipation rates in a turbulent flow," Phys. Fluids, **26**, 1157-1158 (1983).

43. S. G. Speziale, "Analytical methods for the development of Reynolds stress closure in turbulence," Annual Review of Fluid Mechanics **23**, 107-157 (1991)

44. S. C. Crow, "Viscoelastic properties of fine grained incompressible turbulence," J. Fluid Mech. **33**, 1-20 (1968).

45. M. J. Lee and W. C. Reynolds, "Numerical experiments on the structure of homogeneous turbulence," Standford University Tech. Rep TF-24 (1985).

46. B. E. Launder and B. I. Sharma, "Application of the Energy-Dissipation Model of Turbulence to the Calcualtion of Flow Near a Spinning Disc", Letters in Heat and Mass Transfer, **1**, 131-138 (1974).

47. J. B. Perot and P. Moin, "Shear-Free Turbulent Boundary Layers, Part I: Physical Insights into Near Wall Turbulence," J. Fluid Mech. **295**, 199-227 (1995).

48. R. D. Moser, J. Kim and N. Mansour, "Direct numerical simulation of turbulent channel flow up to Re=590" Phys. Fluids. **11**, 943-945, (1999)

49. Kristoffersen, R., Andersson, H.I. 1993 "Direct simulations of low-Reynolds-number turbulent flow in a rotating channel" *J. Fluid Mech.*, **256**, 163-197.

50. H. Le, P. Moin, and J. Kim, "Direct numerical simulation of turbulent flow over a backward-facing step," J. Fluid Mech. **330**, 349-374, (1997).

51. S. Natu, "A Reynolds stress transport model for the near wall region," Masters Thesis, University of Massachusetts, Amherst, (2003).

52. U. Schumann, "Relizability of Reynolds Stress Turbulence Models," Physics of Fluids, Vol. 20, pp. 721-725, (1977)

53. J. P. Laval, B. Dubrulle and J. C. McWilliams, "Langevin Models of Turbulence: Renormalization Group, Distant Interaction Algorithms or Rapid Distortion Theory?," Physics of Fluids, Vol. 15, No. 5 (2003)

54. T. S. Lungren, "Distribution functions in the statistical theory of turbulence," Physics of Fluids, Vol. 10, No. 5 (1967).

55. S. B. Pope, Lagrangian PDF methods for turbulent flows. *Annual Rev. Fluid Mech.* **26**, 23-63, 1994.

56. M. Chen & Z. Hong, A PDF description of turbulent axisymmetric free jet flow, *J. Fluids Eng.*, **121**, 73-79, 1999.

57. L. I. Zaichik, A statistical model of particle transport and heat transfer in turbulent shear flow, *Phys. Fluids*, **11** (6), 1521-1534, 1999.

58. A. J. Wagner, Derivation of a non-objective Oldroyd model from the Boltzmann equation, preprint *cond-mat/0105067*, 2001.

59. P. Degond & M. Lemou, Turbulence models for incompressible fluids derived from kinetic theory, *J. Math. Fluid Mech.*, **4** (3), 257-284, 2002.

60. J. B. Perot & P. Moin, *A Near Wall Model for the Dissipation Tensor*, Eleventh Australasian Fluid Mechanics Conference, December 13-18, 1992, Hobart, Tasmania, Australia.

61. W. C. Reynolds & S. C. Kassinos, A one-point model for the evolution of the Reynolds stress and structure tensors in rapidly deformed homogeneous turbulence, *Proc. R. Soc. London*, Ser A **451**, 87, 1995.

62. P. R. Van Slooten & S. B. Pope, PDF modeling for inhomogeneous turbulent with exact representation of rapid distortions, *Phys. Fluids*, **9**, 1085, 1997.

63. S. M. de Bruyn Kops & J. J. Riley, Direct numerical simulation of laboratory experiments in isotropic turbulence, *Phys. Fluids*, **10** (9), 2125-2127, 1998.

64. G. Comte-Bellot & S. Corrsin, Simple Eularian time correlation of full and narrow-band velocity signals in grid-generated, 'isotropic' turbulence, *J. Fluid Mech.* **48**, 273, 1971.

65. J. B. Perot & P. Moin, *Shear-Free Turbulent Boundary Layers, Part II: New Concepts for Reynolds Stress Transport Equation Modeling of Inhomogeneous Flows*, Journal of Fluid Mechanics, **295**, 1995.

66. J. B. Perot & S. Natu, A model for the dissipation tensor in inhomogeneous and anisotropic turbulence, Submitted to *Phys. Fluids*, May 2003.

67. J. C. R. Hunt & J. M. Graham, Free-stream turbulence near plane boundaries, *J. Fluid Mech.* **84**, 209-235, 1978.

68. W. C. Reynolds, Effects of rotation on homogeneous turbulence, Proceedings of the 10th Australasian Fluid Mechanics Conference, University of Melbourne, Australia, 1989.

69. J. B. Perot & P. Moin, Shear-Free Turbulent Boundary Layers, Part I: Physical Insights into Near Wall Turbulence, *J. Fluid Mech.*, **295**, 1995.

70. J. Katz, Private Communication.

71. J. B. Perot & R. Nallapati, *A Moving Unstructured Staggered Mesh Method for the Simulation of Incompressible Free-Surface Flows*, Journal of Computational Physics, **184**, 192-214, 2003.

72. W. Chang & J. B. Perot, *Prediction of Turbulent Transition in Boundary Layers Using the Turbulent Potential Model*, Journal of Turbulence, **3**, January. 2002.

73. R. Rubinstein, C. L. Rumsey, M. D. Salas & J. L. Thomas, eds. *Turbulence modeling workshop*, ICASE Interim Report No. 37, NASA/CR-2001-210841.

Appendix A: Moments of the PDF Equation

In theory, the PDF contains enough information to calculate all single point statistics involving the velocity. This means that from a particular collision model we can derive the resulting mass, momentum, total kinetic energy, and Reynolds stress equations. In this appendix a very general model form is assumed, and the resulting equations determined.

The general PDF evolution equation is given by,

$$\frac{\partial f}{\partial t}+v_i\frac{\partial f}{\partial x_i}+(a_i-a_{mesh})\frac{\partial f}{\partial v_i}=-\frac{\partial}{\partial v_i}\Big[G_{ij}\left(v_j-u_j\right)f\Big]+\frac{\partial}{\partial v_i}H_{ij}\frac{\partial f}{\partial v_j}+\frac{\partial}{\partial x_j}\mu\frac{\partial f}{\partial x_j}$$
$$+\frac{\partial}{\partial v_i}\left[(J_{ij}+\mu u_{i,j})\frac{\partial f}{\partial x_j}\right]+\frac{\partial}{\partial v_i}\left[\mu K_{,n}\frac{\partial\left(fv_i'/K\right)}{\partial x_n}\right] \qquad (A.1)$$

1. $\dfrac{\partial f}{\partial t}$

Mass: $$\int\frac{\partial f}{\partial t}d\bar{v}=\frac{\partial}{\partial t}\int f d\bar{v}=0 \qquad (A.2)$$

Momentum: $$\int v_k\frac{\partial f}{\partial t}d\bar{v}=\frac{\partial}{\partial t}\int v_k f d\bar{v}=\frac{\partial u_k}{\partial t} \qquad (A.3)$$

Turbulence: $$\int v_m'v_n'\frac{\partial f}{\partial t}d\bar{v}=\frac{\partial R_{mn}}{\partial t} \qquad (A.4)$$

Energy: $$\tfrac{1}{2}\int v_k v_k\frac{\partial f}{\partial t}d\bar{v}=\frac{\partial E}{\partial t} \qquad (A.5)$$

2. $v_i\dfrac{\partial f}{\partial x_i}$

Mass: $$\int v_i\frac{\partial f}{\partial x_i}d\bar{v}=\frac{\partial}{\partial x_i}\int v_i f d\bar{v}=\frac{\partial u_i}{\partial x_i} \qquad (A.6)$$

Momentum: $$\int v_i v_k\frac{\partial f}{\partial x_i}d\bar{v}=\frac{\partial}{\partial x_i}\int v_i v_k f d\bar{v} \qquad (A.7)$$

Writing v in terms of v' gives:

$$=\frac{\partial}{\partial x_i}\int(v_i'+u_i)(v_k'+u_k)f d\bar{v} \qquad (A.8)$$

$$=\frac{\partial}{\partial x_i}\int(v_i'v_k'+v_i'u_k+u_iv_k'+u_ku_i)f d\bar{v} \qquad (A.9)$$

$$= \frac{\partial R_{ik}}{\partial x_i} + \frac{\partial u_i u_k}{\partial x_i} \tag{A.10}$$

Turbulence: $$\int v'_m v'_n v_i \frac{\partial f}{\partial x_i} d\vec{v} = \int v'_m v'_n \frac{\partial v_i f}{\partial x_i} d\vec{v} \tag{A.11}$$

$$= \int \frac{\partial v'_m v'_n v_i f}{\partial x_i} - v_i f \frac{\partial v'_m v'_n}{\partial x_i} d\vec{v} \tag{A.12}$$

$$= \int \frac{\partial v'_m v'_n v'_i f}{\partial x_i} + \frac{\partial v'_m v'_n u_i f}{\partial x_i} - v_i f \left(v'_m \frac{\partial v'_n}{\partial x_i} + v'_n \frac{\partial v'_m}{\partial x_i} \right) d\vec{v} \tag{A.13}$$

$$= \frac{\partial}{\partial x_i} \overline{v'_m v'_n v'_i} + \frac{\partial}{\partial x_i} u_i R_{mn} + \frac{\partial u_n}{\partial x_i} \int v'_m v_i f d\vec{v} + \frac{\partial u_m}{\partial x_i} \int v'_n v_i f d\vec{v} \tag{A.14}$$

$$= \frac{\partial}{\partial x_i} \overline{v'_m v'_n v'_i} + \frac{\partial}{\partial x_i} u_i R_{mn} + \frac{\partial u_n}{\partial x_i} \int v'_m \left(v'_i + u_i \right) f d\vec{v} + \frac{\partial u_m}{\partial x_i} \int v'_n \left(v'_i + u_i \right) f d\vec{v} \tag{A.15}$$

Since $\int u_i v'_m f d\vec{v} = 0$ we get the following.

$$= \frac{\partial}{\partial x_i} \overline{v'_m v'_n v'_i} + \frac{\partial}{\partial x_i} u_i R_{mn} + \frac{\partial u_n}{\partial x_i} \int v'_m v'_i f d\vec{v} + \frac{\partial u_m}{\partial x_i} \int v'_n v'_i f d\vec{v} \tag{A.16}$$

$$= \underbrace{\frac{\partial}{\partial x_i} u_i R_{mn}}_{\text{Convection}} + \underbrace{\frac{\partial}{\partial x_i} \overline{v'_m v'_n v'_i}}_{\text{Turbulent Transport}} + \underbrace{R_{ni} \frac{\partial u_m}{\partial x_i} + R_{mi} \frac{\partial u_n}{\partial x_i}}_{\text{Production}} \tag{A.17}$$

Energy: $$\tfrac{1}{2} \int v_k v_k v_i \frac{\partial f}{\partial x_i} d\vec{v} = \tfrac{1}{2} \int v_k v_k \frac{\partial v_i f}{\partial x_i} d\vec{v}$$

$$= \tfrac{1}{2} \frac{\partial}{\partial x_i} \int v_k v_k v_i f d\vec{v} = \tfrac{1}{2} \frac{\partial}{\partial x_i} \overline{v_k v_k v_i} \tag{A.18}$$

$$= \frac{\partial}{\partial x_i} \left[\tfrac{1}{2} \overline{\left(u_i + v'_i \right) v_k v_k} \right] = \frac{\partial}{\partial x_i} \left[\tfrac{1}{2} u_i \overline{v_k v_k} + \tfrac{1}{2} \overline{v'_i \left(u_k + v'_k \right)^2} \right] \tag{A.19}$$

Since $\int u_k v'_i f d\vec{v} = 0$ we get the following.

$$= \frac{\partial}{\partial x_i} \left[u_i E + u_k \overline{v'_i v'_k} + \tfrac{1}{2} \overline{v'_i v'_k v'_k} \right] \tag{A.20}$$

$$= \frac{\partial}{\partial x_i} \left[u_i E + u_k R_{ik} + \tfrac{1}{2} \overline{v'_i v'_k v'_k} \right] \tag{A.21}$$

3. $$a_i \frac{\partial f}{\partial v_i} + \frac{\partial}{\partial v_i} \left(G_{ij} v'_j f \right) = \frac{\partial}{\partial v_i} \left[\left(a_i + G_{ij} v'_j \right) f \right]$$

Mass: $$\int \frac{\partial}{\partial v_i}\left[\left(a_i + G_{ij}v_j'\right) f\right] d\vec{v} = \int_{\partial\Omega\to\infty} \left(a_i + G_{ij}v_j'\right) f n_i d\vec{s} \to 0 \qquad \text{(A.22)}$$

By using Gauss's divergence theorem, we can convert this volume integral into a surface integral, where $\boldsymbol{n}$ is the normal vector to the cell face. Evaluation this integral over all velocity space means this term is zero, since the probability density function goes to zero as $\boldsymbol{v}$ foes to infinity. .

Momentum: $$\int v_k \frac{\partial}{\partial v_i}\left[\left(a_i + G_{ij}v_j'\right) f\right] d\vec{v}$$

$$= \int \frac{\partial}{\partial v_i}\left[v_k\left(a_i + G_{ij}v_j'\right) f\right] d\vec{v} - \int \left(a_k + G_{kj}v_j'\right) f d\vec{v} \qquad \text{(A.23)}$$

$$= \int_{\partial\Omega\to\infty} v_k\left(a_i + G_{ij}v_j'\right) f n_i dS - a_k \int f d\vec{v} - G_{kj}\int v_j' f d\vec{v} \qquad \text{(A.24)}$$

The first term is zero by Gauss's Theorem and the last because the average of the fluctuations is zero. $\int v_m' f d\vec{v} = 0$.

$$= -a_k$$

Turbulence: $$\int v_m' v_n' \frac{\partial}{\partial v_i}\left[\left(a_i + G_{ij}v_j'\right) f\right] d\vec{v}$$

Writing v' in terms of v gives:

$$= \int (v_m v_n - v_m u_n - v_n u_m + u_m u_n) \frac{\partial}{\partial v_i}\left[\left(a_i + G_{ij}v_j'\right) f\right] d\vec{v} \qquad \text{(A.25)}$$

$$= \int \frac{\partial}{\partial v_i}\left[(v_m v_n - v_m u_n - v_n u_m + u_m u_n)\left(a_i + G_{ij}v_j'\right) f\right] d\vec{v}$$
$$- \int \left(a_i + G_{ij}v_j'\right) f \frac{\partial}{\partial v_i}(v_m v_n - v_m u_n - v_n u_m + u_m u_n) d\vec{v} \qquad \text{(A.26)}$$

By Gauss's Theorem we can eliminate the first term.

$$= -\int \left(a_i + G_{ij}v_j'\right) f\left[\delta_{mi}v_n + \delta_{ni}v_m - \delta_{mi}u_n - \delta_{ni}u_m\right] d\vec{v} \qquad \text{(A.27)}$$

$$= -\int \left(a_i + G_{ij}v_j'\right) f\left(\delta_{mi}v_n' + \delta_{ni}v_m'\right) d\vec{v} \qquad \text{(A.28)}$$

$$= -\left(G_{mj}R_{jn} + G_{nj}R_{jm}\right) \qquad \text{(A.29)}$$

Energy: $$\tfrac{1}{2}\int v_k v_k \frac{\partial}{\partial v_i}\left[\left(a_i + G_{ij}v_j'\right) f\right] d\vec{v}$$

$$= \int \tfrac{1}{2} a_i \frac{\partial}{\partial v_i} v_k v_k f - a_i v_k f \frac{\partial v_k}{\partial v_i} + \tfrac{1}{2}\frac{\partial}{\partial v_i} v_k v_k G_{ij} v_j' f - v_k G_{ij} v_j' f \frac{\partial v_k}{\partial v_i} d\vec{v} \qquad \text{(A.30)}$$

By Gauss's Theorem we can eliminate the first and third terms.

$$= -\int a_i v_i f d\vec{v} - \int v_k G_{kj} v_j' f d\vec{v} = -a_i u_i - G_{kj}\overline{v_k v_j'} \qquad \text{(A.31)}$$

$$= -a_i u_i - G_{kj}\overline{(u_k + v_k')v_j'} \qquad \text{(A.32)}$$

Since $\int u_k v_j' f d\vec{v} = 0$ we get the following.

$$= -a_i u_i - G_{kj}\overline{v_k' v_j'} \tag{A.33}$$

$$= -a_i u_i - G_{kj} R_{jk} \tag{A.34}$$

4. $\dfrac{\partial}{\partial v_i}\left[H_{ij} \dfrac{\partial f}{\partial v_j}\right]$

Mass:
$$\int \frac{\partial}{\partial v_i}\left[H_{ij} \frac{\partial f}{\partial v_j}\right] d\vec{v} = \int_{\partial\Omega}\left(H_{ij} \frac{\partial f}{\partial v_j}\right) n_i dS = 0 \tag{A.35}$$

Momentum:
$$\int v_k \frac{\partial}{\partial v_i}\left[H_{ij} \frac{\partial f}{\partial v_j}\right] d\vec{v} = \int \frac{\partial}{\partial v_i}\left[v_k H_{ij} \frac{\partial f}{\partial v_j}\right] d\vec{v} - \int H_{ij} \frac{\partial f}{\partial v_j} \delta_{ik} d\vec{v} \tag{A.36}$$

$$= -\int \frac{\partial}{\partial v_j}\left(H_{jk} f\right) d\vec{v} = 0 \tag{A.37}$$

Turbulence:
$$\int v_m' v_n' \frac{\partial}{\partial v_i}\left[H_{ij} \frac{\partial f}{\partial v_j}\right] d\vec{v} = \int \frac{\partial}{\partial v_i}\left[v_m' v_n' H_{ij} \frac{\partial f}{\partial v_j}\right] d\vec{v} - \int H_{ij} \frac{\partial f}{\partial v_j} \frac{\partial v_m' v_n'}{\partial v_i} d\vec{v} \tag{A.38}$$

$$= -\int H_{ij} \frac{\partial f}{\partial v_j}\left(\delta_{mi} v_n' + \delta_{ni} v_m'\right) d\vec{v} \tag{A.39}$$

$$= \int H_{ij} f\left(\delta_{mi}\delta_{nj} + \delta_{ni}\delta_{mj}\right) d\vec{v} \tag{A.40}$$

$$= \left(H_{mn} + H_{nm}\right) \tag{A.41}$$

Energy:
$$\int \tfrac{1}{2} v_k v_k \frac{\partial}{\partial v_i}\left[H_{ij} \frac{\partial f}{\partial v_j}\right] d\vec{v}$$

$$= \int \tfrac{1}{2} H_{ij} \frac{\partial}{\partial v_i}\left[v_k v_k \frac{\partial f}{\partial v_j}\right] d\vec{v} - \int H_{ij} v_k \frac{\partial f}{\partial v_j} \frac{\partial v_k}{\partial v_i} d\vec{v} \tag{A.42}$$

By Gauss's Theorem we can eliminate the first term.

$$= -\int H_{jk} v_k \frac{\partial f}{\partial v_j} d\vec{v} \tag{A.43}$$

$$= -\int H_{jk} \frac{\partial}{\partial v_j}\left(v_k f\right) d\vec{v} + \int H_{jk} f \frac{\partial v_k}{\partial v_j} d\vec{v} \tag{A.44}$$

Again, from Gauss, we see the first term is zero.

$$= H_{kk} \tag{A.45}$$

5. $\dfrac{\partial}{\partial x_i} \mu \dfrac{\partial f}{\partial x_i}$

Mass:
$$\int \frac{\partial}{\partial x_i}\mu\frac{\partial f}{\partial x_i}d\vec{v} = \frac{\partial}{\partial x_i}\mu\frac{\partial}{\partial x_i}\int f d\vec{v} = 0 \tag{A.46}$$

Momentum:
$$\int v_k \frac{\partial}{\partial x_i}\mu\frac{\partial f}{\partial x_i}d\vec{v} = \frac{\partial}{\partial x_i}\mu\frac{\partial}{\partial x_i}\int v_k f d\vec{v} = \frac{\partial}{\partial x_i}\mu\frac{\partial u_k}{\partial x_i} \tag{A.47}$$

Turbulence:
$$\int v'_m v'_n \frac{\partial}{\partial x_i}\mu\frac{\partial f}{\partial x_i}d\vec{v}$$
$$= \int \frac{\partial}{\partial x_i}\left[v'_m v'_n \mu\frac{\partial f}{\partial x_i}\right]_{\rfloor} - \left[\mu\frac{\partial f}{\partial x_i}\right]_{\rfloor}\frac{\partial v'_m v'_n}{\partial x_i}d\vec{v} \tag{A.48}$$

We note that $\frac{\partial v'_m v'_n}{\partial x_j} = -v'_m u_{n,i} - v'_n u_{m,i}$,

$$= \int \frac{\partial}{\partial x_i}\left[v'_m v'_n \mu\frac{\partial f}{\partial x_i}\right]_{\rfloor} + \left[\mu\frac{\partial f}{\partial x_i}\right]_{\rfloor}\left(v'_m u_{n,i} + v'_n u_{m,i}\right)d\vec{v} \tag{A.49}$$

$$= \int \frac{\partial}{\partial x_i}\left[\mu\frac{\partial v'_m v'_n f}{\partial x_i} - \mu f\frac{\partial v'_m v'_n}{\partial x_i}\right]_{\rfloor} + \mu\frac{\partial f}{\partial x_i}\left(v'_m u_{n,i} + v'_n u_{m,i}\right)d\vec{v} \tag{A.50}$$

$$= \frac{\partial}{\partial x_i}\mu\frac{\partial}{\partial x_i}\int v'_m v'_n f d\vec{v} + \frac{\partial}{\partial x_i}\int \mu f\left(v'_m u_{n,i} + v'_n u_{m,i}\right)d\vec{v} + \mu\int\frac{\partial f}{\partial x_i}\left(v'_m u_{n,i} + v'_n u_{m,i}\right)d\vec{v} \tag{A.51}$$

The middle term is zero due to the fact that $\int v'_m f d\vec{v} = 0$

$$= \frac{\partial}{\partial x_i}\mu\frac{\partial R_{mn}}{\partial x_i} + \mu\int\frac{\partial f}{\partial x_i}\left(v'_m u_{n,i} + v'_n u_{m,i}\right)d\vec{v} \tag{A.52}$$

$$= \frac{\partial}{\partial x_i}\mu\frac{\partial R_{mn}}{\partial x_i} + \mu\int\frac{\partial f\left(v'_m u_{n,i} + v'_n u_{m,i}\right)}{\partial x_i} - f\frac{\partial\left(v'_m u_{n,i} + v'_n u_{m,i}\right)}{\partial x_i}d\vec{v} \tag{A.53}$$

Again the middle term is zero.

$$= \frac{\partial}{\partial x_i}\mu\frac{\partial R_{mn}}{\partial x_i} - \mu\int f\left(v'_m\frac{\partial u_{n,i}}{\partial x_i} + u_{n,i}\frac{\partial v'_m}{\partial x_i} + v'_n\frac{\partial u_{m,i}}{\partial x_i} + u_{m,i}\frac{\partial v'_n}{\partial x_i}\right)d\vec{v} \tag{A.54}$$

$$= \frac{\partial}{\partial x_i}\mu\frac{\partial R_{mn}}{\partial x_i} - \mu\int f\left(u_{n,i}\frac{\partial v'_m}{\partial x_i} + u_{m,i}\frac{\partial v'_n}{\partial x_i}\right)d\vec{v} \tag{A.55}$$

$$= \frac{\partial}{\partial x_i}\mu\frac{\partial R_{mn}}{\partial x_i} + 2\mu u_{m,i}u_{n,i} \tag{A.56}$$

Energy:
$$\tfrac{1}{2}\int v_k v_k \frac{\partial}{\partial x_i}\mu\frac{\partial f}{\partial x_i}d\vec{v}$$
$$= \tfrac{1}{2}\frac{\partial}{\partial x_i}\mu\frac{\partial}{\partial x_i}\int v_k v_k f d\vec{v} \tag{A.57}$$

$$= \tfrac{1}{2}\frac{\partial}{\partial x_i}\mu\frac{\partial}{\partial x_i}\left(u_k u_k + \overline{v'_k v'_k}\right) \tag{A.58}$$

$$= \frac{\partial}{\partial x_i} \mu \frac{\partial E}{\partial x_i}$$

6. $$\frac{\partial}{\partial v_i}\left[(J_{ij} + \mu u_{j,i}) \frac{\partial f}{\partial x_j}\right]_{\rfloor}^{\lceil} = (J_{ij} + \mu u_{j,i}) \frac{\partial^2 f}{\partial v_i \partial x_j} \quad \text{(A.59)}$$

Mass: $$\int (J_{ij} + \mu u_{j,i}) \frac{\partial^2 f}{\partial v_i \partial x_j} \partial \vec{v} = 0 \quad \text{(A.60)}$$

Momentum: $$\int v_k (J_{ij} + \mu u_{j,i}) \frac{\partial^2 f}{\partial v_i \partial x_j} d\vec{v} \quad \text{(A.61)}$$

$$= (J_{ij} + \mu u_{j,i}) \int \frac{\partial}{\partial v_i}\left[v_k \frac{\partial f}{\partial x_j}\right]_{\rfloor}^{\lceil} - \delta_{ki} \frac{\partial f}{\partial x_j} d\vec{v} \quad \text{(A.62)}$$

$$= (J_{ij} + \mu u_{j,i}) \frac{\partial}{\partial x_j} \int \frac{\partial v_k f}{\partial v_i} d\vec{v} - (J_{kj} + \mu u_{j,k}) \frac{\partial}{\partial x_j} \int f d\vec{v} \quad \text{(A.63)}$$

Using Gauss's theorem,

$$= 0 \quad \text{(A.64)}$$

Turbulence: $$\int v'_m v'_n (J_{ij} + \mu u_{j,i}) \frac{\partial^2 f}{\partial v_i \partial x_j} d\vec{v} = (J_{ij} + \mu u_{j,i}) \int v'_m v'_n \frac{\partial^2 f}{\partial v_i \partial x_j} d\vec{v} \quad \text{(A.65)}$$

$$= (J_{ij} + \mu u_{j,i}) \int \frac{\partial}{\partial x_i}\left[v'_m v'_n \frac{\partial f}{\partial v_j}\right]_{\rfloor}^{\lceil} - \frac{\partial f}{\partial v_j} \frac{\partial v'_m v'_n}{\partial x_i} d\vec{v} \quad \text{(A.66)}$$

$$= (J_{ij} + \mu u_{j,i}) \int \frac{\partial}{\partial x_i}\left[\frac{\partial f v'_m v'_n}{\partial v_j} - f \frac{\partial v'_m v'_n}{\partial v_j}\right]_{\rfloor}^{\lceil} + \int \left(v'_m u_{n,i} + v'_n u_{m,i}\right) \frac{\partial f}{\partial v_j} d\vec{v} \quad \text{(A.67)}$$

Gauss's divergence theorem eliminates the first term.

$$= (J_{ij} + \mu u_{j,i}) \left\{ \frac{\partial}{\partial x_i} \int -f \left(v'_m \delta_{nj} + v'_n \delta_{mj}\right) d\vec{v} + \int \left(v'_m u_{n,i} + v'_n u_{m,i}\right) \frac{\partial f}{\partial v_j} d\vec{v} \right\}_{\rfloor} \quad \text{(A.68)}$$

First term is zero.

$$= (J_{ij} + \mu u_{j,i}) \int \frac{\partial \left(v'_m u_{n,i} + v'_n u_{m,i}\right) f}{\partial v_j} - f \frac{\partial \left(v'_m u_{n,i} + v'_n u_{m,i}\right)}{\partial v_j} d\vec{v} \quad \text{(A.69)}$$

Gauss's theorem eliminates the first term.

$$= -(J_{ij} + \mu u_{j,i}) \int u_{n,i} f \delta_{mj} + u_{m,i} f \delta_{nj} d\vec{v} \quad \text{(A.70)}$$

$$= -(J_{ij} + \mu u_{j,i}) \left\{ u_{m,i} \delta_{nj} + u_{n,i} \delta_{mj}\right\} \quad \text{(A.71)}$$

$$= -\rho \left\{ J_{in} u_{m,i} + J_{im} u_{n,i} + 2\mu u_{n,i} u_{m,i}\right\}$$

Energy: $$\int \tfrac{1}{2} v_k v_k (J_{ij} + \mu u_{j,i}) \frac{\partial^2 f}{\partial v_i \partial x_j} d\vec{v}$$

$$= \tfrac{1}{2}(J_{ij} + \mu u_{j,i}) \int \frac{\partial}{\partial x_i} \left[v_k v_k \frac{\partial f}{\partial v_j} \right]^{\prime} d\vec{v} \tag{A.72}$$

$$= \tfrac{1}{2}(J_{ij} + \mu u_{j,i}) \int \frac{\partial}{\partial x_i} \left(\frac{\partial v_k v_k f}{\partial v_j} - 2 f v_k \frac{\partial v_k}{\partial v_j} \right) d\vec{v} \tag{A.73}$$

Gauss's theorem eliminates the first term.

$$= -(J_{ij} + \mu u_{j,i}) \frac{\partial}{\partial x_i} \int f v_j d\vec{v} \tag{A.74}$$

$$= -(J_{ij} + \mu u_{j,i}) \frac{\partial u_j}{\partial x_i} \tag{A.75}$$

7. $$\frac{\partial}{\partial v_i} \mu K_{,l} \frac{\partial}{\partial x_l} \left[\frac{f v_i'}{K} \right]^{\prime} = \mu K_{,l} \frac{\partial}{\partial x_l} \frac{\partial}{\partial v_i} \left[\frac{f v_i'}{K} \right]^{\prime} \tag{A.76}$$

Mass: $$\int \mu K_{,l} \frac{\partial}{\partial x_l} \frac{\partial}{\partial v_i} \left[\frac{f v_i'}{K} \right]^{\prime} d\vec{v} = \mu K_{,l} \frac{\partial}{\partial x_l} \frac{\partial}{\partial v_i} \int \left[\frac{f v_i'}{K} \right]^{\prime} d\vec{v} = 0 \tag{A.77}$$

Momentum: $$\int v_m \mu K_{,l} \frac{\partial}{\partial x_l} \frac{\partial}{\partial v_i} \left[\frac{f v_i'}{K} \right]^{\prime} d\vec{v} = \int v_m \frac{\partial}{\partial v_i} \left[\mu K_{,l} \frac{\partial}{\partial x_l} \left[\frac{f v_i'}{K} \right]^{\prime} \right]^{\prime} d\vec{v} \tag{A.78}$$

$$= \int \frac{\partial}{\partial v_i} \left[v_m \mu K_{,l} \frac{\partial}{\partial x_l} \left[\frac{f v_i'}{K} \right]^{\prime} \right]^{\prime} - \frac{\partial v_m}{\partial v_i} \mu K_{,l} \frac{\partial}{\partial x_l} \left[\frac{f v_i'}{K} \right]^{\prime} d\vec{v} \tag{A.79}$$

The first term is zero by Gauss's Theorem

$$= -\int \delta_{mi} \mu K_{,l} \frac{\partial}{\partial x_l} \left[\frac{f v_i'}{K} \right]^{\prime} d\vec{v} \tag{A.80}$$

$$= -\mu K_{,l} \frac{\partial}{\partial x_l} \int \left[\frac{f v_m'}{K} \right]^{\prime} d\vec{v} = 0 \tag{A.81}$$

Turbulence: $$\int v_n' v_m' \left(\mu K_{,l} \frac{\partial}{\partial x_l} \frac{\partial}{\partial v_i} \left[\frac{f v_i'}{K} \right]^{\prime} \right) d\vec{v} = \int v_n' v_m' \frac{\partial}{\partial v_i} \left[\mu K_{,l} \frac{\partial}{\partial x_l} \left[\frac{f v_i'}{K} \right]^{\prime} \right]^{\prime} d\vec{v} \tag{A.82}$$

$$= \int \frac{\partial}{\partial v_i} \left[v_n' v_m' \mu K_{,l} \frac{\partial}{\partial x_l} \left[\frac{f v_i'}{K} \right]^{\prime} \right]^{\prime} - \frac{\partial v_n' v_m'}{\partial v_i} \mu K_{,l} \frac{\partial}{\partial x_l} \left[\frac{f v_i'}{K} \right]^{\prime} d\vec{v} \tag{A.83}$$

By Gauss's Theorem we can eliminate the first term

$$= \int -\mu K_{,l} (\delta_{ni} v_m' + \delta_{mi} v_n') \frac{\partial}{\partial x_l} \left[\frac{f v_i'}{K} \right]^{\prime} d\vec{v} \tag{A.84}$$

$$= \int -\mu K_{,l} \left(\frac{\partial}{\partial x_l} \left[\frac{f v_i' (\delta_{ni} v_m' + \delta_{mi} v_n')}{K} \right]^{\prime} - \frac{\partial}{\partial x_l} \left[\delta_{ni} v_m' + \delta_{mi} v_n' \right] \frac{f v_i'}{K} \right) d\vec{v} \tag{A.85}$$

$$= \int -\mu K_{,l}\left(\frac{\partial}{\partial x_l}\left[\frac{fv_n'v_m' + fv_m'v_n'}{K}\right] - \left(-\delta_{ni}u_{m,l} - \delta_{mi}u_{n,l}\right)\frac{fv_i'}{K}\right)d\vec{v} \tag{A.86}$$

Second term is zero

$$= -\mu K_{,l}\frac{\partial}{\partial x_l}\int \frac{fv_n'v_m'}{K} + \frac{fv_m'v_n'}{K}d\vec{v} \tag{A.87}$$

$$= -2\mu K_{,l}\left(\frac{R_{mn}}{K}\right)_{,l} \tag{A.88}$$

Energy: $\frac{1}{2}\int v_k v_k\left(\mu K_{,l}\frac{\partial}{\partial x_l}\frac{\partial}{\partial v_i}\left[\frac{fv_i'}{K}\right]\right)d\vec{v} = \frac{1}{2}\int \mu K_{,l}v_k v_k \frac{\partial}{\partial v_i}\frac{\partial}{\partial x_l}\left[\frac{fv_i'}{K}\right]d\vec{v}$ (A.89)

$$= \frac{1}{2}\int \mu K_{,l}\frac{\partial}{\partial v_i}\left[v_k v_k \frac{\partial}{\partial x_l}\left[\frac{fv_i'}{K}\right]\right]d\vec{v} - \int \mu K_{,l}v_k \frac{\partial v_k}{\partial v_i}\frac{\partial}{\partial x_l}\left[\frac{fv_i'}{K}\right]d\vec{v} \tag{A.90}$$

By Gauss's Theorem we can eliminate the first term

$$= -\mu K_{,l}\int \frac{\partial}{\partial x_l}\left[\frac{fv_i v_i'}{K}\right]d\vec{v} \tag{A.91}$$

$$= -\mu K_{,l}\frac{\partial}{\partial x_l}\int \frac{f(v_i' + u_i)v_i'}{K}d\vec{v} \tag{A.92}$$

Since $\int v_i' f\, d\vec{v} = 0$ we get

$$= -\mu K_{,l}\frac{\partial}{\partial x_l}\int \frac{fv_i'v_i'}{K}d\vec{v} = -\mu K_{,l}\frac{\partial}{\partial x_l}[1] \tag{A.93}$$

$$= 0 \tag{A.94}$$

So, in summary,

Mass: $0 = -\frac{\partial u_i}{\partial x_i}$ (A.95)

Momentum: $\frac{\partial u_k}{\partial t} + \frac{\partial R_{ik}}{\partial x_i} + \frac{\partial u_i u_k}{\partial x_i} - a_k = \frac{\partial}{\partial x_i}\mu\frac{\partial u_k}{\partial x_i}$ (A.96)

Turbulence:

$$\frac{\partial R_{mn}}{\partial t} + \frac{\partial}{\partial x_i}u_i R_{mn} + \frac{\partial}{\partial x_i}\overline{v_m'v_n'v_i'} + R_{ni}\frac{\partial u_m}{\partial x_i} + R_{mi}\frac{\partial u_n}{\partial x_i} = \left(G_{mj}R_{jn} + G_{nj}R_{jm}\right) + \left(H_{mn} + H_{nm}\right) + \frac{\partial}{\partial x_i}\mu\frac{\partial R_{mn}}{\partial x_i} - \left(J_{in}u_{m,i} + J_{im}u_{n,i}\right) - 2\mu\frac{\partial K}{\partial x_l}\left(\frac{R_{mn}}{K}\right)_{,l} \tag{A.97}$$

Energy:

$$\frac{\partial E}{\partial t} + \frac{\partial}{\partial x_i}\left[u_i E + u_k R_{ik} + \frac{1}{2}\overline{v_i'v_k'v_k'}\right] = a_i u_i + G_{kj}R_{jk} + H_{kk} + \frac{\partial}{\partial x_i}\mu\frac{\partial E}{\partial x_i} - (J_{ij} + \mu u_{j,i})\frac{\partial u_j}{\partial x_i} \tag{A.98}$$

Appendix B: Numerical Solution of the PDF Equation

PDF Equation:

$$\frac{\partial f}{\partial t} = -v_i \frac{\partial f}{\partial x_i} - a_i \frac{\partial f}{\partial v_i} - \frac{\partial}{\partial v_i}\left[G_{ij}\left(v_j - u_j\right) f\right] + \frac{\partial}{\partial v_i}\left[H_{ij} \frac{\partial f}{\partial v_j}\right] + \frac{\partial}{\partial x_i}\left[\mu \frac{\partial (f/\rho)}{\partial x_i}\right] + \frac{\partial}{\partial x_i}\left[(J_{ij} + \mu u_{j,i}) \frac{\partial f}{\partial v_j}\right] + \mu K_{,l} \frac{\partial}{\partial x_l} \frac{\partial}{\partial v_i}\left[\frac{f v_i'}{K}\right] \tag{B.1}$$

'F hat' Equation:

$$\hat{f} = \ln[f], \quad \frac{\partial \hat{f}}{\partial t} = \frac{1}{f} \frac{\partial f}{\partial t} \tag{B.2}$$

By defining 'F hat' as the natural log of the PDF function, we arrive at an equivalent evolution equation, which looks like the following

$$\frac{\partial \hat{f}}{\partial t} = \frac{1}{f}\left(-v_i \frac{\partial f}{\partial x_i} - a_i \frac{\partial f}{\partial v_i} - \frac{\partial}{\partial v_i}\left[G_{ij}\left(v_j - u_j\right) f\right] + \frac{\partial}{\partial v_i}\left[H_{ij} \frac{\partial f}{\partial v_j}\right] + \frac{\partial}{\partial x_i}\left[\mu \frac{\partial (f/\rho)}{\partial x_i}\right] + \frac{\partial}{\partial x_i}\left[(J_{ij} + \mu u_{j,i}) \frac{\partial f}{\partial v_j}\right] + \mu K_{,l} \frac{\partial}{\partial x_l} \frac{\partial}{\partial v_i}\left[\frac{f v_i'}{K}\right]\right) \tag{B.3}$$

Each term is derived below based on the 'F hat' equation.

$$-v_i \frac{1}{f} \frac{\partial f}{\partial x_i} = -v_i \frac{\partial \hat{f}}{\partial x_i} \tag{B.4}$$

$$-a_i \frac{1}{f} \frac{\partial f}{\partial v_i} = -a_i \frac{\partial \hat{f}}{\partial v_i} \tag{B.5}$$

$$-\frac{1}{f} \frac{\partial}{\partial v_i}\left[G_{ij}\left(v_j - u_j\right) f\right] = -G_{ij} \frac{1}{f} \frac{\partial}{\partial v_i}\left[v_j' f\right] \tag{B.6}$$

since $\left(v_j - u_j\right) = v_j'$

$$= -G_{ij} \frac{1}{f} f \frac{\partial v_j'}{\partial v_i} - G_{ij} \frac{1}{f} v_j' \frac{\partial f}{\partial v_i} \tag{B.7}$$

$$= -G_{ij} \frac{\partial v_j'}{\partial v_i} - G_{ij} v_j' \frac{\partial \hat{f}}{\partial v_i} \tag{B.8}$$

$$= -G_{ij}\delta_{ij} - G_{ij}v_j^{'}\frac{\partial \hat{f}}{\partial v_i} \tag{B.9}$$

$$= -G_{ii} - G_{ij}v_j^{'}\frac{\partial \hat{f}}{\partial v_i} \tag{B.10}$$

$$\frac{1}{f}\frac{\partial}{\partial v_i}\left[H_{ij}\frac{\partial f}{\partial v_j}\right] = H_{ij}\frac{1}{f}\frac{\partial}{\partial v_i}\frac{\partial f}{\partial v_j} \tag{B.11}$$

$$= H_{ij}\left(\frac{\partial}{\partial v_i}\left[\frac{1}{f}\frac{\partial f}{\partial v_j}\right] - \frac{\partial \frac{1}{f}}{\partial v_i}\frac{\partial f}{\partial v_j}\right) \tag{B.12}$$

$$= H_{ij}\left(\frac{\partial}{\partial v_i}\frac{\partial \hat{f}}{\partial v_j} + \frac{1}{f^2}\frac{\partial f}{\partial v_i}\frac{\partial f}{\partial v_j}\right) \tag{B.13}$$

$$= H_{ij}\left(\frac{\partial}{\partial v_i}\frac{\partial \hat{f}}{\partial v_j} + \frac{\partial \hat{f}}{\partial v_i}\frac{\partial \hat{f}}{\partial v_j}\right) \tag{B.14}$$

$$\frac{1}{f}\frac{\partial}{\partial x_i}\left[\mu\frac{\partial(f/\rho)}{\partial x_i}\right] = \frac{\partial}{\partial x_i}\left[\frac{\mu}{f}\frac{\partial f}{\partial x_i}\right] - \mu\frac{\partial \frac{1}{f}}{\partial x_i}\frac{\partial f}{\partial x_i} \tag{B.15}$$

$$= \frac{\partial}{\partial x_i}\left[\mu\frac{\partial \hat{f}}{\partial x_i}\right] + \frac{\mu}{f^2}\frac{\partial f}{\partial x_i}\frac{\partial f}{\partial x_i} \tag{B.16}$$

$$= \frac{\partial}{\partial x_i}\left[\mu\frac{\partial \hat{f}}{\partial x_i}\right] + \mu\frac{\partial \hat{f}}{\partial x_i}\frac{\partial \hat{f}}{\partial x_i} \tag{B.17}$$

$$\frac{1}{f}\frac{\partial}{\partial x_i}\left[(J_{ij} + \mu u_{j,i})\frac{\partial f}{\partial v_j}\right] = \frac{\partial}{\partial x_i}\left[\frac{(J_{ij} + \mu u_{j,i})}{f}\frac{\partial f}{\partial v_j}\right] - (J_{ij} + \mu u_{j,i})\frac{\partial \frac{1}{f}}{\partial x_i}\frac{\partial f}{\partial v_j} \tag{B.18}$$

$$= \frac{\partial}{\partial x_i}\left[(J_{ij} + \mu u_{j,i})\frac{\partial \hat{f}}{\partial v_j}\right] + \frac{(J_{ij} + \mu u_{j,i})}{f^2}\frac{\partial f}{\partial x_i}\frac{\partial f}{\partial v_j} \tag{B.19}$$

$$= \frac{\partial}{\partial x_i}(J_{ij} + \mu u_{j,i})\frac{\partial \hat{f}}{\partial v_j} + (J_{ij} + \mu u_{j,i})\frac{\partial \hat{f}}{\partial x_i}\frac{\partial \hat{f}}{\partial v_j} \tag{B.20}$$

$$\frac{1}{f}\mu K_{,l}\frac{\partial}{\partial x_l}\frac{\partial}{\partial v_i}\left[\frac{fv_i^{'}}{K}\right] = \mu K_{,l}\left\{\frac{\partial}{\partial x_l}\left[\frac{1}{f}\frac{\partial}{\partial v_i}\left[\frac{fv_i^{'}}{K}\right]\right] - \frac{\partial}{\partial v_i}\left[\frac{fv_i^{'}}{K}\right]\frac{\partial \frac{1}{f}}{\partial x_l}\right\} \tag{B.21}$$

$$= \mu K_{,l}\left\{\frac{\partial}{\partial x_l}\left[\frac{\partial}{\partial v_i}\left[\frac{\frac{1}{f}fv_i^{'}}{K}\right] - \frac{fv_i^{'}}{K}\frac{\partial \frac{1}{f}}{\partial v_i}\right] + \left(\frac{1}{f}\frac{\partial}{\partial v_i}\left[\frac{fv_i^{'}}{K}\right]\right)\frac{\partial \hat{f}}{\partial x_l}\right\} \tag{B.22}$$

$$= \mu K_{,l} \left\{ \left[\frac{\partial}{\partial x_l} \left[\frac{\partial v_i' / K}{\partial v_i} - \frac{v_i'}{K} \frac{\partial \hat{f}}{\partial v_i} \right] \right] + \left(\frac{1}{f} \frac{\partial}{\partial v_i} \left[\frac{f v_i'}{K} \right] \right) \frac{\partial \hat{f}}{\partial x_l} \right\} \tag{B.23}$$

$$= \mu K_{,l} \left\{ \left[\frac{\partial}{\partial x_l} \left[\frac{\partial v_i' / K}{\partial v_i} - \frac{v_i'}{K} \frac{\partial \hat{f}}{\partial v_i} \right] \right] + \left(\frac{\partial v_i' / K}{\partial v_i} - \frac{v_i'}{K} \frac{\partial \hat{f}}{\partial v_i} \right) \frac{\partial \hat{f}}{\partial x_l} \right\} \tag{B.24}$$

$$= \mu K_{,l} \left\{ \left[\frac{\partial}{\partial x_l} \left[\frac{3}{K} - \frac{v_i'}{K} \frac{\partial \hat{f}}{\partial v_i} \right] \right] + \left(\frac{3}{K} - \frac{v_i'}{K} \frac{\partial \hat{f}}{\partial v_i} \right) \frac{\partial \hat{f}}{\partial x_l} \right\} \tag{B.25}$$

The resulting evolution equation for 'F hat' is:

$$\begin{aligned} \frac{\partial \hat{f}}{\partial t} = & -v_i \frac{\partial \hat{f}}{\partial x_i} - a_i \frac{\partial \hat{f}}{\partial v_i} - G_{ii} - G_{ij} v_j' \frac{\partial \hat{f}}{\partial v_i} + H_{ij} \left(\frac{\partial}{\partial v_i} \frac{\partial \hat{f}}{\partial v_j} + \frac{\partial \hat{f}}{\partial v_i} \frac{\partial \hat{f}}{\partial v_j} \right) + \mu \left(\frac{\partial}{\partial x_i} \frac{\partial \hat{f}}{\partial x_i} + \frac{\partial \hat{f}}{\partial x_i} \frac{\partial \hat{f}}{\partial x_i} \right) \\ & + \left(\frac{\partial}{\partial x_i} (J_{ij} + \mu u_{j,i}) \frac{\partial \hat{f}}{\partial v_j} + (J_{ij} + \mu u_{j,i}) \frac{\partial \hat{f}}{\partial x_i} \frac{\partial \hat{f}}{\partial v_j} \right) + \mu K_{,l} \frac{\partial}{\partial x_l} \left[\frac{3}{K} + \frac{v_i'}{K} \frac{\partial \hat{f}}{\partial v_i} \right] \\ & + \mu K_{,l} \left(\frac{3}{K} + \frac{v_i'}{K} \frac{\partial \hat{f}}{\partial v_i} \right) \frac{\partial \hat{f}}{\partial x_l} \end{aligned} \tag{B.26}$$

Appendix C: PDF Models for Return-to-Isotropy

1. Introduction

In most turbulent flows of interest the turbulent velocity fluctuations are anisotropic, that is they differ in magnitude depending on their orientation. One aspect of Reynolds stress transport models (and other more advanced models) that distinguishes them from simple two-equation transport models like k-ε is their ability to more accurately model turbulence anisotropy. The degree of anisotropy is important because it can directly impact how turbulence affects the mean flow.

In the absence of any driving mechanism anisotropic turbulent flows tend to return to an isotropic state (the state of least order). This nonlinear process is often called return-to-isotropy. It was identified early on in the development of Reynolds stress transport models and first modeled by Rotta[1]. Since that time, the return-to-isotropy process has been extensively investigated and modeled[2-10].

The return-to-isotropy problem is of significant theoretical interest in the theory of turbulence because it is entirely due to nonlinear interactions. The return process is irreversible, and is the mathematical consequence of the averaging process. As a result we know that the return process must be modeled, and that there can be no exact representation for this process in terms of Reynolds averaged variables. Existing models for return-to-isotropy tend to make extensive use of mathematical concepts, such as the Cayley-Hamilton theorem, realizability, Taylor series expansions, and fixed point analysis. The resulting models invariably have a least one model 'constant' that must be set via experiments.

In this work, we are interested in deriving models for the return process based on physical ideas as well as the commonly used mathematical tools. We make the assumption that turbulence behaves as a kinetic process, and that kinetic models of turbulence may lead to some useful insights about the return process. The advantage of this approach is that the resulting models can be made to be free of any tunable model constants.

In Section 2, the classic Reynolds stress transport equation approach to modeling return-to-isotropy is briefly reviewed. We use these classic results as a reference since this is the approach that is most widely understood by most readers. In Section 3 we consider return-to-isotropy from the perspective of the BGK[11] approximation to the Boltzmann equation. Classic linear return models result from this kinetic equation. The deficiencies of the BGK approach are largely solved by two parameter-free relaxation collision models developed and tested in Section 4. Section 5 investigates the predictive performance of these models for five different experimental cases. The relaxation model is extended in Section 6 to enable any desired Reynolds stress return behavior, and another parameter free model is proposed that has some unique and interesting properties. Section 7 explores the implications and connections to the Fokker-Planck collision

model, and the results are discussed in Section 8, where some speculation is presented as to what these kinetic models imply about turbulent eddy interactions.

2. Reynolds Stress Transport Models

In the absence of any mean flow the evolution of the Reynolds stress tensor, R_{ij}, in homogeneous but anisotropic turbulence evolves according to the equation

$$\frac{\partial R_{ij}}{\partial t} = -2\nu\overline{u'_{i,k}u'_{j,k}} + \overline{p(u'_{i,j} + u'_{j,i})} \qquad \text{(C.1)}$$

The first term on the right-hand side is the dissipation rate tensor and the second term is the slow pressure-strain. The pressure-strain is considered 'slow' in this situation because the pressure in this term depends only on the turbulence not on the 'rapid' mean flow velocity gradients (since there are none in this situation). Both terms require modeling. However, one half the trace of the dissipation tensor is the dissipation rate, $\varepsilon = \nu\overline{u'_{i,k}u'_{i,k}}$, which is assumed to be known (given by another transport equation model), and the trace of the pressure-strain term is zero in incompressible flows.

The most common modeling approach is to assume that the dissipation tensor is close to isotropic. If small anisotropy in the dissipation tensor exists then it is then included with the pressure-strain model. The slow pressure-strain and anisotropic dissipation are then collectively modeled as a 'return-to-isotropy' term. There are reasons to suggest that modeling dissipation anisotropy and slow pressure-strain separately is advantageous,[12,13] but for simplicity we retain the 'collective' approach described above. The simplest model (due to Rotta) is that the return-to-isotropy term is proportional to the Reynolds stress anisotropy. This gives a Reynolds stress transport model of the form,

$$\frac{\partial R_{ij}}{\partial t} = -\frac{2}{3}\varepsilon\delta_{ij} - \hat{C}_R\varepsilon\left(\frac{R_{ij}}{K} - \frac{2}{3}\delta_{ij}\right) \qquad \text{(C.2)}$$

The 'return-to-isotropy' term will tend to drive the Reynolds stress tensor towards an isotropic state as time proceeds. The rate at which this happens is governed by the Rotta constant, $\hat{C}_R$. This return model is the simplest possible, and is linear in the Reynolds stress anisotropy, $a_{ij} = \left(\frac{R_{ij}}{K} - \frac{2}{3}\delta_{ij}\right)$. Equation C.2 appears to imply return-to-isotropy for any positive value of $\hat{C}_R$. In fact this is not the case, $\hat{C}_R$ must be greater than 1. To see this we look at the evolution equation for $\frac{R_{ij}}{K}$ which should tend towards $\frac{2}{3}\delta_{ij}$.

$$\frac{\partial(R_{ij}/K)}{\partial t} = \frac{1}{K}\frac{\partial R_{ij}}{\partial t} - \frac{R_{ij}}{K^2}\frac{\partial K}{\partial t} = -(\hat{C}_R - 1)\frac{\varepsilon}{K}\left(\frac{R_{ij}}{K} - \frac{2}{3}\delta_{ij}\right) \qquad \text{(C.3)}$$

The isotropic dissipation actually causes the Reynolds stress tensor to move away from isotropy which must be counteracted by the return term. $\hat{C}_R$ is actually a parameter, not a strict constant, that can be (and often is) a function of the Reynolds stress invariants and

turbulent Reynolds number. Due to the strict requirement described above the splitting $\hat{C}_R = 1 + C_R$ is useful. This gives a model equation of the form,

$$\frac{\partial R_{ij}}{\partial t} = -\varepsilon \frac{R_{ij}}{K} - C_R \varepsilon \left(\frac{R_{ij}}{K} - \frac{2}{3}\delta_{ij}\right) \tag{C.4}$$

where $C_R > 0$. Typical values for C_R lie between 0.5 and 1.0 (Durbin)[14]. Launder, Reece and Rodi[15] suggest a value of 0.8. No return to isotropy is the case of $C_R = 0$. Physically, the no return limit appears to occur at low Reynolds numbers. In addition, the no-return limit is often enforced in the two component limit (where one of the Reynolds stress diagonals goes to zero faster than the others, such as near walls). For this reason C_R is often not a constant but is actually a parameter that depends on the turbulent Reynolds number and Reynolds stress invariants[6,16].

It is helpful to propose a general model for the Reynolds stress evolution,

$$\frac{\partial R_{ij}}{\partial t} = -\frac{\varepsilon}{2K}\left(\Pi_{im} R_{mj} + \Pi_{jm} R_{mi}\right) \tag{C.5}$$

where the dimensionless Π_{ij} is some as yet unspecified model. Expanding this model as $\Pi_{ij} = \delta_{ij} + \hat{\Pi}_{ij}$ gives

$$\frac{\partial R_{ij}}{\partial t} = -\frac{\varepsilon}{K} R_{ij} - \frac{\varepsilon}{2K}\left(\hat{\Pi}_{im} R_{mj} + \hat{\Pi}_{jm} R_{mi}\right) \tag{C.6}$$

so it is clear that $\hat{\Pi}_{ij}$ is the return part of the model. The trace of the last term should be zero, so we have a single constraint on the model, $\hat{\Pi}_{ij} R_{ji} = 0$. It is not necessary that $\hat{\Pi}_{ij}$ be symmetric. The explicit inclusion of the Reynolds stress in Eq. (C.5) means that this general model can be strongly realizable (Schumann[17], Lumley[2]) if $\hat{\Pi}_{ij}$ is finite. If one component of the turbulence goes to zero then this model will also make the time derivative of that component go to zero. However, in the unusual circumstance that $\hat{\Pi}_{ij}$ becomes singular (goes to infinity) this model can potentially violate strong realizability. The classic linear return model described above is given by $\hat{\Pi}_{ij} = C_R(\delta_{ij} - \frac{2}{3} K R_{ij}^{-1})$. This model becomes singular in the two component limit (because of the Reynolds stress inverse). The classic linear model satisfies weak realizability[18] if $C_R > 0$, but for the linear model to satisfy strong realizability C_R must go to zero in the two component limit.

Slightly more complex nonlinear models for return-to-isotropy have the general form,

$$\frac{K}{\varepsilon}\frac{\partial a_{ij}}{\partial t} = -C_R\left(a_{ij}\right) + C_N\left(a_{ik}a_{kj} - a_{nk}a_{kn}\frac{\delta_{ij}}{3}\right) \tag{C.7}$$

Cubic and higher order nonlinear models can also be represented by this quadratically nonlinear model due to the Cayley-Hamilton theorem. Sarkar and Speziale[3] suggest values of $C_R = 0.7$ and $C_N = 1.05$.

The realizability conditions are clearer when this model is written in terms of the Reynolds stresses,

$$\frac{\partial R_{ij}}{\partial t} = -\frac{\varepsilon}{K} R_{ij} - \{C_R - C_N[\frac{R_{nk}R_{kn}}{2K^2} - \frac{4}{3}]\}\frac{\varepsilon}{K}\left(R_{ij} - \frac{2}{3}K\delta_{ij}\right) + C_N\frac{\varepsilon}{K^2}\left(R_{ik}R_{kj} - \frac{R_{nk}R_{kn}}{2K}R_{ij}\right) \qquad (C.8)$$

Pre and post-multiplying this expression by the eigenvector matrix $\mathbf{Q}$ diagonalizes the Reynolds stress tensor ($\mathbf{Q}^T\mathbf{R}\mathbf{Q} = \mathbf{D}$), so

$$\mathbf{Q}^T\frac{\partial \mathbf{R}}{\partial t}\mathbf{Q} = -\frac{\varepsilon}{K}\mathbf{D} - \{C_R - C_N[\frac{R_{nk}R_{kn}}{2K^2} - \frac{4}{3}]\}\frac{\varepsilon}{K}\left(\mathbf{D} - \frac{2}{3}K\mathbf{I}\right) + C_N\frac{\varepsilon}{K^2}\left(\mathbf{D}\mathbf{D} - \frac{R_{nk}R_{kn}}{2K}\mathbf{D}\right) \qquad (C.9)$$

since $\mathbf{Q}^T\frac{\partial \mathbf{R}}{\partial t}\mathbf{Q} = \frac{\partial \mathbf{D}}{\partial t} + \mathbf{D}(\frac{\partial \mathbf{Q}^T}{\partial t}\mathbf{Q}) - (\frac{\partial \mathbf{Q}^T}{\partial t}\mathbf{Q})\mathbf{D}$ the off diagonal evolution is trivial, and the diagonal components individually satisfy the right-hand side of Eq. (C.9). Weak realizability is satisfied as long as $C_R - C_N[\frac{R_{nk}R_{kn}}{2K^2} - \frac{4}{3}] \geq 0$. Strong realizability requires equality on this previous expression and $1 + C_N[\frac{R_{nk}R_{kn}}{2K^2}] \geq 0$. The quantity $\frac{R_{nk}R_{kn}}{2K^2}$ appears frequently and is related to the second invariant of the anisotropy tensor via $\frac{R_{nk}R_{kn}}{2K^2} = \frac{2}{3} + \frac{1}{2}a_{nk}a_{kn}$.

The model expression for the nonlinear return model is

$$\Pi_{ij} = \delta_{ij} + \{C_R - C_N[\frac{R_{nk}R_{kn}}{2K^2} - \frac{4}{3}]\}(\delta_{ij} - \frac{2}{3}KR_{ij}^{-1}) - C_N\left(\frac{R_{ij}}{K} - \frac{R_{nk}R_{kn}}{2K^2}\delta_{ij}\right) \qquad (C.10)$$

The singularity due to R_{ij}^{-1} is weakly realizable as long as the leading coefficient is positive. It is strongly realizable if this leading coefficient is zero in the 2-component limit and the coefficient of δ_{ij} is positive.

3. BGK Collision Models

In homogeneous turbulence in the absence of mean accelerations or mean pressure gradients the evolution equation for the velocity probability density function (PDF) is

$$\frac{\partial f}{\partial t} = \left.\frac{df}{dt}\right|_{collisions} \qquad (C.11)$$

This equation governs the decay of anisotropic homogeneous turbulence, which is the focus of this work. One of the simplest collision models is a relaxation of the PDF to some known equilibrium form.

$$\frac{\partial f}{\partial t} = -\frac{\varepsilon}{K}C_{BGK}(f - f^{eq}) \qquad (C.12)$$

where the constant $C_{BGK}(\mathbf{x},t)$ might be a function of position and time but is not a function of the velocity. This model is similar to the BGK approximation for collisions used in Lattice-Boltzmann methods. The constant C_{BGK} should always be greater than 0 for a well-posed method. Unlike molecules, turbulence particles do not conserve kinetic energy when they collide, so the form of f^{eq}, the equilibrium target distribution, must be slightly different from classical theory. If we take the target distribution to be

$$f^{eq}(\hat{K}) = (\tfrac{4}{3}\pi\hat{K})^{-3/2} e^{-\frac{3v'_n v'_n}{4\hat{K}}} \tag{C.13}$$

where $0 < \hat{K} < K$, then (as shown in Appendix I) mass and momentum are conserved and turbulent kinetic energy obeys the equation, $\frac{\partial K}{\partial t} = -\frac{\varepsilon}{K} C_{BGK}(K - \hat{K})$. This implies that $C_{BGK} = \frac{1}{(1-\hat{K}/K)}$, and the dissipating collision model is

$$\frac{\partial f}{\partial t} = -\frac{\varepsilon}{(K-\hat{K})}\left(f - (\tfrac{4}{3}\pi\hat{K})^{-3/2} e^{-\frac{3v'_n v'_n}{4\hat{K}}} \right) \tag{C.14}$$

This is a model in which the PDF relaxes towards a spherical Gaussian PDF with less turbulent kinetic energy (see Figure 1). Those portions of the PDF which are farthest from the target spherical distribution decay faster than those portions of the PDF which are closer to the target.

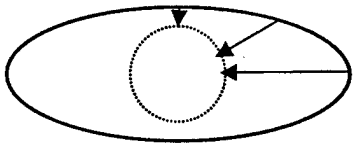

Figure 1: BGK relaxation model. Solid line represents an isocontour for an anisotropic PDF. Dashed line is the spherical target

The equivalent Reynolds stress transport equation is obtained by multiplying by $v'_i v'_j$ and integrating over all velocities. This is shown in Appendix I, and results in the following equation.

$$\frac{\partial R_{ij}}{\partial t} = -\frac{\varepsilon}{(K-\hat{K})}(R_{ij} - \tfrac{2}{3}\hat{K}\delta_{ij}) = -\frac{\varepsilon}{K} R_{ij} - \frac{\varepsilon}{K}\frac{1}{(K/\hat{K}-1)}(R_{ij} - \tfrac{2}{3}K\delta_{ij}) \tag{C.15}$$

In terms of $\hat{\Pi}$, this model is $\hat{\Pi}_{ij} = \frac{\hat{K}-1}{K}(\delta_{ij} - \frac{2}{3}KR_{ij}^{-1})$. Which is identical to the classic return model if $C_R = \frac{1}{(K/\hat{K}-1)}$, or equivalently $\hat{K} = K\frac{C_R}{(1+C_R)}$. This implies the relation $C_{BGK} = 1 + C_R = \hat{C}_R$ between the BGK relaxation constant and the Rotta constant.

From this analysis it can be seen that there is no return to isotropy if $C_R = 0$ (or $\hat{K} = 0$). Under the condition $\hat{K} = 0$, f^{eq} becomes a delta function. This observation suggests an alternative model of the form,

$$\frac{\partial f}{\partial t} = -\frac{\varepsilon}{k}(f - \delta(v')) - \frac{\varepsilon}{k} C_R (f - f^{eq}(K)) \tag{C.16}$$

The first term (involving a delta function) produces pure decay and the second produces return to isotropy with no decay (relaxation to a spherical PDF of the same energy). This two-part model has been proposed by Degond & Lemou[10].

While both C.14 and C.16 result in an identical equation for the Reynolds stress evolution (the classic linear Rotta model), the models themselves are not identical. Differences exist in the evolution of the higher turbulence moments. The model given by Eq. (C.16) will tend to produce a spike in the PDF around its mean value (due to the delta function). Eq. (C.14) has a smoother influence on the PDF in general but will also produce a spike if C_R goes to zero (in the two-component or low Reynolds number limits).

Neither model has the ellipsoidal (Eq. 23) or spherical (Eq. 18) Gaussian as a solution. This implies that even if the turbulence starts with a Gaussian PDF it does not stay Gaussian. It is not a strict fact that turbulence should be Gaussian. Certainly under the influence of inhomogeneity we know it is not Gaussian at all. Even in homogeneous turbulence the tails of the PDF are not expected to be Gaussian. However, statistical arguments based on the central limit theorem would suggest that decaying homogeneous turbulence ought to be close to Gaussian or at least evolve in that direction for most of the core portion of the PDF. Experiments (Tavoularis & Corrsin)[19] of homogeneous turbulent shear flows support the hypothesis that homogeneous turbulence (even when sheared) has a central core that is closely approximated by an elliptical Gaussian PDF (sometimes called a trivariate normal distribution).

4. Relaxation Collision Models

A more general form than the BGK model (Eq. C.12) for collisions is the linear relaxation model,

$$\frac{\partial f}{\partial t} = g(\mathbf{v}) - h(\mathbf{v}) f \qquad \text{(C.17)}$$

where $g(\mathbf{v}) > 0$ and $h(\mathbf{v}) > 0$ are some positive functions of the velocity (and possibly position and time as well). The positivity requirements keep the governing equation stable and the probability always greater than zero.

In addition, the model should conserve the total probability (or mass), so that $\int g(\mathbf{v}) d\mathbf{v} = \int h(\mathbf{v}) f d\mathbf{v}$, and it should not cause any mean flow to be created, implying $\int v'_n [g - hf] d\mathbf{v} = 0$. Finally the model should dissipate energy at the correct rate, $\int \frac{v'_n v'_n}{2} [hf - g] d\mathbf{v} = \varepsilon$.

One way to determine a suitable choice for the model functions is to insert a desired solution for the PDF function f and then derive the parameters from Eq. (C.17). In isotropic decaying turbulence there is evidence that the core of the PDF is very close to a Gaussian and retains this shape during the decay process (Yeung and Pope)[20]. If we assume the PDF equation (17) has a Gaussian solution,

$$f(\mathbf{v},t) = (\tfrac{4}{3}\pi K)^{-3/2} e^{-\frac{3v'_n v'_n}{4K}} \tag{C.18}$$

where $v'_n = v_n - u_n$ and u_n is the mean velocity, then taking the time derivative gives,

$$\tfrac{\partial f}{\partial t} = (\tfrac{4}{3}\pi K)^{-3/2} e^{-\frac{3v'_n v'_n}{4K}} (1 - \tfrac{v'_n v'_n}{2K}) \tfrac{3}{2} \tfrac{\varepsilon}{K} \tag{C.19}$$

Comparing with Eq. (C.17) suggests that a suitable choice for the model functions is $g(\mathbf{v}) = f^{eq}(\mathbf{v}) \tfrac{3\varepsilon}{2K}$ and $h(\mathbf{v}) = \tfrac{3\varepsilon}{2K} \tfrac{v'_n v'_n}{2K}$. Actually, these functions do not conserve momentum or dissipate energy at the correct rate. They must be generalized slightly to,

$$g(\mathbf{v}) = C_M \tfrac{3\varepsilon}{2K} (\tfrac{4}{3}\pi \hat{K})^{-3/2} e^{-\frac{3\hat{v}'_n \hat{v}'_n}{4\hat{K}}} \qquad h(\mathbf{v}) = C_M \tfrac{3\varepsilon}{2K} \tfrac{\tilde{v}'_n \tilde{v}'_n}{[2K + (u-\tilde{u})^2]} \tag{C.20}$$

where we expect $C_M \to 1$, $\hat{K} \to K$, $\hat{v}'_i \to \tilde{v}'_i \to v'_i$ when the PDF approaches a spherical Gaussian (Eq. (C.18)). Conservation of mass is already satisfied. Conservation of momentum implies a relationship exists between the hat and tilde velocities,

$$(\hat{u}_p - u_p)[2K + (u-\tilde{u})^2] = 2R_{ip}(u_i - \tilde{u}_i) + \int v'_p v'_i v'_i \, f d\mathbf{v} \tag{C.21}$$

This implies that either $\hat{u}_p$ or $\tilde{u}_p$ can be specified arbitrarily and then the other determined by Eq. (C.21). The two simplest choices are $\hat{u}_p = u_p$ which implies $\tilde{u}_i = u_i + \tfrac{R_{ip}^{-1}}{2} \int v'_p v'_n v'_n \, f d\mathbf{v}$, and $\tilde{u}_p = u_p$ which implies $\hat{u}_i = u_i + \tfrac{1}{2K} \int v'_i v'_n v'_n \, f d\mathbf{v}$. In either case, if the PDF is symmetric then the odd order integral is zero and $\tilde{u}_p = \hat{u}_p = u_p$. Since by definition $v_i = \hat{u}_i + \hat{v}'_i = \tilde{u}_i + \tilde{v}'_i = u_i + v'_i$, this also implies $\hat{v}'_i = \tilde{v}'_i = v'_i$ as well. Therefore the hat and tilde quantities in Eq. (C.20) can be viewed as a small perturbation imposed when the PDF is skewed (not symmetric), and are largely a formal technicality to enforce conservation of momentum.

Conservation of energy imposes a relation between C_M and $\hat{K}/K$ (Appendix J).

$$\begin{aligned} &[\tfrac{\hat{K}}{K} + \tfrac{1}{2K}(\hat{u}-u)^2 + \tfrac{1}{C_M}\tfrac{2}{3}][2K + (u-\tilde{u})^2] \\ &\quad = \tfrac{1}{2K} \int v'_p v'_p v'_i v'_i \, f d\mathbf{v} + \tfrac{(u_p - \tilde{u}_p)}{K} \int v'_p v'_i v'_i \, f d\mathbf{v} + (u-\tilde{u})^2 \end{aligned} \tag{C.22}$$

If f is symmetric this simplifies considerably to $\tfrac{\hat{K}}{K} + \tfrac{1}{C_M}\tfrac{2}{3} = \tfrac{1}{4K^2} \int v'_p v'_p v'_i v'_i \, f d\mathbf{v}$. If f is an elliptic Gaussian given by

$$f = [(2\pi)^3 \det(R_{nm})]^{-1/2} e^{-\frac{1}{2} R_{nm}^{-1} v'_n v'_m} \tag{C.23}$$

then the integral can be evaluated and is $4K^2 + 2R_{nm}R_{mn}$ (Appendix K). Then $\tfrac{\hat{K}}{K} = 1 + \tfrac{R_{nm}R_{mn}}{2K^2} - \tfrac{2}{3}\tfrac{1}{C_M}$ or perhaps even more informatively $\tfrac{3}{2} C_M = (1 + \tfrac{R_{nm}R_{mn}}{2K^2} - \tfrac{\hat{K}}{K})^{-1}$. The

relaxation model therefore has one free parameter (either C_M or $\hat{K}/K$). Both of these parameters should go to 1 when the turbulence is isotropic (i.e. when f is a spherical Gaussian). Since $\frac{R_{nn}R_{mn}}{2K^2} \to \frac{2}{3}$ in isotropic turbulence, forcing one of these conditions is sufficient to guarantee the other.

The derivation of the equivalent Reynolds stress equation is given in Appendix J. The result is that Eq. (C.20) is equivalent to

$$\frac{\partial R_{ij}}{\partial t} = -\frac{\varepsilon}{\left[1+\frac{R_{mn}R_{nm}}{2K^2}-\frac{\hat{K}}{K}\right]}\left(\frac{R_{ij}}{K}+\frac{R_{in}R_{nj}}{K^2}-\frac{2}{3}\frac{\hat{K}}{K}\delta_{ij}\right) \tag{C.24}$$

if an elliptic Gaussian is assumed for the PDF. Eq. (C.24) in turn implies the return parameters

$$C_R = \frac{\left[\frac{4}{3}-\frac{R_{mn}R_{nm}}{2K^2}+\frac{\hat{K}}{K}\right]}{\left[1+\frac{R_{mn}R_{nm}}{2K^2}-\frac{\hat{K}}{K}\right]} \quad \text{and} \quad C_N = \frac{-1}{\left[1+\frac{R_{mn}R_{nm}}{2K^2}-\frac{\hat{K}}{K}\right]} \tag{C.25}$$

or, in terms of C_M,

$$C_R = \tfrac{7}{2}C_M - 1 \qquad \text{and} \quad C_N = -\tfrac{3}{2}C_M \tag{C.26}$$

Note that this model, and the other models derived in this work, tend to imply that C_N is less than zero. In contrast, the widely used nonlinear model of Sarkar and Speziale[3] has a positive value for this constant. The implications of this difference are examined in detail in Section 8.

Various choices of C_M are possible. The simple choice $C_M = 1$ leads to $C_R = \frac{5}{2}$, and $C_N = -\frac{3}{2}$. These values produce a model which is very similar to the two models examined in detail below.

The equally simple choice $\frac{\hat{K}}{K} = 1$ implies

$$C_R = \tfrac{7}{3}\frac{2K^2}{R_{mn}R_{nm}} - 1 \quad \text{and} \quad C_N = -\frac{2K^2}{R_{mn}R_{nm}} \tag{C.27}$$

This choice of $\frac{\hat{K}}{K}$ implies the 'target' distribution has the same energy as the PDF but a spherical shape. The performance of this model is shown in Section 5 and is referred to as Model-1. The realizability condition, $C_R - C_N[\frac{R_{nk}R_{kn}}{2K^2} - \frac{4}{3}] = \frac{2K^2}{R_{mn}R_{nm}}$, indicates that Model-1 is weakly realizable.

In general the realizability condition for these relaxation models is $C_R - C_N[\frac{R_{nk}R_{kn}}{2K^2} - \frac{4}{3}] = \frac{\hat{K}}{K}/(1+\frac{R_{nm}R_{mn}}{2K^2}-\frac{\hat{K}}{K})$ so choices where $\frac{\hat{K}}{K}$ vanish in the 2-component limit will satisfy the strong realizability condition. The quantity $F = \det(R_{ij})/(\frac{2}{3}K)^3$ is 1 in isotropic turbulence and 0 in the two component limit. The choice $\frac{\hat{K}}{K} = F$ means that

$$C_R = \frac{\left[\frac{4}{3} - \frac{R_{mn}R_{nm}}{2K^2} + F\right]}{\left[1 + \frac{R_{mn}R_{nm}}{2K^2} - F\right]} \text{ and } C_N = \frac{-1}{\left[1 + \frac{R_{mn}R_{nm}}{2K^2} - F\right]} \tag{C.28}$$

The other strong realizability condition ($C_N \geq -\frac{2K^2}{R_{mn}R_{nn}}$ when F=0) is also satisfied by this model. Referred to as Model-F, the performance of this model is also shown in Section 5. This model has a target distribution that has less energy, and in this sense it is similar to the simple BGK model of Section 3. However, unlike the BGK model, this model has the spherical Gaussian as a solution, is strongly realizable, and does not produce a spike in the PDF in the 2-component limit. In addition, unlike the simple BGK model, the decay constant, h, now depends on the velocity, $\mathbf{v}$, and acts preferentially on the tails of the distribution, damping extreme events more strongly.

5. Model Performance

In this section the performance of these models is compared with experimental data for return to isotropy. For each test case, we present both the Reynolds stresses as a function of time and the Reynolds stress anisotropy as a function of time. The anisotropy is the standard method for looking at return-to-isotropy, since it eliminates much of the dependence on the dissipation. However, due to the nondimensionalization with respect to K the anisotropy can cause errors in one turbulence component (possibly even experimental errors) to appear as a general failure of the entire model. For this reason we retain the direct Reynolds stress decay plots as well.

In all models the dissipation is determined from the model transport equation

$$\frac{\partial \varepsilon}{\partial t} = -C_{\varepsilon 2}\frac{\varepsilon^2}{K} \tag{C.29}$$

The value of $C_{\varepsilon 2}$ is taken to be 11/6, which is the high Reynolds number analytical solution for turbulence with a low wavenumber k^2 spectrum[21]. In most of the experiments the initial value of the dissipation is not known, and is obtained by attempting to match the K profile as well as possible.

In each case, we have solved the Reynolds stress ODE associated with the model, using fourth order Runge-Kutta and very small time-steps. We have also solved the corresponding PDF relaxation models and obtained very similar results. However, there are further numerical issues associated with solving the PDF equations which we do not wish to address here, so we simple present the ODE results in this paper.

Because $C_{\varepsilon 2}$ and the return process are believed to be Reynolds number dependent we have selected only high Re number experiments for comparison and no DNS test cases. It must be noted that there is some uncertainty associated with the experimental results. First, while the geometry of these experiments changes abruptly from a straining section to a straight section, the actual cessation of the mean strain may not be quite so abrupt due to the long range effects of pressure. As a result, these decay experiments may have some residual straining in them at early times. The translation of the zero time in the Le Penven experiment, case III < 0, suggests that the experimenters were aware of this

problem. More importantly, the initial turbulence for these experiments has structure, due to the strains imposed to make the turbulence anisotropic. It is likely that at early times the relaxation of these structures also affects the return process.

Figures 2 and 3 are Le Penven et al cases III > 0 (expansion) and III < 0 (contraction). Figures 4, 5 and 6 are the data of Choi & Lumley[6] for their cases A (plane distortion), B (axisymmetric expansion) and C-2 (axisymmetric contraction) respectively.

Despite the fact that model-F is strongly realizable and Model-1 is not, the two models behave very similarly for all five experimental test cases. With the exception of Figure 3 (Le Penven, case III < 0) and Figure 6 (Choi & Lumley, case C-2) the models show poor agreement with the experimental data, and tend to return to isotropy too quickly.

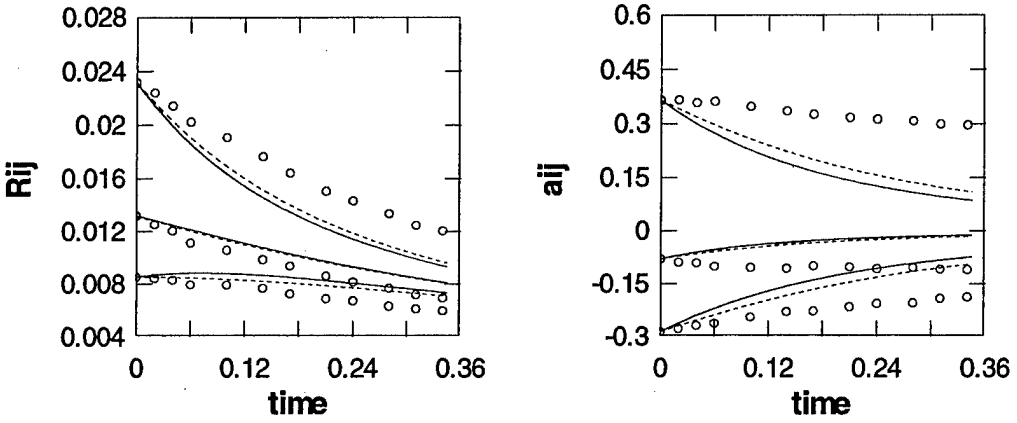

Figure 2: Reynolds Stresses and anisotropy for the case III > 0 from Le Penven, Gence and Comte-Bellot. Symbols are the experimental data, lines are the Model-1 predictions, and the dotted lines are the Model-F predictions.

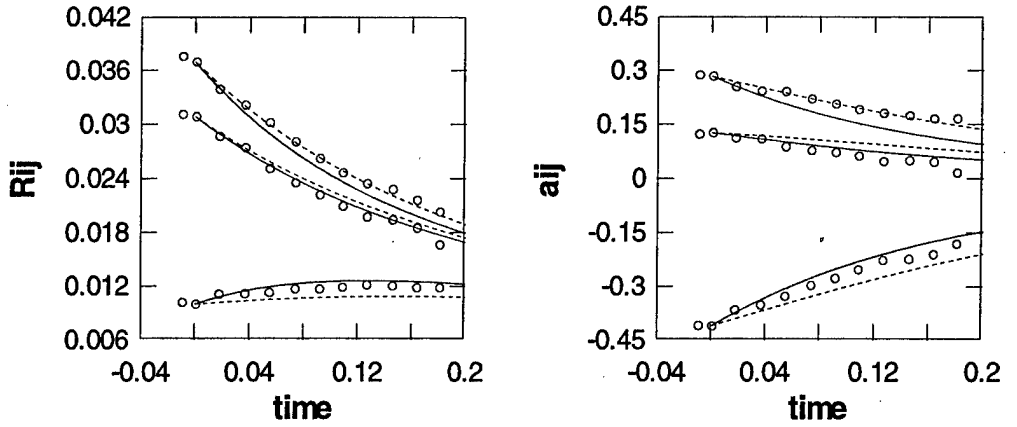

Figure 3: Reynolds Stresses and anisotropy for case III < 0 from Le Penven, Gence and Comte-Bellot. Symbols are the experimental data, lines are the Model-1 predictions, and the dotted lines are the Model-F predictions.

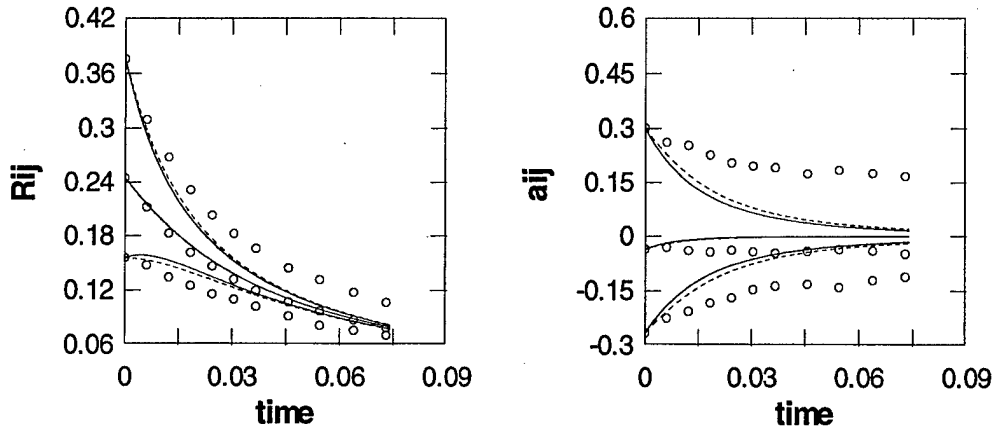

Figure 4: Reynolds Stresses and anisotropy for case A of Choi and Lumley. Symbols are the experimental data, lines are the Model-1 predictions, and the dotted lines are the Model-F predictions.

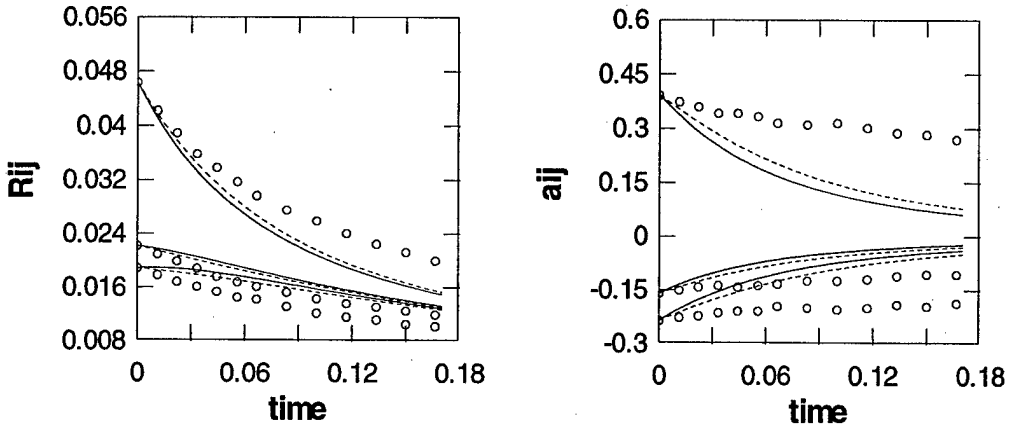

Figure 5: Reynolds Stresses and anisotropy for case B of Choi and Lumley. Symbols are the experimental data, lines are the Model-1 predictions, and the dotted lines are the Model-F predictions.

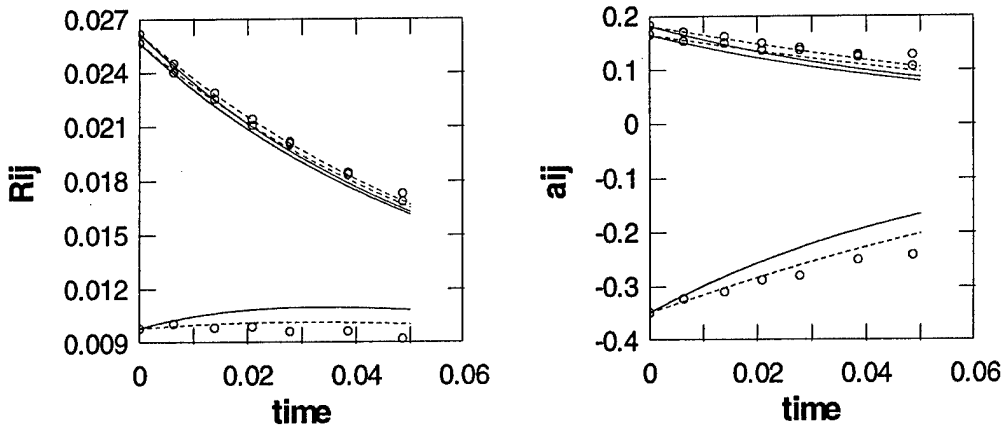

Figure 6: Reynolds Stresses and anisotropy for case C-2 of Choi and Lumley. Symbols are the experimental data, lines are the Model-1 predictions, and the dotted lines are the Model-F predictions.

6. General Relaxation Models

Rather than assuming a spherical Gaussian let us assume that the anisotropic ellipsoidal Gaussian (Eq. (C.23)) is a solution to the relaxation equation (Eq. (C.17)). Then

$$\frac{\partial f}{\partial t} = -\frac{1}{2} f \left(\frac{\frac{\partial}{\partial t}\det(R_{nm})}{\det(R_{nm})} + \frac{\partial R^{-1}_{nm}}{\partial t} v'_n v'_m \right) \tag{C.30}$$

Since $\frac{\partial R^{-1}_{ij}}{\partial t} = -R^{-1}_{im} \frac{\partial R_{mn}}{\partial t} R^{-1}_{nj}$ and $\frac{\partial}{\partial t}\det(R_{nm}) = \det(R_{nm}) \frac{\partial R_{ip}}{\partial t} R^{-1}_{pi}$ (Jacobi's formula) this reduces to

$$\frac{\partial f}{\partial t} = -\frac{1}{2} f \left(R^{-1}_{ij} - R^{-1}_{im} R^{-1}_{nj} v'_n v'_m \right) \frac{\partial R_{ij}}{\partial t} \tag{C.31}$$

Let us further assume that $\frac{\partial R_{ij}}{\partial t} = -\frac{\varepsilon}{2K} \left(\Pi_{im} R_{mj} + \Pi_{jm} R_{mi} \right)$ which is the general Reynolds stress transport model (Eq. (C.5)). Then

$$\frac{\partial f}{\partial t} = \frac{\varepsilon}{2K} f \left(\Pi_{ii} - \Pi_{in} R^{-1}_{im} v'_m v'_n \right) \tag{C.32}$$

This implies that for any desired Reynolds stress model, Π_{ij}, a corresponding relaxation model can be constructed,

$$g(\mathbf{v}) = C_M \Pi_{ii} \frac{\varepsilon}{2K} \frac{e^{-\frac{1}{2}\hat{R}^{-1}_{nm} \hat{v}'_n \hat{v}'_m}}{[(2\pi)^3 \det(\hat{R}_{nm})]^{1/2}}, \quad h(\mathbf{v}) = C_M \frac{\varepsilon}{2K} \frac{\Pi_{in} R^{-1}_{im} \tilde{v}'_m \tilde{v}'_n}{\left[1 + (u_n - \tilde{u}_n)(u_m - \tilde{u}_m) R^{-1}_{im} \frac{\Pi_{in}}{\Pi_{pp}} \right]} \tag{C.33}$$

When the PDF is an elliptic Gaussian we expect $C_M = 1$, $\tilde{v}'_n = \hat{v}'_n = v'_n$, and $\hat{R}_{nm} = R_{nm}$. The constant C_M can be a function of tilde and hat quantities (such as $\tilde{u}_p - u_p$ and

$\hat{u}_p - u_p$) but it can no longer be a function of the Reynolds stress invariants (like it was in the simpler spherical relaxation model). This is because the elliptic Gaussian PDF (unlike the spherical Gaussian PDF) can represent any state of the Reynolds stress invariants.

Note that the relaxation equation places constraints on the underlying Reynolds stress model. It implies that $\Pi_{ii} > 0$, and $\prod_{in} R_{im}^{-1}$ must be a positive definite tensor.

Conservation of probability (or mass) is already satisfied by this model. Conservation of momentum requires a relation between $\hat{u}_p$ and $\tilde{u}_p$ (see Appendix L).

$$\begin{aligned}(\hat{u}_p - u_p)\left[1 + (u_n - \tilde{u}_n)(u_m - \tilde{u}_m)R_{im}^{-1}\frac{\Pi_{in}}{\Pi_{pp}}\right] \\ = \frac{\Pi_{in}}{\Pi_{ii}} R_{im}^{-1}\left\{\int v'_p v'_m v'_n f d\mathbf{v} + R_{np}(u_m - \tilde{u}_m) + R_{mp}(u_n - \tilde{u}_n)\right\}\end{aligned} \tag{C.34}$$

The simplest choice is $\tilde{u}_p = u_p$ then

$$\hat{u}_p = u_p + \frac{\Pi_{in}}{\Pi_{ii}} R_{im}^{-1} \int v'_p v'_m v'_n f d\mathbf{v} \tag{C.35}$$

The choice $\hat{u}_p = u_p$ is more complicated and requires a symmetric matrix inversion $(\prod_{ip} R_{in}^{-1} + \prod_{in} R_{ip}^{-1})(\tilde{u}_n - u_n) = \prod_{in} R_{im}^{-1} R_{tp}^{-1} \int v'_t v'_m v'_n f d\mathbf{v}$. For certain models (like the one shown below), this matrix problem is easy to invert analytically, and this choice is also viable.

The Reynolds stress transport equation is derived in Appendix M. Assuming the choice $\tilde{u}_p = u_p$ it requires that,

$$\hat{R}_{ij} = \frac{\Pi_{pn}}{\Pi_{ss}} R_{pm}^{-1} \int v'_m v'_n v'_i v'_j f d\mathbf{v} - \frac{1}{C_M}\left(\frac{\Pi_{im}}{\Pi_{ss}} R_{mj} + \frac{\Pi_{jm}}{\Pi_{ss}} R_{mi}\right) - (\hat{u}_i - u_i)(\hat{u}_j - u_j) \tag{C.36}$$

If the PDF is an ellipsoidal Gaussian then $\hat{u}_p = u_p$ (by Eq. (C.35)), and $C_M = 1$ (by definition). In addition, since

$$\int v'_m v'_n v'_i v'_j f d\mathbf{v} = R_{mn}R_{ij} + R_{mi}R_{nj} + R_{mj}R_{ni} \tag{C.37}$$

Eq. (C.36) gives the correct limit, $\hat{R}_{ij} = R_{ij}$ for an elliptic Gaussian PDF. The hat and tilde quantities can be seen to be slight perturbations to the standard quantities that precisely account for any deviation of the PDF from an elliptic Gaussian shape.

The model given by Eqs. (C.33)-(C.36) represents the general relaxation model. Using this formulation, any Reynolds stress transport model can also be implemented as a PDF relaxation model, that has the elliptic Gaussian as a solution. Remember that $\Pi_{ij} = \delta_{ij}$ corresponds to the case of no return-to-isotropy, and $\Pi_{ij} = \delta_{ij} + C_R(\delta_{ij} - \frac{2}{3} K R_{ij}^{-1})$ is the

classic linear return-to-isotropy model. Substituting these expressions into Eqs. (33)-(36) will produce the corresponding PDF relaxation model. However, in this paper, we do not wish to specify Π_{ij}, but to determine what the general relaxation model (Eqs. (33)-(36)) imply about how it should be specified.

The general relaxation model as described above has singular h, $\hat{u}_p$, and $\hat{R}_{ij}$ in the two-component limit due to the presence of R_{ij}^{-1}. This singularity is removed by the parameter-free Reynolds stress model $\Pi_{ij} = \frac{2K}{R_{nm}R_{mn}} R_{ij}$. Making Π_{ij} directly proportional to the Reynolds stress tensor removes the singularities. The constant of proportionality is determined from the decay condition $\Pi_{ij}R_{ij} = 2K$ (see Section 2). In the relaxation context this model is given by

$$g = C_M \frac{\varepsilon}{K} \frac{2K^2}{R_{nm}R_{mn}} \frac{e^{-\frac{1}{2}\hat{R}^{-1}_{nm}\hat{v}'_n\hat{v}'_m}}{[(2\pi)^3 \det(\hat{R}_{nm})]^{1/2}} \qquad h = C_M \frac{\varepsilon}{K} \frac{2K^2}{R_{nm}R_{mn}} \frac{\tilde{v}'_n\tilde{v}'_n}{[2K+(u-\tilde{u})^2]} \tag{C.38}$$

where

$$(\hat{u}_p - u_p)[2K + (u-\tilde{u})^2] = 2R_{ip}(u_i - \tilde{u}_i) + \int v'_p v'_i v'_i \, f d\mathbf{v} \tag{C.39}$$

Note that Eq. (C.39) is a particular case of the general Eq. (C.34) (for this Π_{ij} model). It also happens to be identical to Eq. (C.21), the general expression for the spherical relaxation models in Section 4. As in Section 4, the choice of $\hat{u}_p = u_p$ or $\tilde{u}_p = u_p$ is up to the user. For symmetric PDFs if makes no difference what the choice is, since then $\hat{u}_p = \tilde{u}_p = u_p$. For inhomogeneous flows, the PDFs will be skewed and this choice may make some difference.

For this model we also require the condition on $\hat{R}_{ij}$ that,

$$\begin{aligned}\left[\hat{R}_{ij} + (\hat{u}_i - u_i)(\hat{u}_j - u_j) + \tfrac{1}{C_M}\tfrac{R_{im}R_{mj}}{K}\right]\left[2K + (u-\tilde{u})^2\right] \\ = \int v'_n v'_n v'_i v'_j f d\mathbf{v} + (u_n - \tilde{u}_n)\int v'_n v'_i v'_j f d\mathbf{v} + R_{ij}(u-\tilde{u})^2\end{aligned} \tag{C.40}$$

This model (Eqs. (C.38)-(C.40)) differs from those in Section 4 in that it has the ellipsoidal Gaussian as a solution.

The choices for C_M are now far more restrictive. The simplest choice is simply to set $C_M = 1$. Eqs. (C.40) and (C.39) are simplified considerably by choosing $\tilde{u}_p = u_p$. Then the hat quantities are defined by $\hat{u}_p = u_p + \frac{1}{2K}\int v'_p v'_i v'_i \, f d\mathbf{v}$ and $\hat{R}_{ij} = \frac{1}{2K}\int v'_n v'_n v'_i v'_j f d\mathbf{v} - (\hat{u}_i - u_i)(\hat{u}_j - u_j) - \frac{1}{C_M}\frac{R_{im}R_{mj}}{K}$.

The equivalent Reynolds stress transport model can be derived from this relaxation model by assuming the PDF is an elliptic Gaussian. Under this assumption, the various possible choices of the hat and tilde quantities are irrelevant and we find that all these choices are equivalent to,

$$\frac{\partial R_{ij}}{\partial t} = -2\varepsilon \frac{R_{is}R_{sj}}{R_{mn}R_{nm}} \tag{41}$$

which implies the model parameters are,

$$C_R = \frac{4}{3}\frac{2K^2}{R_{mn}R_{nm}} - 1 \text{ and } C_N = -\frac{2K^2}{R_{mn}R_{nm}} \tag{42}$$

We note that this model satisfies the strong realizability constraint, $C_R - C_N[\frac{R_{nk}R_{kn}}{2K^2} - \frac{4}{3}] = 0$, and sits on the cusp of the strong realizability condition $C_N \geq -\frac{2K^2}{R_{mn}R_{nm}}$. In the 2-component limit, this model returns to isotropy as slowly as physically possible. The performance of this model is shown below and it is referred to as Model-EG (for elliptic Gaussian). The fact that the resulting Reynolds stress model is very simple, entirely nonlinear, contains no model parameters, and satisfies strong realizability at its cusp, makes Model-EG very intriguing.

In Figures 7 through 11 the performance of Model-EG is compared with experimental data for return-to-isotropy, the classic linear Rotta model (with $C_R = 0.8$), and the nonlinear model of Sarkar and Speziale ($C_R = 0.7$, $C_N = 1.05$). The most interesting result is that these three very different models perform very similarly for all five test cases. The Sarkar and Speziale is slightly better than the other two, but it has two adjustable model constants that were tuned to exactly these test cases. The linear Rotta model also performs surprisingly well. It can be made even better by adjusting the standard value (0.8) downwards (to 0.7 or 0.6). Model-EG matches the data the least well, but gives quite good agreement considering there are no adjustable parameters in this model.

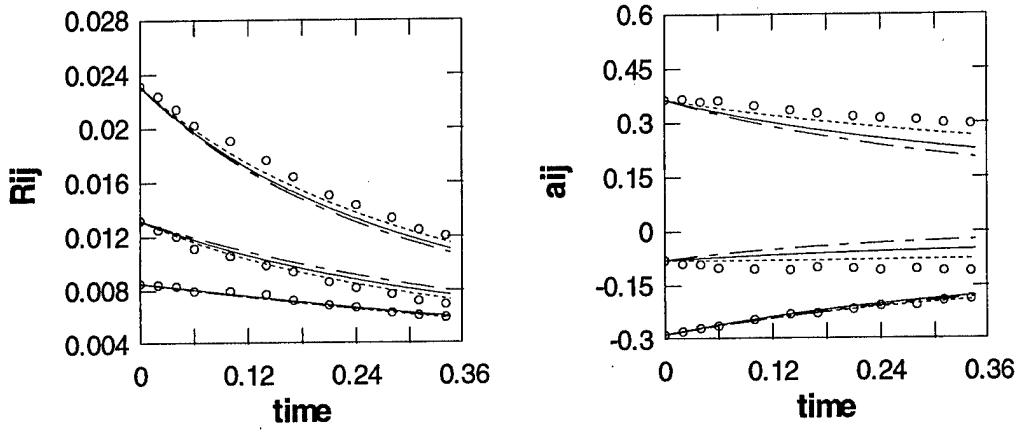

Figure 7: Reynolds Stresses and anisotropy for the case III > 0 from Le Penven, Gence and Comte-Bellot. Symbols are the experimental data, lines are the Rotta Model predictions (C_R = 0.8), the dotted lines are the SS Model predictions, and dashed lines are

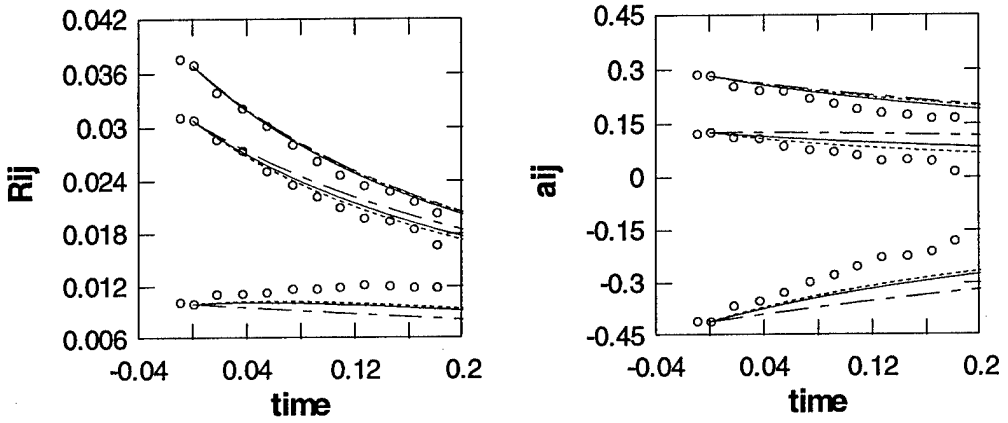

Figure 8: Reynolds Stresses and anisotropy for case III < 0 from Le Penven, Gence and Comte-Bellot. Symbols are the experimental data, lines are the Rotta Model predictions ($C_R = 0.8$), the dotted lines are the SS Model predictions, and dashed lines are the Model-EG predictions.

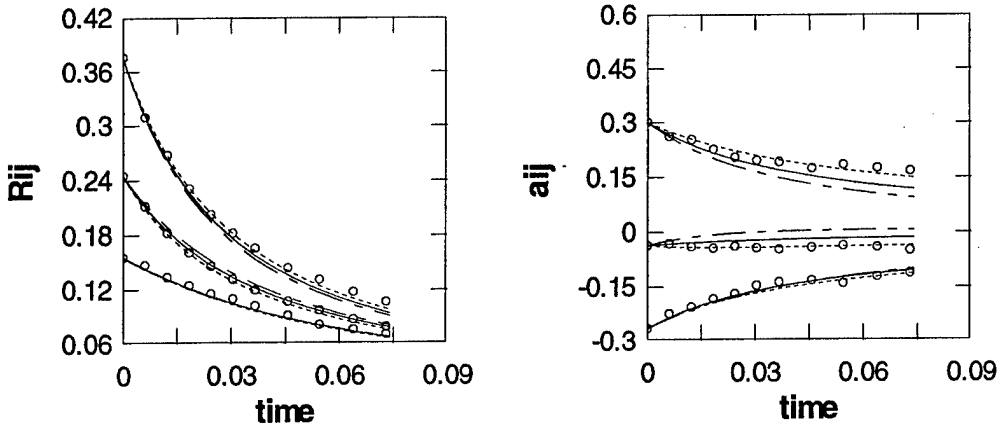

Figure 9: Reynolds Stresses and anisotropy for case A of Choi and Lumley. Symbols are the experimental data, lines are the Rotta Model predictions (C_R = 0.8), the dotted lines are the SS Model predictions, and dashed lines are the Model-EG predictions.

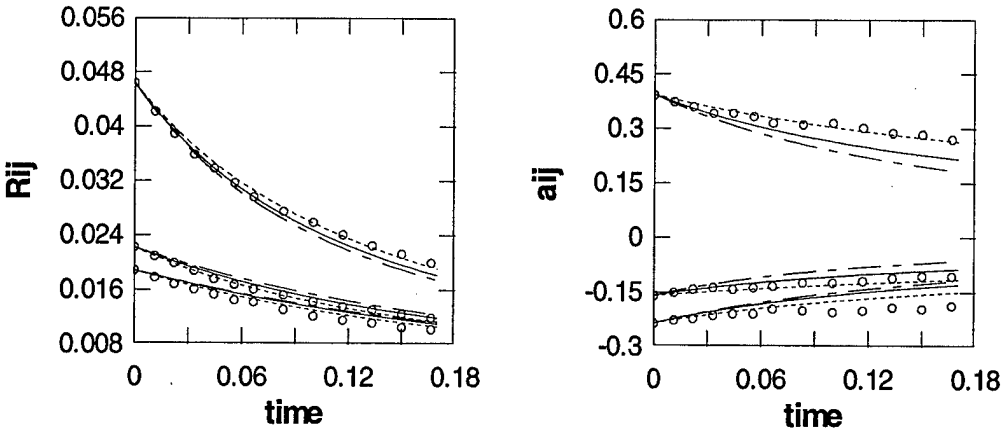

Figure 10: Reynolds Stresses and anisotropy for case B of Choi and Lumley. Symbols are the experimental data, lines are the Rotta Model predictions (C_R = 0.8), the dotted lines are the SS Model predictions, and dashed lines are the Model-EG predictions.

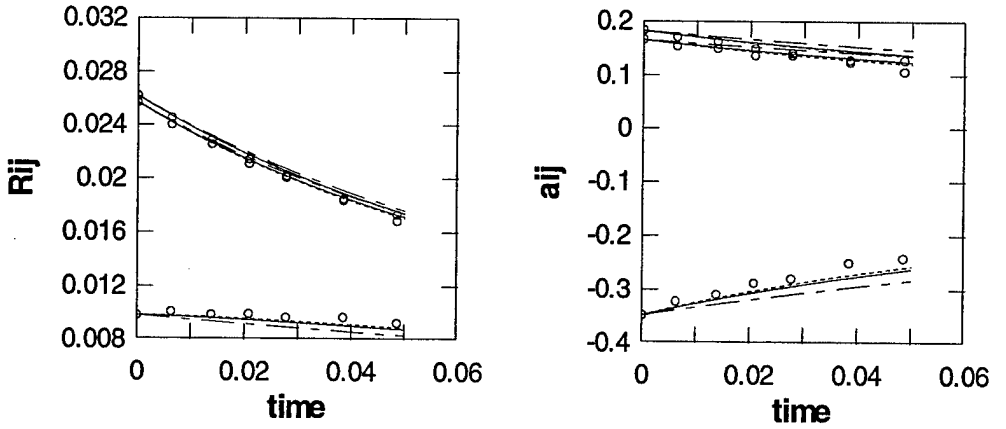

Figure 11: Reynolds Stresses and anisotropy for case C-2 of Choi and Lumley. Symbols are the experimental data, lines are the Rotta Model predictions (C_R = 0.8), the dotted lines are the SS Model predictions, and dashed lines are the Model-EG predictions.

As noted earlier, the greatest uncertainty in both the models and the experiments lies in the initial conditions. To see that the assessment of the models performance is not affected by these initial conditions Figure 8 was recalculated using a later time for initialization. Figure 12 shows that the point of initialization does not fundamentally change the results.

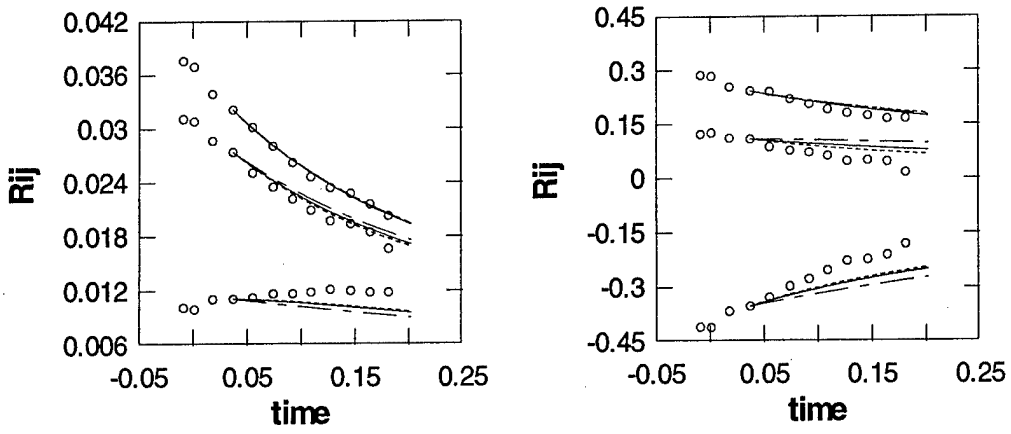

Figure 12: Reynolds Stresses and anisotropy for the case III < 0 from Le Penven, Gence and Comte-Bellot, initialized at 0.037 seconds. Symbols are the experimental data, lines are the Rotta Model predictions (C_R = 0.8), the dotted lines are the SS Model predictions, and dashed lines are the Model-EG predictions.

We conclude this section by noting that other return models have been proposed that are nonlinear, that parameterize C_R and C_N as functions of the Reynolds stress invariants (or anisotropy invariants), and which satisfy strong realizability[6,16]. However, these models assume that C_R and C_N are polynomial functions of the invariants. In contrast, the model described above uses linear *rational* polynomial functions of the invariants to represent the return parameters C_R and C_N. We note that rational polynomials tend to have better fitting properties than polynomials, and that the formulated rational polynomials are the result of physical assumptions not assumptions about functional behavior.

7. Fokker-Planck Collision Models

An alternative to relaxation models is the Fokker-Planck collision model. This model is frequently used to model Brownian motion, liquid collisions, and some plasmas. Langevin models for turbulence[18,22], are directly related to the Fokker-Planck equation and therefore effectively use this type of model. A generalized Fokker-Planck collision operator involves two as yet unspecified matrices, G_{ij} and H_{ij}.

$$-\frac{\partial f}{\partial t} = -\frac{\partial (G_{ij} v'_j f)}{\partial V_i} + \frac{\partial}{\partial V_i}\left[H_{ij} \frac{\partial f}{\partial V_j} \right] \qquad \text{(C.43)}$$

The tensor H_{ij} should be positive definite for stability reasons. In Langevin models it is convenient to make H_{ij} isotropic as well. However, in general the Fokker-Planck collision model has considerable flexibility in the choice of both the model tensors. The model automatically satisfies conservation of probability and momentum. It also has the ellipsoidal Gaussian as a solution[23]. Multiplying equation (C.43) by $v'_n v'_m$ and

integrating over all velocity space gives the equivalent Reynolds stress transport equation.

$$\frac{\partial R_{nm}}{\partial t} = G_{mj}R_{jn} + G_{nj}R_{jm} + H_{mn} + H_{nm} \tag{C.44}$$

By comparing this with the generic Reynolds stress transport equation, (Eq. (C.5)) it can be seen that,

$$G_{ij} + H_{im}R_{mj}^{-1} = -\frac{\varepsilon}{2K}\Pi_{ij} \tag{C.45}$$

In this way, classic return models (given in terms of Π_{ij}) can be implemented in the generalized Fokker-Planck context. This transformation is also discussed in Pope[18]. The general nonlinear Reynolds stress return model (Eq. (C.8)) is equivalent to

$$\Pi_{ij} = \delta_{ij} + \left\{C_R + C_N[\tfrac{4}{3} - \tfrac{R_{nk}R_{kn}}{2K^2}]\right\}(\delta_{ij} - \tfrac{2}{3}KR_{ij}^{-1}) - C_N\left(\frac{R_{ij}}{K} - \frac{R_{nk}R_{kn}}{2K^2}\delta_{ij}\right) \tag{C.46}$$

In the Fokker-Planck context this implies that

$$G_{ij} + H_{im}R_{mj}^{-1} = -\frac{\varepsilon}{2K}\left[\delta_{ij} + \left\{C_R + C_N[\tfrac{4}{3} - \tfrac{R_{nk}R_{kn}}{2K^2}]\right\}(\delta_{ij} - \tfrac{2}{3}KR_{ij}^{-1}) - C_N\left(\frac{R_{ij}}{K} - \frac{R_{nk}R_{kn}}{2K^2}\delta_{ij}\right)\right] \tag{C.47}$$

There are many possible choices of G_{ij} and H_{ij} which satisfy this constraint.

The simplest and most numerically attractive choice for H_{ij} is that this tensor is isotropic, $H_{ij} = C_D\varepsilon\delta_{ij}$ where C_D is an arbitrary model constant. This means that

$$G_{ij} = -\frac{\varepsilon}{2K}\left[(1 + C_R + \tfrac{4}{3}C_N)\delta_{ij} - C_N\frac{R_{ij}}{K}\right] + \frac{\varepsilon}{3}(C_R + C_N[\tfrac{4}{3} - \tfrac{R_{nk}R_{kn}}{2K^2}] - 3C_D)R_{ij}^{-1} \tag{C.48}$$

The singularity in G_{ij} is removed by the particular choice $3C_D = C_R + C_N[\tfrac{4}{3} - \tfrac{R_{nk}R_{kn}}{2K^2}]$, which is the choice used in most Langevin turbulence models. This gives the following model constants,

$$H_{ij} = \left[C_R + C_N(\tfrac{4}{3} - \tfrac{R_{nk}R_{kn}}{2K^2})\right]\frac{\varepsilon}{3}\delta_{ij} \quad \text{and} \quad G_{ij} = -\frac{\varepsilon}{2K}\left[(1 + C_R)\delta_{ij} + C_N(\tfrac{4}{3}\delta_{ij} - \frac{R_{ij}}{K})\right] \tag{C.49}$$

Note that with this choice the realizability constraint $C_R + C_N[\tfrac{4}{3} - \tfrac{R_{nk}R_{kn}}{2K^2}] \geq 0$ is equivalent to the requirement that H_{ij} be positive definite. Under these circumstances, the classic linear return model (with $C_N = 0$) is obtained using $G_{ij} = -\frac{\varepsilon}{2K}(1 + C_R)\delta_{ij}$ and $H_{im} = \frac{\varepsilon}{3}C_R\delta_{im}$. Model-1 given in Section 4 (with $C_R = \frac{7}{3}\frac{2K^2}{R_{nk}R_{kn}} - 1$ and $C_N = -\frac{2K^2}{R_{nk}R_{kn}}$), is obtained using $H_{ij} = \left(\frac{2K^2}{R_{nk}R_{kn}}\right)\frac{\varepsilon}{3}\delta_{ij}$ and $G_{ij} = -\frac{\varepsilon}{2K}(\frac{2K^2}{R_{nk}R_{kn}})\left[\delta_{ij} + \frac{R_{ij}}{K}\right]$. Model-F (with

$C_R = \frac{\left[\frac{4}{3}\frac{R_{mn}R_{nm}}{2K^2}+F\right]}{\left[1+\frac{R_{mn}R_{nm}}{2K^2}-F\right]}$ and $C_N = \frac{-1}{\left[1+\frac{R_{mn}R_{nm}}{2K^2}-F\right]}$), is obtained using $H_{ij} = \frac{\varepsilon}{3}\delta_{ij}F/\left[1+\frac{R_{mn}R_{nm}}{2K^2}-F\right]$ and $G_{ij} = -\frac{\varepsilon}{2K}\left[\delta_{ij}+\frac{R_{ij}}{K}\right]/\left[1+\frac{R_{mn}R_{nm}}{2K^2}-F\right]$. Note that in the 2-component limit H_{ij} now goes to zero. This particular splitting (Eq. (7.7)) will be unstable in this limit. Model-EG (with $C_R = \frac{4}{3}\frac{2K^2}{R_{mn}R_{nm}}-1$ and $C_N = -\frac{2K^2}{R_{mn}R_{nm}}$) is obtained using $H_{ij} = 0$ and $G_{ij} = -\frac{\varepsilon}{2K}\left(\frac{2K^2}{R_{mn}R_{nm}}\right)\frac{R_{ij}}{K}$. This model is therefore incompatible with this splitting (unstable). If H_{ij} is assumed to be isotropic (and non-zero), then G_{ij} must become singular in the 2-component limit.

A more general splitting is possible if H_{ij} is allowed to be anisotropic. Classic Langevin models require isotropic H_{ij}, but the Fokker-Planck model itself only requires H_{ij} to be positive definite. Assuming a positive definite form, $H_{ij} = C_D\varepsilon\delta_{ij} + C_E\frac{\varepsilon}{K}R_{ij}$ implies

$$G_{ij} = -\frac{\varepsilon}{2K}(1+C_R+\tfrac{4}{3}C_N+2C_E)\delta_{ij} + (C_S-3C_D)\tfrac{\varepsilon}{3}R_{ij}^{-1} + C_N\frac{\varepsilon}{2K^2}R_{ij} \qquad \text{(C.50)}$$

where $C_S = C_R + C_N(\frac{4}{3}-\frac{R_{nk}R_{kn}}{2K^2})$. Again, to remove the near singularity $C_D = \frac{1}{3}C_S$ can be chosen, but because of the more general form for H_{ij} the (realizability) restriction $C_S \geq 0$ is no longer required for a well posed model. The classic linear return model is obtained using $G_{ij} = -\frac{\varepsilon}{2K}(1+C_R+2C_E)\delta_{ij}$ and $H_{im} = \frac{\varepsilon}{3}C_R\delta_{im} + C_E\frac{\varepsilon}{K}R_{ij}$. Note that this splitting has an extra free parameter C_E which does not change the Reynolds stress evolution, but does change the model. A nonsingular splitting for Model-EG (with $C_R = \frac{4}{3}\frac{2K^2}{R_{nk}R_{kn}}-1$ and $C_N = -\frac{2K^2}{R_{nk}R_{kn}}$) is now given by $G_{ij} = -\frac{\varepsilon}{R_{nk}R_{kn}}R_{ij} - \frac{\varepsilon}{K}C_E\delta_{ij}$ and $H_{ij} = \frac{\varepsilon}{K}C_E R_{ij}$, where C_E is again an arbitrary parameter. Note that C_E can actually be determined by a dispersion analysis and is related to the Kolmorgorov constant.

8. Discussion

The return-to-isotropy problem of anisotropic turbulence has been studied via three very different collision models for the evolution of the velocity PDF. The simplest collision operator is the BGK approximation to the Boltzmann collision integral. This collision model, $-\frac{\varepsilon}{k}C_{BGK}(f-f^{eq})$, is characterized by an inverse timescale (which does not depend on the velocity). It was shown that if this model is to dissipate energy correctly, the target state must have considerably less energy than the current PDF state. Some models even use a target state with zero energy (a delta function). The BGK model produces the classic linear return-to-isotropy model, with the rate of return $C_R = \frac{1}{(K/\hat{K}-1)}$ determined by the energy of the target state. The Gaussian PDF is not a solution of the BGK model even though theoretical and experimental evidence might suggest that this is desirable.

To overcome the limitations of the BGK model, more general relaxation models were constructed in which the collision operator $g(v)-h(v)f$ has a positive-definite velocity dependent source term and a velocity dependent sink term that is proportional to the PDF. Previous analysis of this collision model in the context of turbulence is unknown to the authors. In Section 4 prescriptions for the model parameters g and h were derived such that the spherical Gaussian is a solution to the evolution equation. Two models were derived from this analysis, Model-1 assumed that the target distribution has the same energy as the PDF, $\frac{\hat{K}}{K}=1$. It is only weakly realizable. Model-F assumed that the target distribution has less energy than the PDF in the ratio $\frac{\hat{K}}{K}=F$. This ratio was chosen because it makes the resulting model strongly realizable. While these models

While these initial parameter-free relaxation models did not perform as well as might be hoped, they set the stage for the development of Model-EG. This model was shown to be the only nonsingular relaxation model that has the elliptic Gaussian as a solution. The equivalent Reynolds stress transport model is totally nonlinear in the Reynolds stresses and was shown to be strongly realizable. Interestingly, the performance of Model-EG is quite similar to the linear return to isotropy model. Even the Sarkar and Speziale model with an opposite sign for the nonlinear term, C_N, performs similarly.

To investigate these models further, their trajectories on the anisotropy invariant map were plotted, and are presented in Figure 13. It is well known that the linear Rotta model has linear trajectories when plotted on this anisotropy invariant map. The trajectories of the model of Sarkar and Speziale tend to move downwards and from left to right on this map. This means that turbulence with two large Reynolds stresses and one small stress will tend to first approach a state with only one large stress before approaching full isotropy. This implies that the intermediate stress decays faster than the maximum and minimum stresses, and is somewhat counter intuitive. The models developed in this paper tend to have the opposite behavior. Turbulence with one large stress will first decay to a state with two large stresses before approaching total isotropy. There is no experimental data in the middle of the triangle that allows us to determine which behavior is actually correct.

The top boundary of the 'triangle' is the 2-component line. The strongly realizable models have trajectories that stay on this line and move to the left if they start on the 2-component line. This means that if one component of the turbulence is zero it stays zero for all time, and the two non-zero stresses approach each other (mutual isotropy). This is the expected behavior for two-dimensional turbulence, which is sometimes (but by no means always) found when the turbulence is two-component. More information about the turbulence (than the Reynolds stress) is clearly necessary to make return models behave correctly in the 2-component limit. Strong realizability seems appropriate when the 2-component turbulence is also two dimensional, and weak realizability seems appropriate otherwise.

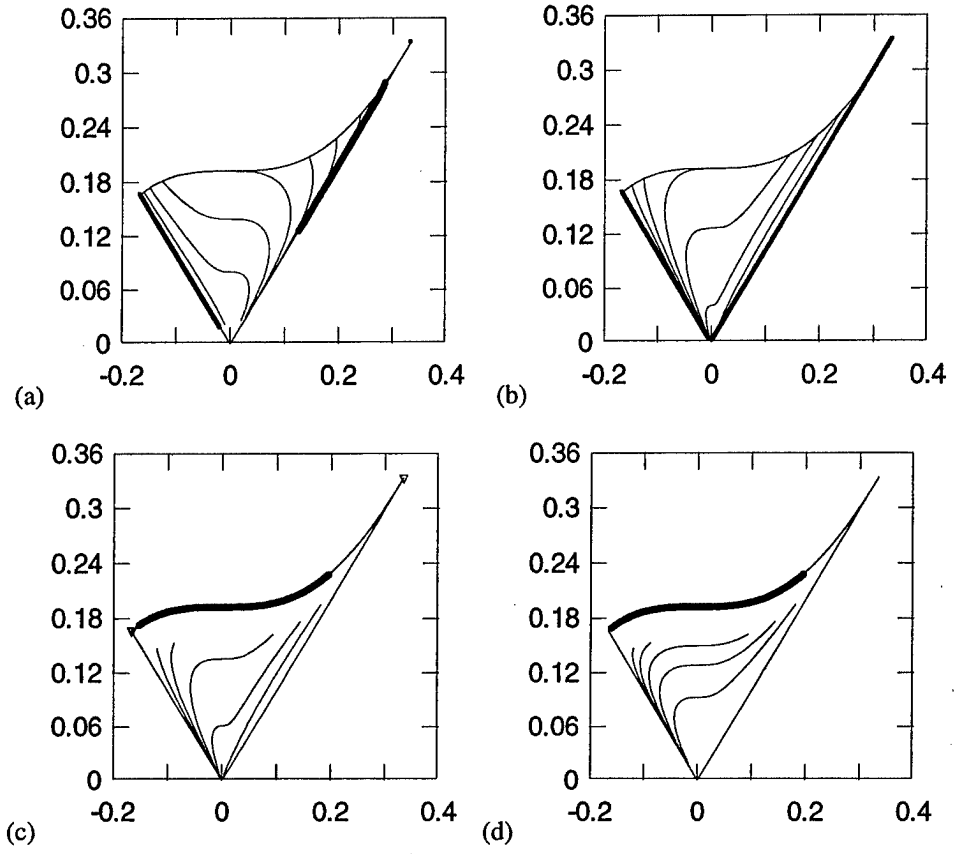

Figure 13: Invariant triangle. (a) Sarkar and Speziale, (b) Model-1, (c) Model-F, (d) Model-EG.

Finally, the relationship between the relaxation models and the Fokker-Planck collision model ($-\frac{\partial(G_{ij}v'_j f)}{\partial V_i}+\frac{\partial}{\partial V_i}H_{ij}\frac{\partial f}{\partial V_j}$) was investigated. Like the general relaxation model (Section 6) the Fokker-Planck model has the ellipsoidal Gaussian as a solution. Because it involves derivatives in velocity space, the Fokker-Planck model is more difficult to implement numerically than relaxation models. However, the Fokker-Planck model (with isotropic H_{ij}) has a direct correspondence with the Langevin models. Examination of Model-EG in this context showed that this model can not be implemented with isotropic H_{ij}. Instead, the diffusion coefficient H_{ij} must be proportional to R_{ij}.

It is not entirely clear that high Reynolds number decaying anisotropic turbulence should retain exactly an ellipsoidal Gaussian distribution during the return process. Nevertheless the assumption of ellipsoidal Gaussian evolution is probably a very good starting point that applies everywhere but the PDF tails. It has lead to the development of a novel parameter free return-to-isotropy model with interesting properties, and reasonable agreement with the data.

Acknowledgments

We gratefully acknowledge the financial support of this work by the Office of Naval Research (grant number N00014-01-1-0483) under the supervision of Ron Joslin.

References

1. J. Rotta, "Stastische theorie nichthomegener turbulenz I," Z. für Physik **129**, 547-572 (1951).
2. J. L. Lumley, "Computation modeling of turbulent flows", Advances in Applied Mechanics **18**, 126-176. (1978).
3. S. Sarkar and C. G. Speziale, "A Simple Nonlinear Model for the Return to Isotropy inn Turbulence," Physics of Fluids, Vol. A2, No. 1, pp. 84-93 (1990).
4. D. C. Haworth, and S. B. Pope, "A Generalized Langevin Model for Turbulent Flows," Physics of Fluids, Vol. 29, No. 2, (1986).
5. K. S. Choi and J. L. Lumley, "Turbulence and Chaotic Phenomena in Fluids," *Proceedings of the IUTAM Symposium* (Kyoto, Japan), edited by T. Tatsumi, North-Holland, Amsterdam, p. 267, (1984).
6. K. S. Choi and J. L. Lumley, "The return to isotropy of homogeneous turbulence," J. Fluid Mech., Vol. 436, pp 57-84 (2001).
7. T. J. Craft and B. E. Launder, "Computation of Impinging Flows Using Second-Moment Closure," *Proceedings of the Eighth Symposium on Turbulent Shear Flows*, Technical University of Munich, Munich, Germany, pp. 8-5-1 – 8-5-6 (1991).
8. M. Yamamoto and C. Arakawa, "Study on the Pressure-Strain Term in Reynolds Stress models." *Proceedings of the Eighth Symposium on Turbulent Shear Flows*, Technical University of Munich, Munich, Germany, pp. III-17-1 – III-17-2 (1991).
9. C. G. Speziale, S. Sarkar and T. B. Gatski, "Modeling the pressure-strain correlation of turbulence: an invariant dynamical systems approach," J. Fluid Mech., Vol. 227, pp 245-272 (1991)
10. P. Degond and M. Lemou, "Toward a Kinetic Model of Turbulent Incompressible Fluids," Université Paul Sabatier, (2000).
11. P. Bhatnagar, E. P. Gross, and M. K. Krook, Phys. Rev. **94**, 511 (1954)
12. M. Hallbäck, J. Groth & A. V. Johansson, "An algebraic model for nonisotropic turbulent dissipation rate in Reynolds stress closures," Phys. Fluids, **2** (10, 1859-1866, (1990).
13. J. B. Perot and P. Moin, "A Near Wall Model for the Dissipation Tensor," Eleventh Australasian Fluid Mechanics Conference, Hobart, Tasmania, Australia, 13-18 (1992).
14. P. A. Durbin & B. A. Pettersson Reif , *Statistical Theory and Modeling for Turbulent Flows*. Wiley & Sons, 2001.
15. B. E. Launder, G. J. Reece & W. Rodi, "Progress in the development of a Reynolds stress turbulence closure", J. Fluid Mech. **68**, 537-566 (1975).
16. T. Sjögren and A. V. Johansson, "Development and calibration of algebraic nonlinear models for terms in the Reynolds stress transport equation," Phys. Fluids **12**, 1554-1572 (2000).

17. U. Schumann, "Realizability of Reynolds Stress Turbulence Models," Physics of Fluids, Vol. 20, pp. 721-725, (1977)
18. S. B. Pope, *Turbulent Flows*, Cambridge University Press, 2000.
19. S. Tavoularis and S. Corrsin, "Experiments in nearly homogeneous turbulent shear flow with a uniform mean temperature gradient. Part1," J. Fluid Mech. **104**, 311-347 (1981).
20. P. K. Yeung and S. B. Pope, "Lagrangian statistics from direct numerical simulations of isotropic turbulence," J. Fluid Mech., **207**, 531-586 (1989)
21. P. G. Saffman, "Note on decay of homogeneous turbulence," Physics of fluids **10**, 1349, (1967).
22. J. P. Laval, B. Dubrulle and J. C. McWilliams, "Langevin Models of Turbulence: Renormalization Group, Distant Interaction Algorithms or Rapid Distortion Theory?," Physics of Fluids, Vol. 15, No. 5 (2003)
23. C. Chartrand, "Eddy collision models for turbulence," Masters Thesis, University of Massachusetts, Amherst, (2003).

Appendix D: Fast Pressure-Strain Modeling

The pressure strain is an important term in turbulence modeling. We are modeling the two pressure related terms (pressure-strain and pressure-transport) together as a pressure-gradient velocity correlation given by Π_{ij}.

$$\Pi_{ij} = -\overline{p'(\frac{\partial u_i'}{\partial x_j} + \frac{\partial u_j'}{\partial x_i})} - \frac{\partial(\overline{p'u_i'})}{\partial x_j} - \frac{\partial(\overline{p'u_j'})}{\partial x_i} = \pi_{ij} - (\frac{\partial T_i^p}{\partial x_j} + \frac{\partial T_j^p}{\partial x_i}) \quad \text{(D.1)}$$

In the standard approach, Π_{ij} is modeled as rapid and slow pressure strain separately.

Analysis(cf. Chou 1945) shows that in homogenous turbulence the rapid pressure term in the Reynolds stress equations is given by,

$$\Pi_{ij} = 2\frac{\partial \overline{u_p}}{\partial x_q} M_{ijpq}$$

where M is the fourth rank tensor given by,

$$M_{ijpq} = 2\int(\frac{k_p k_j}{k^2}\hat{u}_i\hat{u}_q^* + \frac{k_p k_i}{k^2}\hat{u}_j\hat{u}_q^*)d\mathbf{k} = -\int(\frac{\partial^2 u_i(x)u_q(x')}{\partial r_p \partial r_j} + \frac{\partial^2 u_j(x)u_q(x')}{\partial r_p \partial r_i})\frac{1}{2\pi|\mathbf{r}|}d\mathbf{r}$$

The problem is therefore reduced to modeling the fourth rank tensor, **M**, which possesses the following symmetry, incompressibility, and amplitude constraints,

$$\begin{aligned} M_{ijpq} &= M_{jipq} \\ M_{iipq} &= 0 \\ M_{ijpp} &= 0 \\ M_{ippq} &= 2R_{iq} \end{aligned} \quad \text{(D.2)}$$

The first two constraints directly affect the resulting pressure-strain tensor and must be satisfied by any model. The last two constraints are true of the exact M tensor but do *not* have to be satisfied in order to obtain a viable pressure-strain model. Durbin, in his book, has argued that satisfying the third constraint is overly restrictive for single point closure models. Further constraints, such as realizability of the pressure-strain term or invariance to system rotation in the 2D limit (limited MFI) can also be imposed. Realizabity [Shuman] requires that when a Reynolds stress (in the principal or diagonal coordinate system) is zero then the pressure strain term does not cause the Reynolds stress to be come negative, which would be unphysical. The realizability constraint is an issue only for two component (2C) turbulence where one Reynolds stress is zero. It can be satisfied by making certain parameters in the model proportional to the two component parameter F(which is 0 in the 2C limit and 1 in isotropic turbulence).

The standard approach is to model M as a tensor expansion in terms of the identity tensor δ_{ij} and the dimensionless Reynolds stress anisotropy tensor, $a_{ij} = \frac{R_{ij}}{K} - \frac{2}{3}\delta_{ij}$, where $K = \frac{1}{2}R_{ii}$ is the turbulent kinetic energy. Launder(1975), proposed the most general linear expansion. The anisotropy tensor is not linear in the Reynolds stresses, but

$Ka_{ij} = R_{ij} - \frac{2}{3}\delta_{ij}K$ is linear and this is how the anisotropy terms appear in the final model. Higher order expansion in the anisotropy tensor allows the model to satisfy realizability and all the incompressibility constraints. The Cayley-Hamilton theorem allows one to truncate the expansion at third order in the tensors. The expansion to this order is performed in Johanson et al. The scalar parameters in the expansion are functions of the invariants, and Johannson et al assume these functions are low order polynomials in the invariants.

In this work a simple linear model will be used, to maintain model simplicity. However, unlike LRR, the model parameters will not be constants and will be functions of the turbulence.

We begin by looking at the basic linear model in which M is expanded in terms of the Reynolds stress gradients and identity tensor.

$$\begin{aligned} M_{ijpq} &= A_1\delta_{ij}\delta_{pq} + A_2(\delta_{ip}\delta_{jq} + \delta_{iq}\delta_{jp}) \\ &+ B_1R_{ij}\delta_{pq} + B_2\delta_{ij}R_{pq} + B_3(R_{ip}\delta_{jq} + R_{jp}\delta_{iq}) + B_4(R_{iq}\delta_{jp} + R_{jq}\delta_{ip}) \end{aligned} \tag{D.3}$$

This is the most general linear expansion of M that satisfies the constraints given by the first constraint in equation (D.2). Imposing the first incompressibility constraint (second constraint in equation (D.2) gives,

$$\begin{aligned} 3A_1 + 2A_2 + 2KB_1 &= 0 \\ 3B_2 + 2B_3 + 2B_4 &= 0 \end{aligned} \tag{D.4}$$

So the most general rapid pressure-strain model in which M is a linear function of only the Reynolds stresses contains four unknown functions and is given by

$$\begin{aligned} M_{ijpq} &= A_2(\delta_{ip}\delta_{jq} + \delta_{iq}\delta_{jp} - \tfrac{2}{3}\delta_{ij}\delta_{pq}) + B_1(R_{ij} - \tfrac{2}{3}K\delta_{ij})\delta_{pq} \\ &+ B_3(R_{ip}\delta_{jq} + R_{jp}\delta_{iq} - \tfrac{2}{3}\delta_{ij}R_{pq}) + B_4(R_{iq}\delta_{jp} + R_{jq}\delta_{ip} - \tfrac{2}{3}\delta_{ij}R_{pq}) \end{aligned} \tag{D.5}$$

If this model is going to be strictly linear in the Reynolds stress tensor and the unknown functions are only functions of the Reynolds stress invariants then the functions are highly constrained and $A_2 \propto K$ and the Bs must be constants. However, in this model this condition will be relaxed and parameters will be allowed to be functions. For incompressible mean flows the term involving B_1 does not appear in the pressure-strain model and there are only three unknown functions.

$$\begin{aligned} \Pi_{ij} &= 2A_2\left(\frac{\partial U_i}{\partial x_j} + \frac{\partial U_j}{\partial x_i}\right) + 2B_3\left(R_{ip}\frac{\partial U_p}{\partial x_j} + R_{jp}\frac{\partial U_p}{\partial x_i} - \tfrac{2}{3}\delta_{ij}R_{pq}\frac{\partial U_p}{\partial x_q}\right) \\ &+ 2B_4\left(R_{iq}\frac{\partial U_j}{\partial x_p} + R_{jq}\frac{\partial U_i}{\partial x_q} - \tfrac{2}{3}\delta_{ij}R_{pq}\frac{\partial U_p}{\partial x_q}\right) \end{aligned} \tag{D.6}$$

This equation is can be presented in an alternative form,

$$\Pi_{ij} = 4A_2S_{ij} + 2(B_3 + B_4)(R_{ip}S_{pj} + R_{jp}S_{pi} - \tfrac{2}{3}\delta_{ij}R_{pq}S_{pq}) + 2(B_3 - B_4)(R_{ip}W_{pj} + R_{jp}W_{pi}) \tag{D.7}$$

where $S_{ij} = \frac{1}{2}\left(\frac{\partial U_i}{\partial x_j} + \frac{\partial U_j}{\partial x_i}\right)$ and $W_{ij} = \frac{1}{2}\left(\frac{\partial U_i}{\partial x_j} - \frac{\partial U_j}{\partial x_i}\right)$. In general, this linear model satisfies only the most basic constraints on the M tensor.

We are modeling this Π_{ij} as,

$$\Pi_{ij} = C_p^* K S_{ij} + C_{p2}^s (R_{ip} S_{pj} + R_{jp} S_{pi} - \tfrac{2}{3}\delta_{ij} R_{pq} S_{pq}) + C_{p2}^w (R_{ip} W_{pj} + R_{jp} W_{pi}) \quad \text{(D.8)}$$

where,

$$C_p^* K = 4A$$

$$C_{p2}^s = 2(B_3 + B_4) \quad \text{(D.9)}$$

$$C_{p2}^w = 2(B_3 - B_4)$$

C_{p2}^s, C_p^* and C_{p2}^w are parameters to be determined.

The classic model for the slow pressure term in the Reynolds stress equations is the Rotta(1951) return to isotropy model given by,

$$\Pi_{ij}^{slow} = -C_1 \frac{\varepsilon}{K}(R_{ij} - \frac{2}{3} K \delta_{ij}) \quad \text{(D.10)}$$

Return to isotropy has been shown to occur in homogenous turbulence in the experiments of Lumley & Newman (1977). Speziale(1991) uses a C_1 which depends on the prediction. We follow his example in this work and define,

$$C_1 = C_{p1}^{'} + C_{p2}^{'} \frac{P}{\hat{\varepsilon}} \quad \text{(D.11)}$$

where we found that $C_{p2}^{'} = -C_{p2}^s$.

The slow pressure strain model then given by,

$$\Pi_{ij}^{slow} = -(C_{p1}^{'} - C_{p2}^s \frac{P}{\hat{\varepsilon}}) \frac{\hat{\varepsilon}}{K}(R_{ij} - \frac{2}{3} K \delta_{ij}) \quad \text{(D.12)}$$

The model developed above is for homogenous (or quasi-homogenous) turbulence. As with the dissipation model it is likely that we need an additional term near wall to take into consideration inhomogeneities. We are using near wall term developed by Amitabh in his master's thesis (2001) by working on asymptotic analysis.

The new term that is proposed is $-\upsilon \frac{\partial K}{\partial x_k} \frac{\partial (R_{ij}/K)}{\partial x_k}$, adding this term in (D.12) gives,

$$\Pi_{ij}^{slow} = -(C_{p1}^{'} - C_{p2}^s \frac{P}{\hat{\varepsilon}}) \frac{\hat{\varepsilon}}{K}(R_{ij} - \frac{2}{3} K \delta_{ij}) - \upsilon \frac{\partial K}{\partial x_k} \frac{\partial (R_{ij}/K)}{\partial x_k} \quad \text{(D.13)}$$

Adding the slow and fast pressure terms we get,

$$\Pi_{ij}^{total} = C_p^* K S_{ij} + C_{p2}^s (R_{ip} S_{pj} + R_{jp} S_{pi} - \tfrac{2}{3}\delta_{ij} R_{pq} S_{pq}) + C_{p2}^w (R_{ip} W_{pj} + R_{jp} W_{pi})$$
$$-(C_{p1}^{'} - C_{p2}^s \frac{P}{\hat{\varepsilon}}) \frac{\hat{\varepsilon}}{K}(R_{ij} - \frac{2}{3} K \delta_{ij}) - \upsilon \frac{\partial K}{\partial x_k} \frac{\partial (R_{ij}/K)}{\partial x_k} \quad \text{(D.14)}$$

From above equation(D.14) with dissipation tensor (described in Appendix E), we get

$$\Pi_{ij}^{total} - \varepsilon_{ij} = C_p^* K S_{ij} + C_{p2}^s (R_{ip} S_{pj} + R_{jp} S_{pi} - \tfrac{2}{3}\delta_{ij} R_{pq} S_{pq}) + C_{p2}^w (R_{ip} W_{pj} + R_{jp} W_{pi})$$
$$-(C_{p1}^{'} - C_{p2}^s \frac{P}{\hat{\varepsilon}}) \frac{\hat{\varepsilon}}{K} (R_{ij} - \frac{2}{3} K \delta_{ij})$$
$$+(1-\alpha)\hat{\varepsilon}(\frac{R_{ij}}{K} - \frac{2}{3}\delta_{ij}) - \frac{\varepsilon}{K} R_{ij} - C^* S_{ij} K$$
$$-2\upsilon \frac{\partial K}{\partial x_k} \frac{\partial (R_{ij}/K)}{\partial x_k} - 2\nu [\frac{(\frac{\partial \sqrt{F}}{\partial x_s})(\frac{\partial \sqrt{F}}{\partial x_t}) R_{st}}{F}][\delta_{ij} - \frac{3}{2}\frac{R_{ij}}{K}] \quad \text{(D.15)}$$

Combining terms, we get,

$$\Pi_{ij}^{total} - \varepsilon_{ij} = C_{p2}^* K S_{ij} + C_{p2}^s (R_{ip} S_{pj} + R_{jp} S_{pi} + \frac{P}{K} R_{ij}) + C_{p2}^w (R_{ip} W_{pj} + R_{jp} W_{pi})$$
$$+C_{p1}(1-\alpha)\hat{\varepsilon}(\frac{2}{3}\delta_{ij} - \frac{R_{ij}}{K}) - \frac{\varepsilon}{K} R_{ij}$$
$$-2\upsilon \frac{\partial K}{\partial x_k} \frac{\partial (R_{ij}/K)}{\partial x_k} - 2\nu [\frac{(\frac{\partial \sqrt{F}}{\partial x_s})(\frac{\partial \sqrt{F}}{\partial x_t}) R_{st}}{F}][\delta_{ij} - \frac{3}{2}\frac{R_{ij}}{K}] \quad \text{(D.16)}$$

Where,

$$C_{p2}^* = \frac{3}{4}(C_p^* - C^*) \quad \text{(D.17)}$$

$$(C_{p1} - 1)(1-\alpha) = C_{p1}^{'} \quad \text{(D.18)}$$

Appendix E: A Model for the Dissipation Rate Tensor in Inhomogeneous and Anisotropic Turbulence

Summary

By including terms that depend on gradients a dissipation model is developed that is exact in the limit of very strong inhomogeneity (such as near solid walls or free-surfaces). Rapid distortion theory (RDT) and equilibrium theory are used to motivate the anisotropic terms in the model. The resulting model has only one free constant (from the equilibrium theory) which is determined via comparisons with turbulent channel flow at Re=590. *A priori* tests of the model for two shear-free boundary layers, channel flow at lower Reynolds numbers, and a backward facing step are presented. Full simulations using the model in channel flow are also performed. Comparisons are made with a variety of existing tensor dissipation rate models.

1. Introduction

Reynolds stress transport (RST) equation closures for turbulence (also referred to as single-point second-moment closures) are theoretically capable of predicting a wide variety of complex industrial flows. However, after many years of development RST are still not widely used in industrial applications. This may be because in practice RST models often do not perform significantly better than two equation models in complex flows. Why has the potential of RST models not been achieved? One possible explanation is that the development of RST models is largely based on quasi-homogeneous or quasi-isotropic assumptions[1,2]. These assumptions are frequently not applicable in engineering flows, particularly those involving walls.

In this work, the modeling of strongly inhomogeneous turbulence is explored. In particular, the focus of this paper is on the modeling of one of the unclosed terms in the RST equations, often referred to as the dissipation rate tensor. As pointed out in Bradshaw & Perot[3], this tensor is not actually equal to the dissipation rate in inhomogeneous turbulent flows (the case of interest in this paper), so for brevity and historical reasons we simply refer to this tensor as the dissipation tensor in this paper. Our particular interest in the dissipation tensor is due to the fact that this term dominates in the region near a wall. Correct prediction of the dissipation tensor is therefore an important first step towards accurate RST models for complex wall bounded turbulent flows.

The Reynolds stress transport equation can be written as,

$$\frac{D\mathbf{R}_{ij}}{Dt} = -(\mathbf{R}_{ik}U_{j,k} + \mathbf{R}_{jk}U_{i,k}) + \nu\mathbf{R}_{ij,kk} - \boldsymbol{\varepsilon}_{ij} + \boldsymbol{\Pi}_{ij} - \mathbf{T}_{ijk,k} \qquad \text{(E.1)}$$

The first term on the right hand side is the production term. It does not need to be modeled. The next two terms are the viscous diffusion and dissipation (rate) terms. The diffusion term does not require a model, and the dissipation term is given by

$\varepsilon_{ij} = 2\nu\overline{u'_{i,k}u'_{j,k}}$. This dissipation term is the focus of this paper. The final two terms, the pressure-gradient velocity correlation $\Pi_{ij} = -\overline{(p'_{,j}u'_i + p'_{,i}u'_j)}$, and the turbulent transport term $\mathbf{T}_{ijk} = \overline{u'_i u'_j u'_k}$ also require models. Near a wall, the turbulent transport is small and is not critical. The pressure-gradient velocity correlation (closely related to the pressure-strain term) is important just away from the wall.

Early models for the dissipation tensor[4,5] assumed that the dissipation tensor was isotropic and given by the expression $\varepsilon_{ij} = \frac{2}{3}\varepsilon\delta_{ij}$. Note that the dissipation, ε, is a scalar equal to one half of the trace of the dissipation tensor. The scalar dissipation is assumed to be a known quantity that is determined by its own transport equation. The assumption of isotropy is based on the argument that large velocity derivatives should primarily occur at the smallest turbulence scales and turbulence is thought to be isotropic at the smallest scales (Kolmogorov[6]).

While small-scale isotropy of turbulence has support from some experiments[7], it is contradicted by some others[8-10]. The recent theoretical analyses of Hallbäck *et al.*[11] and Durbin & Speziale[12] suggest that under the action of mean velocity gradients, even the smallest scales and hence the dissipation tensor must become anisotropic. Brasseur[13] discusses the issue in detail.

Since it is now widely recognized that the dissipation tensor is not isotropic in practice, it is often argued that the dissipation anisotropy should be modeled along with the pressure-gradient velocity correlation following the practice of Lumley & Newman[14]. There is, indeed, significant evidence to suggest that the *slow* pressure-strain correlation and the dissipation tensor anisotropy are closely related. However, it should be observed that the dependence is one way. The pressure terms respond to, and tend to counteract the production and dissipation terms. Fast pressure-strain reduces the production anisotropy, and slow pressure-stain counteracts the dissipation anisotropy. In order to develop effective slow pressure-strain models it is important to be able to model the dissipation tensor anisotropy first.

Some insight into the dissipation tensor anisotropy in homogeneous turbulence can be obtained by using a Fourier decomposition of the fluctuating velocity field. The dissipation tensor can then be written as $\varepsilon_{ij} = \int 2\nu k^2 \widehat{u'_i}\widehat{u'_j}^* d\mathbf{k}$. If the turbulence exists almost entirely at one wavenumber magnitude then k^2 can be removed from the integral and $\varepsilon_{ij} = 2\nu k^2 \mathbf{R}_{ij}$, or solving in terms of the scalar dissipation $\varepsilon_{ij} = \frac{\varepsilon}{K}\mathbf{R}_{ij}$. This model was first proposed by Rotta[15]. It suggests that the dissipation anisotropy is equal to the Reynolds stress anisotropy, $e_{ij} = \frac{\varepsilon_{ij}}{\varepsilon} - \frac{2}{3}\delta_{ij} = \frac{R_{ij}}{K} - \frac{2}{3}\delta_{ij} = a_{ij}$. In decaying turbulence, at low turbulent Reynolds numbers only the large-scale structures (a single significant k magnitude) exists and this model for the dissipation tensor becomes exact. The Rotta model is therefore frequently referred to as the low Reynolds number limit. However, it should be noted that in many low turbulent Reynolds numbers situations (such as near walls) this critical hypothesis of a single wave number magnitude is not satisfied.

A number of dissipation tensor models[16,17] are based on the idea of blending the isotropic model and the Rotta model using a function that depends on the turbulent Reynolds number. These models have the form,

$$\varepsilon_{ij} = (1-f)\tfrac{2}{3}\varepsilon\delta_{ij} + f\tfrac{\varepsilon}{K}R_{ij} = \tfrac{2}{3}\varepsilon\delta_{ij} + f\varepsilon a_{ij} \qquad \text{(E.2)}$$

where f is 1 at low turbulent Reynolds numbers and 0 at high Reynolds numbers. The model of Hanjalic & Launder[17] used $f = 1/(1+0.1\frac{k^2}{\nu\varepsilon})$. This model did not show very good agreement with DNS data of channel flow at Re=180[18] where the simpler expression $f = 1$ (i.e. the Rotta model) was shown to perform better. Hallbäck, Johansson & Burden[19] proposed $f = 1/(1+\frac{.31}{5\pi}\frac{k^{1/2}L_f}{\nu})$ where L_f is the integral length scale. Note that the turbulent Reynolds number approaches zero near a wall, so any formulation that uses a Reynolds number dependent blending function (such as those described above) will go from approximately isotropic dissipation in the free-stream to the Rotta model near the wall. An asymptotic expansion of the dissipation tensor near the wall (Section 3) shows that the Rotta model captures the zeroth order terms correctly at a wall, so these models show improvement over pure isotropic dissipation for wall bounded flows.

Other researchers[20,21] have proposed using models other than the Rotta model for the near wall (or low Reynolds number) region. These models have the form, $\varepsilon_{ij} = \frac{2}{3}\varepsilon\delta_{ij} + fe_{ij}^{wall}$, where the wall model e_{ij}^{wall} is trace free. Often, e_{ij}^{wall} is defined in terms of the wall normal vector, which is ill-defined away from the wall or at corners. In addition, in these models the form of e_{ij}^{wall} is formulated specifically for walls and is incorrect at a free-surface or at any other boundary other than a wall.

While Reynolds number dependent models capture the near wall region better, they all revert to the isotropic model at high Re numbers and evidence suggests that even in the high Re limit the dissipation tensor is not isotropic. In the rapid distortion limit Hällback *et al.*[11] have shown that the dissipation tensor anisotropy is not zero, but half of the Reynolds stress anisotropy. The work of Speziale & Gatski[22] suggests that in equilibrium the dissipation tensor anisotropy should depend on the shear-stress. Finally, Perot[23] has shown that these Reynolds number dependent models are not correct for boundaries other than walls, such as slip walls or free-surfaces.

In order to account for the RDT limit Hällback, Groth & Johansson[11] (HGJ) proposed a nonlinear dissipation tensor model. This model adds an additional term proportional to the square of the anisotropy and has the form

$$\varepsilon_{ij} = \tfrac{2}{3}\varepsilon\delta_{ij} + f_1\varepsilon a_{ij} + f_2\varepsilon(a_{ik}a_{kj} - \tfrac{1}{3}II_a\delta_{ij}) \qquad \text{(E.3)}$$

where $II_a = a_{ij}a_{ji}$ and the functions are given by $f_1 = \frac{1}{2} + \frac{3}{8}II_a$ and $f_2 = -\frac{3}{4}$. This model is realizable, meaning that the dissipation tensor in a certain direction is zero if the turbulence in that direction is zero. A similar model that depends on the two-componentality parameter, $F = \det(\frac{3R_{ij}}{2k})$ was suggested by Sjögren & Johansson[24] (SJ). The two-componentality factor F is 1 in isotropic turbulence and 0 in two-component (2C) turbulence such as near a wall or a free-surface. In the SJ model $f_1 = 1 - 0.67F$ and

$f_2 = -1.18F$. This model goes to the Rotta model in the 2C limit, but does not satisfy the RDT condition that the dissipation anisotropy is half the Reynolds stress anisotropy under the action of large mean strains. These more complex models perform well (away from boundaries) and will be used for comparison in Section 5 where the model performance is evaluated.

Speziale & Gatski[22] have proposed an algebraic formulation for the dissipation tensor that is similar in construction to algebraic models for the Reynolds stress tensor. In the resulting model the dissipation tensor anisotropy is solely a function of the mean velocity gradients. Unfortunately, the resulting model reverts to the (incorrect) isotropic model in the absence of mean velocity gradients. This model is therefore incapable of representing the shear-free boundary layers studied in Section 5. However, the basic premise of using mean velocity gradients to parameterize the dissipation anisotropy (particularly in the equilibrium limit) is a reasonable idea which is adopted later.

Transport equations for the dissipation tensor can also be formulated[25-27]. The Speziale & Gatski model mentioned above is a simplification of such a transport equation. However, this level of complexity may be unwarranted at this time given the level of model uncertainty in the other RST model terms (particularly the pressure-strain).

In Section 2 of this paper, near boundary terms for the dissipation tensor are developed that are accurate near walls and surfaces. These near wall terms are derived from first principles and introduce no model constants. Section 3 analyzes the near wall asymptotics of these models near both walls and free-surfaces, and considers the limit of strong inhomogeneity. In Section 4 the model development in regions away from boundaries is considered. *A priori* tests of the model are presented in Section 5 and compared with a variety of existing model formulations. A brief discussion and conclusions appear in Section 6.

2. Modeling Strong Inhomogeneity

In strongly inhomogeneous flows, turbulent correlations such as the dissipation tensor change rapidly as a function of their position. Some of the change with position is due a change in the underlying structure of the turbulence. However, most of the change is simply due to the spatial change in the turbulence intensity. In the specific case of the dissipation tensor, $\varepsilon_{ij} = 2\nu\overline{u'_{i,k}u'_{j,k}}$, the dissipation can change spatially for two reasons. Either the gradients correlate differently, or (more likely) the magnitude of the velocity fluctuations has simply changed. These different effects can be isolated by using the following decomposition. Let the fluctuating velocity be decomposed as $u'_i = Q_{ij}\tilde{u}_j$. The tensor Q_{ij} is assumed to be a known quantity (related to the velocity fluctuation magnitude). It is an average quantity and does not change in time for statistically steady flows or along homogeneous directions. The underlying temporal and spatial fluctuations of the velocity field are captured by the dimensionless quantity $\tilde{u}_j$. Changes in the

dissipation due to changes in the turbulence magnitude will be captured by Q_{ij}. Changes in the underlying turbulent structure will be manifest in $\tilde{u}_j$.

Substituting this formula into the equation for the Reynolds stress tensor gives a relationship between the structure correlation and the Reynolds stress tensor.

$$R_{ij} = \overline{u_i' u_j'} = \overline{Q_{in}\tilde{u}_n Q_{jm}\tilde{u}_m} = Q_{in}\overline{\tilde{u}_n\tilde{u}_m}Q_{jm} \tag{E.4}$$

The magnitude tensor is not a fluctuating quantity and therefore can come out of the average. Substituting this decomposition into the dissipation tensor formula gives,

$$\begin{aligned}\varepsilon_{ij} &= 2\nu\overline{u_{i,k}' u_{j,k}'} = 2\nu\overline{(Q_{in,k}\tilde{u}_n + Q_{in}\tilde{u}_{n,k})(Q_{jm,k}\tilde{u}_m + Q_{jm}\tilde{u}_{m,k})} \\ &= 2\nu\{Q_{in,k}Q_{jm,k}\overline{\tilde{u}_n\tilde{u}_m} + \tfrac{1}{2}(Q_{in}Q_{jm})_{,k}(\overline{\tilde{u}_m\tilde{u}_n})_{,k} \\ &\quad + Q_{in}Q_{jm}\overline{\tilde{u}_{n,k}\tilde{u}_{m,k}} + \tfrac{1}{2}(Q_{in,k}Q_{jm} - Q_{in}Q_{jm,k})(\overline{\tilde{u}_{m,k}\tilde{u}_n} - \overline{\tilde{u}_m\tilde{u}_{n,k}})\}\end{aligned} \tag{E.5}$$

If it is required that Q_{ij} be invertible then the first two terms in the expression can be found from Eqn. (E.4) and are exact. The third term is the dissipation of the velocity structure. It requires a model. However, the velocity structure is quasi-homogeneous (by design), and so standard dissipation models are expected to perform well in this context. The final term is the product of two differences. It is assumed to be small and evidence to that effect can be found in Perot & Moin.[28] In regions of strong inhomogeneity the first term dominates and Eqn. (E.5) becomes exact irrespective of the model used for the third term in Eqn. (E.5) or the size of the fourth term.

One possible definition for Q_{ij} is that it represents all the magnitude information (Perot, & Moin,[29]). In this case $\overline{\tilde{u}_n\tilde{u}_m} = \delta_{nm}$ and Eqn (E.4) becomes $R_{ij} = Q_{in}Q_{jn}$ or $R = QQ^T$ and Q is the matrix square root of the Reynolds stress tensor. This definition of Q is actually not unique, Q can be symmetric or lower triangular for example. The symmetric square root however, seems to be the most natural. Like regular square roots, the sign of Q is also not well defined. Since Q always appears in pairs, this distinction is not important. With this definition of Q, the second term of Eqn (E.5) is identically zero, and the model is given by

$$\varepsilon_{ij} = 2\nu Q_{in,k}Q_{jn,k} + Q_{in}\tilde{\varepsilon}_{nm}Q_{jm} \tag{E.6}$$

where the fourth term of Eqn. (E.5) is assumed to be negligible.

This near wall model is elegant, but inconvenient to implement. Finding Q requires determining the eigenvectors and eigenvalues of R. In this paper we consider a simpler implementation of Eqn (E.5). In order to gain implementation simplicity we therefore assume that Q is isotropic and is scaled by the turbulent kinetic energy, $Q_{ij} = K^{1/2}\delta_{ij}$. With this definition of Q, Eqn (E.4) gives the relation $\frac{R_{ij}}{K} = \overline{\tilde{u}_i\tilde{u}_j}$ and the fourth term in Eqn. (E.5) is identically zero. Eqn. (E.5) then becomes,

$$\varepsilon_{ij} = 2\nu(K^{1/2})_{,n}(K^{1/2})_{,n}\tfrac{R_{ij}}{K} + \nu K_{,n}(\tfrac{R_{ij}}{K})_{,n} + K\tilde{\varepsilon}_{ij} \tag{E.7a}$$

which is an exact relation. This can alternatively be written as

$$\varepsilon_{ij} = 2\nu(K^{1/2})_{,n}\left(\frac{R_{ij}}{K^{1/2}}\right)_{,n} + K\tilde{\varepsilon}_{ij} \tag{E.7b}$$

Note that Eqn. (E.7) only becomes a dissipation tensor model when a quasi-homogeneous dissipation tensor model (for $K\tilde{\varepsilon}_{ij}$) is hypothesized. The quasi-homogeneous dissipation tensor should be significantly easier to model than the dissipation tensor itself. The quasi-homogeneous model is discussed in section 4. In the next section, the near wall behavior of Eqn. (E.7) is analyzed.

3. Asymptotic Analysis Near Boundaries

The behavior of turbulence quantities near a boundary can be determined by using Taylor series expansions in the coordinate direction normal to the boundary (Launder & Reynolds[30]). Using the convention that y is the direction normal to a wall the fluctuating velocity can be expanded as,

$$u_i' = a_i(x,z,t) + yb_i(x,z,t) + y^2 c_i(x,z,t) + \ldots \tag{E.8}$$

At a solid wall the velocity goes to zero, so all the a_i are zero. Continuity applied very close to the wall implies $b_2 = 0$.

Substituting Eqn (E.8) into the definition for the dissipation tells us that near a wall,

$$\begin{aligned}
\varepsilon_{11} &= 2\nu\{(\overline{b_1^2}) + y(4\overline{b_1 c_1}) + y^2(4\overline{c_1^2} + 6\overline{b_1 d_1} + \overline{b_{1,1}^2} + \overline{b_{1,3}^2}) + \ldots\} \\
\varepsilon_{12} &= 2\nu\{y(2\overline{b_1 c_2}) + y^2(3\overline{b_1 d_2} + 4\overline{c_1 c_2}) + y^3(4\overline{b_1 e_2} + 6\overline{c_1 d_2} + 6\overline{d_1 c_2} + \overline{b_{1,1} c_{2,1}} + \overline{b_{1,3} c_{2,3}}) + \ldots\} \\
\varepsilon_{22} &= 2\nu\{y^2(4\overline{c_2^2}) + y^3(12\overline{c_2 d_2}) + y^4(9\overline{d_2^2} + 16\overline{c_2 e_2} + \overline{c_{2,1}^2} + \overline{c_{2,3}^2}) + \ldots\}
\end{aligned} \tag{E.9}$$

The ε_{33} component behaves just like ε_{11}. A similar expansion for the Reynolds stress tensor can also be performed.

$$\begin{aligned}
R_{11} &= y^2(\overline{b_1^2}) + y^3(2\overline{b_1 c_1}) + \ldots \\
R_{12} &= y^3(\overline{b_1 c_2}) + y^4(\overline{b_1 d_2} + \overline{c_1 c_2}) + \ldots \\
R_{22} &= y^4(\overline{c_2^2}) + y^5(2\overline{c_2 d_2}) + \ldots
\end{aligned} \tag{E.10}$$

The leading order terms in the dissipation tensor and the Reynolds stress tensor are very similar. However, the coefficient is different in each case. Rotta's model gets the 0(1) terms of the dissipation tensor correctly (i.e. the leading term of the ε_{11} and ε_{33} expansion), but it will under predict the leading order terms of the other two dissipation components. Although the wall is at a low turbulent Reynolds number, Rotta's model does not work entirely correctly. The amplitude of fluctuations normal to the wall and those parallel to the wall are very different, and the basic assumptions used to derive the Rotta model are violated.

Even if leading order terms of ε_{12} and ε_{22} are wrong, does it matter? They still go to zero at the wall. Interestingly, if wall functions are not used it matters a great deal (using wall functions with a RST model largely defeats the purpose of having a RST model, see Speziale[31]). Near the wall, the dissipation and pressure-gradient velocity correlation exactly balance the diffusion term. If the leading order behavior of the dissipation is incorrect, the Reynolds stresses are too large near the wall and as a result they are also too large away from the wall. Trying to reduce these Reynolds stresses via terms in the model (rather than fixing the root cause) often leads to instability in the wall bounded

RST equation system. Note that one reason elliptic relaxation models work well has nothing to do with ellipticity. These models allow an extra boundary condition to be imposed (because they hypothesize an extra equation). This additional boundary condition forces the correct near wall behavior of the Reynolds stresses. In essence, the elliptic relation forces the near wall behavior of the dissipation tensor to be correct via additional boundary conditions. In standard RST models (where six additional equations and their boundary conditions are not available), correct leading order behavior of each dissipation term is highly desirable.

As mentioned earlier, it is also possible to formulate models with the correct near wall asymptotics by using the wall normal vector or distance to the wall along with a blending function. This works, and is standard practice, but these models have serious deficiencies in their generality. Typically they work *only* at walls.

The boundary conditions at a slip wall (or stationary free-surface), impose different constraints on the expansion. We now find that $b_1 = a_2 = b_3 = 0$, and continuity implies $a_{1,x} + a_{3,z} + b_2 = 0$.

At a stationary free-surface the dissipation behaves as,

$$\begin{aligned}
\varepsilon_{11} &= 2\nu\{(\overline{a_{1,1}^2} + \overline{a_{1,3}^2}) + y^2(\overline{a_{1,1}c_{1,1}} + \overline{a_{1,3}c_{1,3}} + 4\overline{c_1^2}) + \ldots\} \\
\varepsilon_{12} &= 2\nu\{y(\overline{a_{1,1}b_{2,1}} + \overline{a_{1,3}b_{2,3}} + 2\overline{c_1 b_2}) + y^2(\overline{a_{1,1}c_{2,1}} + \overline{a_{1,3}c_{2,3}} + 3\overline{d_1 b_2} + 4\overline{c_1 c_2}) + \ldots\} \\
\varepsilon_{22} &= 2\nu\{(\overline{b_2^2}) + y(4\overline{c_2 b_2}) + \ldots\}
\end{aligned} \tag{E.11}$$

and the Reynolds stress tensor is,

$$\begin{aligned}
R_{11} &= (\overline{a_1^2}) + y^2(2\overline{a_1 c_1}) + \ldots \\
R_{12} &= y(\overline{a_1 b_2}) + y^2(\overline{a_1 c_2}) + \ldots \\
R_{22} &= y^2(\overline{b_2^2}) + y^3(2\overline{b_2 c_2}) + \ldots
\end{aligned} \tag{E.12}$$

At a free-surface there is no longer a clear relationship between the dissipation tensor and the Reynolds stress tensor. Rotta's model will cause ε_{22} to be zero at the surface when it should be finite. Also note that a free-surface is no longer a low turbulent Reynolds number situation, so blending models (Eqn E.2) will produce the isotropic limit near the surface. The isotropic model does give a finite value for ε_{22} but it will be shown in Section 5 that it is far too large, and that the dissipation near a free-surface is not close to isotropic.

The near boundary behavior of the proposed model can be determined from the behavior of the Reynolds stresses. For a no-slip wall we find that

$$K = y^2 \tfrac{1}{2}(\overline{b_1^2} + \overline{b_3^2}) + y^3 \tfrac{1}{2}(2\overline{b_1 c_1} + 2\overline{b_3 c_3}) + \ldots \tag{E.13}$$

and

$$(K^{1/2})_{,k}(K^{1/2})_{,k}\tfrac{1}{K} = (\tfrac{K_k}{2K})^2 = \tfrac{1}{y^2}\{1 + y\tfrac{(2\overline{b_1 c_1} + 2\overline{b_3 c_3})}{(\overline{b_1^2} + \overline{b_3^2})} + \ldots\} \tag{E.14}$$

plugging into the model equation (Eqn. E.7) gives,

$$\varepsilon_{11} = 2\nu\{(\overline{b_1^2}) + y(4\overline{b_1 c_1}) + O(y^2)\} + K\tilde{\varepsilon}_{11}$$
$$\varepsilon_{12} = 2\nu\{y(2\overline{b_1 c_2}) + y^2(3\overline{b_1 d_2} + 3\overline{c_1 c_2} + \overline{b_1 c_2}\frac{(\overline{b_1 c_1} + \overline{b_3 c_3})}{(\overline{b_1^2} + \overline{b_3^2})}) + O(y^3)\} + K\tilde{\varepsilon}_{12} \quad \text{(E.15)}$$
$$\varepsilon_{22} = 2\nu\{y^2(3\overline{c_2^2}) + y^3(8\overline{c_2 d_2} + 2\overline{c_2^2}\frac{(\overline{b_1 c_1} + \overline{b_3 c_3})}{(\overline{b_1^2} + \overline{b_3^2})}) + O(y^4)\} + K\tilde{\varepsilon}_{22}$$

So the proposed expression for the dissipation tensor (Eqn E.7) captures the O(1) and O(y) terms exactly and at least 75% of the $O(y^2)$ terms, when implemented near a wall. Since K is $O(y^2)$ this analysis shows that the quasi-homogeneous dissipation model can be as high as O(1) at the walls, without affecting the near wall asymptotics described above. Before considering the behavior of the quasi-homogeneous dissipation tensor in any more detail, let us consider the behavior of the proposed decomposition (Eqn. E.7) near a free surface.

Near a free surface the kinetic energy is given by

$$K = \tfrac{1}{2}(\overline{a_1^2} + \overline{a_3^2}) + y^2\tfrac{1}{2}(\overline{b_2 c_2} + 2\overline{a_1 c_1} + 2\overline{a_3 c_3}) + \ldots \quad \text{(E.16)}$$

and

$$(\tfrac{K_{,k}}{2K})^2 = \{[\tfrac{1}{2}(\overline{a_1^2} + \overline{a_3^2})_{,1}]^2 + [\tfrac{1}{2}(\overline{a_1^2} + \overline{a_3^2})_{,3}]^2\}/[(\overline{a_1^2} + \overline{a_3^2})]^2 + O(y^2) \quad \text{(E.17a)}$$

we can also show that

$$K_{,k}(\tfrac{R_{11}}{K})_{,k} = O(1)$$
$$K_{,k}(\tfrac{R_{12}}{K})_{,k} = O(y) \quad \text{(E.17b)}$$
$$K_{,k}(\tfrac{R_{22}}{K})_{,k} = O(y^2)$$

so the near boundary terms in Eqn. (E.7) have the same type of behavior. This requires the $\tilde{\varepsilon}_{12}$ model to go like O(y) near the surface and $\tilde{\varepsilon}_{22}$ to be O(1). Looking at the exact expressions for the dissipation tensor near a free-surface it is clear that capturing the leading order ε_{11} and ε_{12} terms exactly is not possible. Derivative information is not available to a RST model. However, the leading two terms of the ε_{22} expression can, in theory, be obtained exactly from Reynolds stress information. Also note that the error in both the wall and free-surface expressions for ε_{22} can be represented by $\frac{2\nu}{y^2}R_{22}$. The error is the same irrespective of the boundary type. At both boundaries, the flow becomes two-component, so we will use the 2C parameter F to model this missing contribution for ε_{22}. This extra term is $2\nu(F^{1/2})_{,n}(F^{1/2})_{,m}R_{nm}\delta_{ij}/F$. Technically we are now modeling the quasi-homogeneous dissipation, $K\tilde{\varepsilon}_{ij}$. This is the near boundary contribution of the quasi-homogeneous dissipation due to the 2C nature of the turbulence near these boundaries. This term is higher order for ε_{11} for ε_{12} terms near both walls and free-surfaces, and so it only affects the ε_{22} dissipation component. At a solid wall, this enhancement has only a very small affect on the model. However, at a free surface the 2C affects can be seen very clearly. The importance of this 2C correction is demonstrated in Section 5.

4. Quasi-Homogeneous Dissipation

In homogeneous turbulence, the boundary (or gradient) terms drop out entirely and the quasi-homogeneous dissipation remains to be modeled. Hallbäck *et al.*[19] show that in initially isotropic homogeneous turbulence the dissipation anisotropy should be half of the Reynolds stress anisotropy under the action of rapid irrotational strain or shear. This will be referred to as the RDT limit. The experiments of Crow[32] and Lee & Reynolds[33] show that this ratio does not remain ½ when the turbulence is anisotropic, and in the extreme limit of axisymmetric 2C turbulence it is seen to be close to 1 (which is the Rotta model).

The practice of expanding model parameters in polynomial expansions of the potential unknowns is a rational way to proceed, and is certainly viable when the unknowns are known to be small. However, when the objective is to capture an entire functional range the use of polynomial expansions can be detrimental. Rational polynomials have a greater fitting capability. In this work, we propose a simple tensorally linear model for the quasi-homogeneous dissipation, in which the blending parameter f is a function of F. This is similar to the models of Johansson, however we hypothesize a rational polynomial expansion, $f=\frac{1}{1+F}$, rather than a simple polynomial series. This results in the quasi-homogeneous model $\tilde{\varepsilon}_{ij}=\tilde{\varepsilon}(\frac{F}{1+F}\frac{2}{3}\delta_{ij}+\frac{1}{1+F}\frac{R_{ij}}{K})=\tilde{\varepsilon}(\frac{2}{3}\delta_{ij}+\frac{1}{1+F}a_{ij})$ and $a_{ij}=\frac{R_{ij}}{K}-\frac{2}{3}\delta_{ij}$. In isotropic turbulence, this model gives the correct RDT anisotropy ratio of ½, and in 2C turbulence it gives the correct anisotropy ratio of 1. In theory, a slightly more complex blending might be desired in which $f=\frac{1}{1+g(\mathrm{Re}_T)F}$ where the function g goes to zero as the turbulent Reynolds number becomes small and approaches 1 at high turbulent Reynolds numbers. We have not pursued this added level of complexity at this time.

Finally, we note that the dissipation anisotropy could be a function of the mean flow gradients, not just the Reynolds stress anisotropy. Typically, dissipation anisotropy is not modeled in this way because one does not expect sudden changes in the mean flow to have an instantaneous affect of the dissipation. However, in equilibrium situations, there could be a good correlation between the two tensors. Reynolds stresses are frequently modeled using this type of hypothesis (eddy viscosity hypothesis of Bousinesq). In fact, models which only depend on the Reynolds stress anisotropy will have the dissipation anisotropy aligned along the same principal directions as the Reynolds stress anisotropy. We know that these anisotropy directions are not always aligned (in channel flow they disagree by 8 degrees at y+ =30). In this work we therefore hypothesize that the quasi-homogeneous dissipation tensor can also be a linear function of the shear-stress tensor, $S_{ij}=\frac{1}{2}(U_{i,j}+U_{j,i})$.

The model for the dissipation tensor then becomes,

$$\varepsilon_{ij}=2\nu(K^{1/2}{}_{,n})^2R_{ij}+\nu K_{,k}(\frac{R_{ij}}{K})_{,k}+\tilde{\varepsilon}\frac{F}{1+F}\frac{2}{3}\delta_{ij}K+\tilde{\varepsilon}\frac{1}{1+F}R_{ij}+2\nu\frac{F^{1/2}{}_{,m}R_{mn}F^{1/2}{}_{,n}}{F}\delta_{ij}+C^*KS_{ij} \quad \text{(E.18)}$$

The single parameter $C^*=0.18F/(1+F)^2$ is set by comparing the ε_{12} component of turbulent channel flow at Re=590. In theory, the constant C^* should be a function of

$\frac{\varepsilon}{SK}$, such that C^* goes to zero when $\frac{\varepsilon}{SK}$ is zero (the RDT limit). We have not explored this level of detail in this work.

The scalar $\tilde{\varepsilon} = \frac{1}{2}\tilde{\varepsilon}_{ii}$ is the trace of the quasi-homogeneous dissipation. It has units of inverse time or frequency and can be obtained by taking one half the trace of Eqn. 18, $K\tilde{\varepsilon} = \varepsilon - 2\nu(K^{1/2}{}_{,n})^2 - 3\nu\frac{F^{1/2}{}_{,m}R_{mn}F^{1/2}{}_{,n}}{F}$. The quasi-homogeneous dissipation $\tilde{\varepsilon}$ (or its closely related form $\hat{\varepsilon} = K\tilde{\varepsilon}$) is an interesting inverse timescale that has been used previously in some near wall turbulence models (e.g. Launder & Shima,[32]). It is attractive because at a wall it is finite, whereas the standard inverse timescale $\frac{\varepsilon}{K}$ is singular and goes like y^{-2} at a wall. Note that from its definition, $\tilde{\varepsilon}$ is a positive quantity. However, due to numerical inaccuracy in the calculation of gradients, calculating $\tilde{\varepsilon}$ from the formula above can lead to large errors or negative values when implemented on a computer. In practical implementation either a transport equation is solved directly for $\tilde{\varepsilon}$ rather than the more common ε transport equation (as in many low Re number k/e models), or we sometimes use $\tilde{\varepsilon} = \frac{\varepsilon}{K}\frac{1}{(1+10\nu|\nabla(K^{1/2})|/K)}$ to guarantee a positive inverse timescale with finite near wall behavior.

While the proposed model (Eqn. E.18) looks somewhat complex, it is relatively easy to implement. Many of the terms combine with similar looking terms in the pressure-strain model, and if the Reynolds stress anisotropy equation is solved rather than the RST equation, then some of the terms drop out or simplify even further.

It is important when implementing this model to have a numerical method that is capable of accurately calculating gradients. At the wall, certain terms should exactly balance. Numerically they will only approximately balance and if the disagreement is large enough, the numerical implementation (not the model) becomes unstable. Quantities with high power law behavior ($R_{22} = O(y^4)$) can be quite hard to differentiate accurately with low order numerical methods. For this reason, the anisotropy equations (rather than Reynolds stress equations) are somewhat easier to solve with low order numerical methods.

5. Model Results

In this section, the proposed dissipation model (Eqn. E.18) is compared against experimental and DNS data. The performance of the model is compared to a number of other dissipation tensor models that have been mentioned in the text. The majority of the tests are *a priori* tests using data for the Reynolds stresses and dissipation plugged directly into Eqn 18.

These tests are a useful way to directly isolate if the model can represent the dissipation tensor accurately. However, it is possible to construct models, which perform well in *a priori* tests but do not perform well in practice. These models are unstable and move away from the desired solution rather than towards it. To demonstrate stability we will

also present at the end of this section some solutions of turbulent channel flow that use this dissipation tensor model in a full RST prediction.

Our first test case does not involve the inhomogeneous terms at all. It is a test of the quasi-homogeneous part of the model. Figure 1 shows the model performance in axisymmetric rapid contraction of homogeneous turbulence. In this flow the turbulence is initially isotropic and becomes increasingly 2C as time proceeds. Because the turbulence is axisymmetric only one component of the dissipation need be analyzed. The figure shows the e_{11} component as a function of a_{11}, at various times during the simulation (experiment). The isotropic model gives a flat line, and the dashed line with a slope of 1 is the Rotta model. This is a relatively high Reynolds number test case, so models that switch between the isotropic model and the Rotta model based on a blending parameter which is a function of the turbulent Reynolds number (most models) will be essentially isotropic (very close to a horizontal line through the origin). The HGJ model was designed for this flow and therefore performs well for this case. The SJ model (not shown) performs very like HGJ.

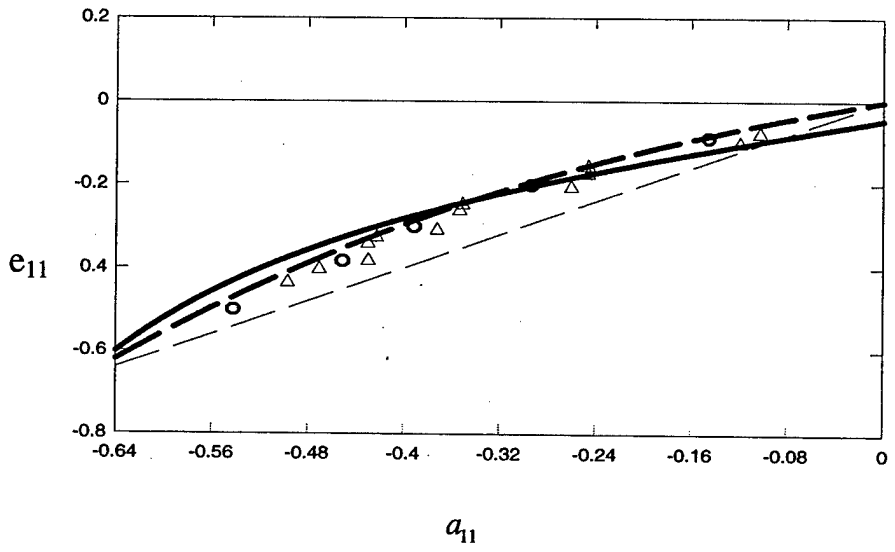

Figure 1. Dissipation anisotropy in axisymmetric contraction. Open triangles denote the experimental data of Crow[32] ($S_2^*(t=0) \approx 0.5-2.0$, $\mathrm{Re}_\lambda \approx 15-100$), open circles denote the experimental data of Lee & Reynolds[33] ($S_2^*(t=0) \approx 0.97$ *to* $.0.71, \mathrm{Re}_\lambda \approx 50$), thick dashed line denotes HGJ model, thin line denotes isotropic model, thin dashed line denotes Rotta model, and thick line denotes the proposed model.

Next, we wish to examine the inhomogeneous terms. The quasi-homogeneous term cannot be completely eliminated in any flow, but shear-free boundary layers provide an opportunity to evaluate the model in a strongly inhomogeneous situation with few other complicating effects. In Figure 2, the model predictions of a shear-free boundary layer next to a solid wall are compared with DNS data[35]. Like the previous case, this flow is

axisymmetric and time developing, but unlike the previous case, it also has strong gradients in the direction normal to the wall. The figure shows the ε_{22} dissipation at two different times after the wall appears. As predicted by the asymptotic analysis, the Rotta model is too small near the wall. The HGJ model transitions from a combination of ½ isotropic and ½ Rotta well away from the wall to all Rotta near the wall where the turbulence is 2C. The SJ model (not shown) is almost identical to HGJ. Other models which blend the isotropic and Rotta models based on the Reynolds number will behave like the Rotta model near the wall. All but the proposed model, underpredict the normal dissipation component near the wall.

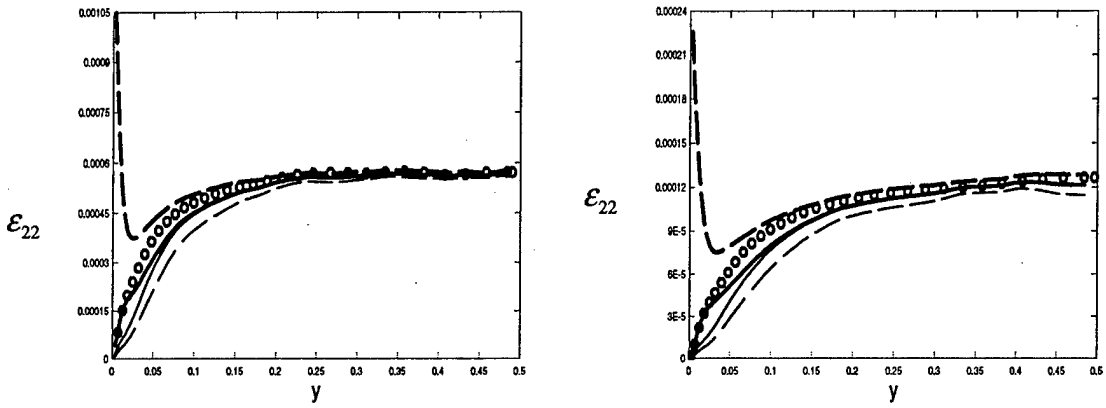

a) After time = 2.01 b) After time = 6.04

Figure 2. Shear-free turbulent boundary layer next to solid wall. Circles denote DNS data of Perot & Moin[35], thick dashed line denotes isotropic model, thin dashed line denotes Rotta model, thin line denotes HGJ model and thick line denotes proposed model.

The shear-free boundary layer next to stationary free surface is shown in Figure 3. Again two times are shown, and the definitions of the lines and symbols are the same as in Figure 2. This flow is no longer low Reynolds number near the surface, and so the under-prediction of the Rotta and HGJ models is even more obvious in this case. Most other models will behave like the isotropic model for this flow. The proposed model captures the near-surface dissipation correctly using no adjustable constants.

In figure 4, the various terms in the present model are split out so the magnitude and location of each contribution can be ascertained. Figure 4(a) is the shear-free surface at time 2.0 and figure 4(b) is the shear-free wall at time 2.0. It is clear that the term involving $2\nu\frac{F^{1/2}{}_{,m}R_{mn}F^{1/2}{}_{,n}}{F}$ is critical in the free-surface case.

In Figure 5 the model is tested in turbulent channel flow at Re 590[36]. The proposed model performs well for all the dissipation components. The other models have difficulty predicting the ε_{12} and ε_{22} components. The value of C^* was tuned for ε_{12} in this case.

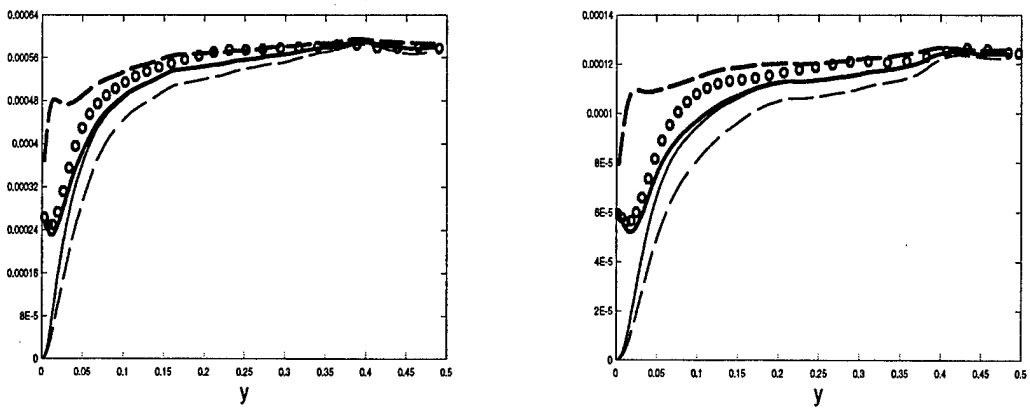

a) After time = 2.01 b) After time = 6.04

Figure 3. Shear-free turbulent boundary layer next to free-surface. (See Figure 2 for caption).

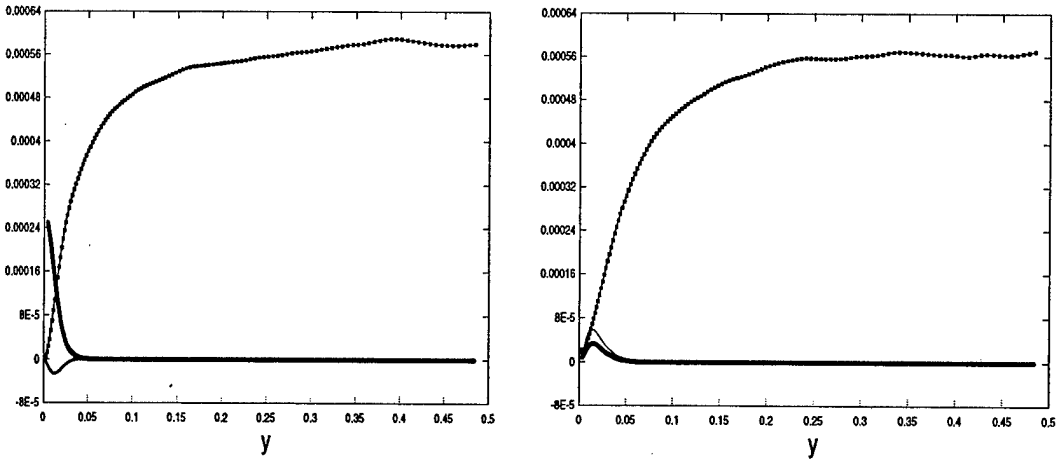

a) Shear-free surface b) Shear-free wall

Figure 4. Each term in equation 18 for shear-free turbulent boundary layers at time 2.0. The chain dotted line denotes $2\nu(K^{1/2}{}_{,n})^2 R_{ij} + \tilde{\varepsilon}\frac{F}{1+F}\frac{2}{3}\delta_{ij}K + \tilde{\varepsilon}\frac{1}{1+F}R_{ij}$, thin line denotes $\nu K_{,k}\left(\frac{R_{ij}}{K}\right)_{,k}$, and thick line denotes $2\nu\frac{F^{1/2}{}_{,m}R_{mn}F^{1/2}{}_{,n}}{F}K\delta_{ij}$. The shear-stress term is zero for both these flows.

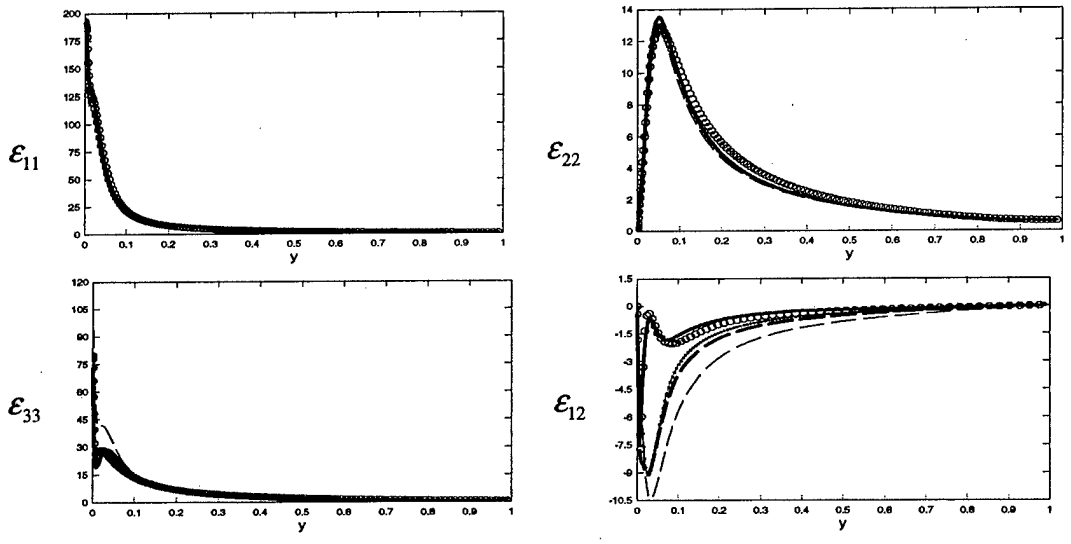

Figure 5. Dissipation tensor in channel flow (Re = 590). Circles denote DNS data from Ref 36, long dashed line denotes SJ model, chained dashed line denotes HGJ model and thick line denotes proposed model. (In the figure of ε_{12}, thick dashed line represents the proposed model without the shear stress term)

With $C^* = 0$, the small dashed line is obtained. The model predictions for channel flow at Re=395 and Re=180 are shown in Figure 6 and Figure 7 respectively. The lowest Reynolds number case shows some discrepancies for ε_{12}. This might be fixed by making C^* a function of ε / SK as suggested earlier.

The behavior of the model in rotating channel flow is shown in figure 8. The test case is the Ro=0.15 DNS case of Andersson and R. Kristoffersen[37] at a Re of 194. The model does a good job of predicting the very different behaviors on each side of the channel (especially given the very low Re number of the simulation).

The proposed model is compared with DNS data for the flow past a backward facing step in Figures 9, 10 and 11. Several locations are shown, both before (4h) and near (6h) reattachment, and well downstream (10h) during the boundary layer recovery. The figures show good agreement with the DNS data[38] in the turning mixing layer. The boundary layer near the wall is more difficult to see, but behaves similarly to the previous channel flow results. In the mixing layer, this tensoraly linear model performs similarly (or better in the ε_{12} case) to the more complex nonlinear model of HGJ and is much more accurate than the isotropic and Rotta models.

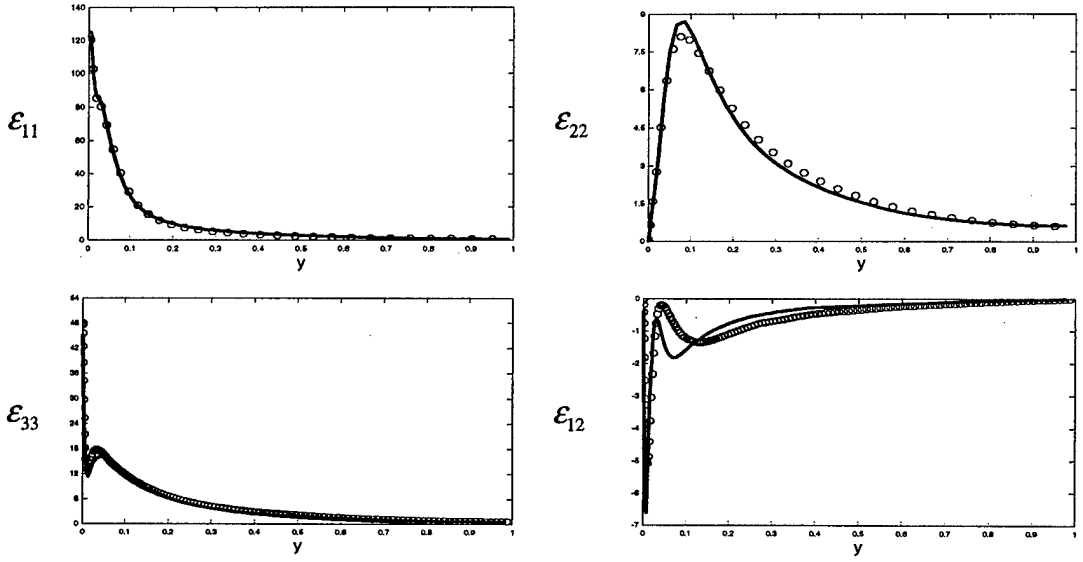

Figure 6. Dissipation anisotropies in channel Flow (Re = 395). Circles denote DNS data from Ref 36 and thick line denotes proposed model.

It is interesting to quantify the effect of the nonlinear term in the SJ and HGJ models. In figure 12, these models are shown with f_2 set to zero, for the 7h downstream location on the backward-facing step. The contribution of the nonlinear term is not that large, given

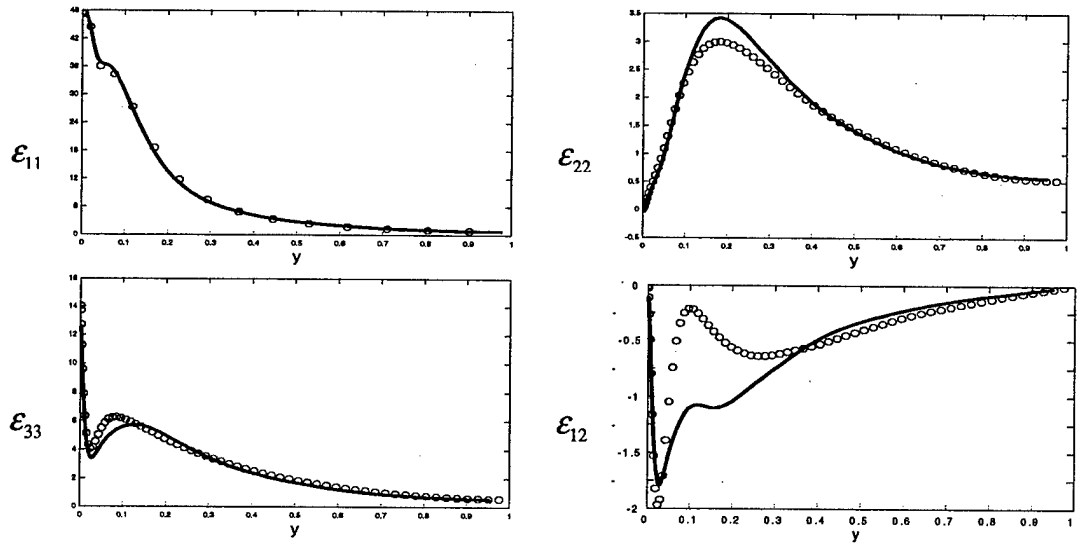

Figure 7. Dissipation anisotropies in channel Flow (Re = 180). Circles denote DNS data from Ref 36 and thick line denotes proposed model.

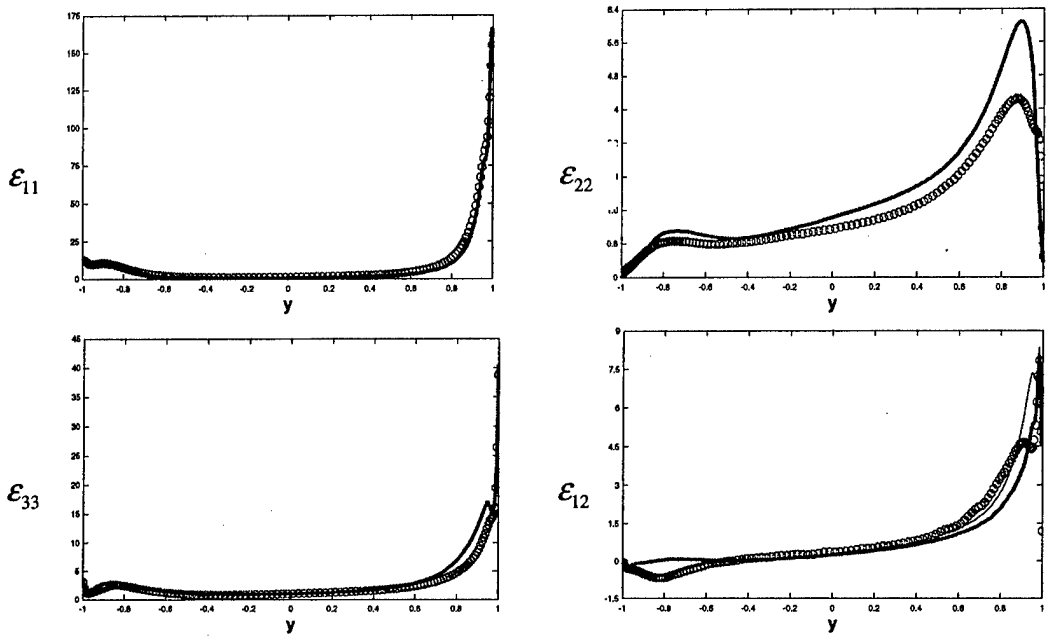

Figure 8. Dissipation anisotropies in rotating channel Flow (Ro=0.15, Re = 194). Circles denote DNS data from Ref 37 and thick line denotes proposed model. Thin line in the last figure is the model with $C^*=0$.

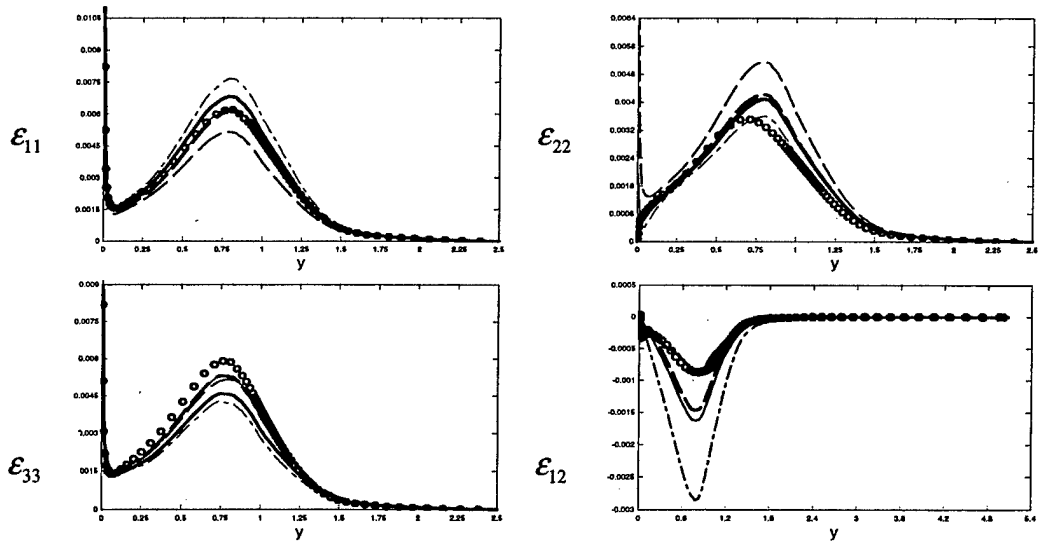

Figure 9. Dissipation tensor in the flow over backward-facing step (at 4h). Circles denote DNS data from Ref 38, long dashed line denotes the isotropic model, chain-dotted line denotes the Rotta model, thin line denotes the SJ model, the small dashed line denotes the HGJ model, and the thick line denotes the proposed model.

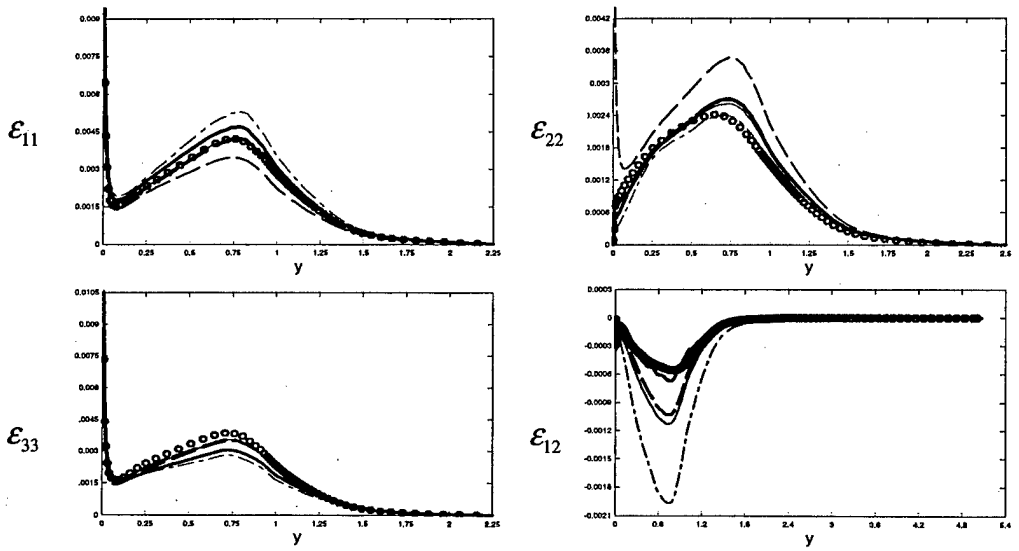

Figure 10. Dissipation tensor in the flow over backward-facing step (at 6h). Circles denote DNS data from Ref 38, long dashed line denotes the isotropic model, chain-dotted line denotes the Rotta model, thin line denotes the SJ model, the small dashed line denotes the HGJ model, and the thick line denotes the proposed model.

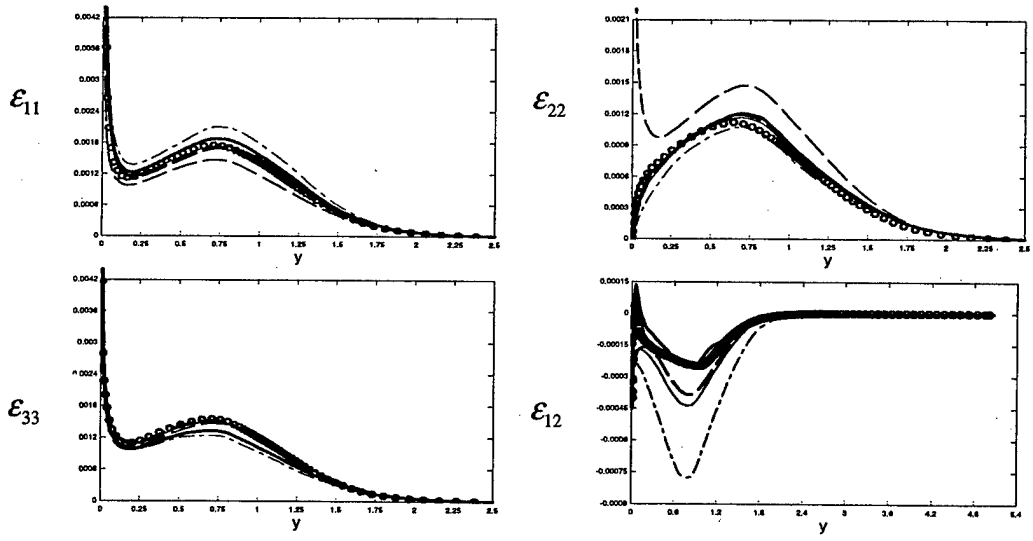

Figure 11. Dissipation tensor in the flow over backward-facing step (at 10h). Circles denote DNS data from Ref 38, long dashed line denotes the isotropic model, chain-dotted line denotes the Rotta model, thin line denotes the SJ model, the small dashed line denotes the HGJ model, and the thick line denotes the proposed model.

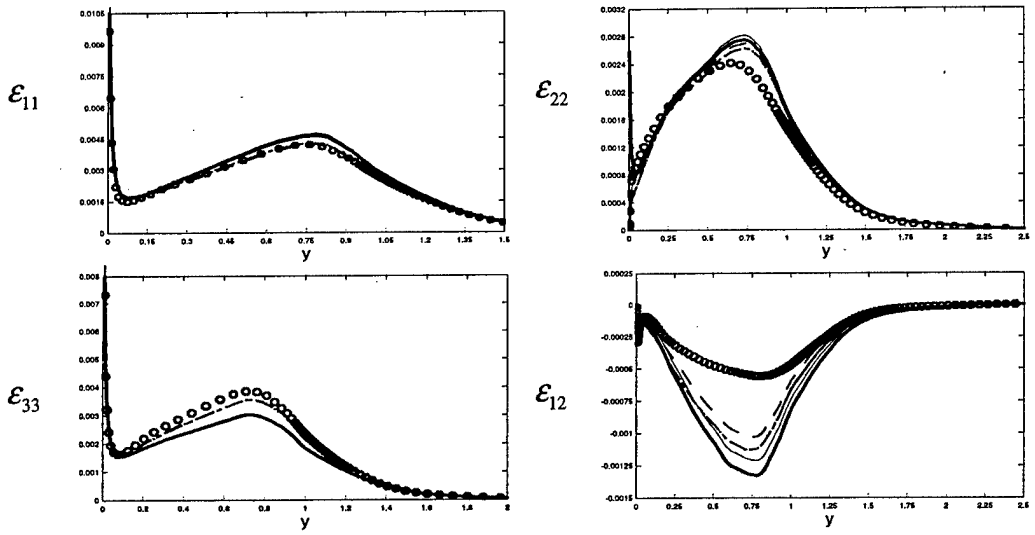

Figure 12. Dissipation anisotropies in flow over backward-facing step (at 6h). Circles denote DNS data from Ref. 38, chained dashed line denotes SJ model, dashed line denotes HGJ model, thin line denotes SJ model without nonlinear term, thick line denotes HGJ model without nonlinear term.

its added complexity we have chosen not to include such a nonlinear term in the proposed model. The choice of the function $f = \frac{1}{1+F}$ allows us to satisfy the RDT limit and realizability without the nonlinear term present.

A priori tests such as those described above can be very informative about the quality of a model. Nevertheless, it is possible to formulate models which work well in *a priori* test but which fail in practice due to the inherent instability of the proposed formulation. The proposed dissipation model has been incorporated into a full RST closure and solved for turbulent channel flow. The details of the full RST closure are given in Natu[39]. Results of these simulations for channel flow at Re=590 are show in Figure 13, and for the rotating channel flow case in figure 14. These full model results are highly dependent on the chosen pressure-strain model. They are not, therefore, an indication of the accuracy of the dissipation tensor model. They are, however, an indication of the dissipation tensor model's stability and computability.

6. Conclusion

The proposed model for the dissipation tensor deviates from all prior models in its use of terms which involve gradients of various turbulence quantities. The appearance of these gradient terms is not particularly surprising. There is no reason to believe that the source terms in the RST equations should not be functions of such gradients and, in fact, there is every reason to believe that gradients should dominate in regions of strong inhomogeneity, such as near walls.

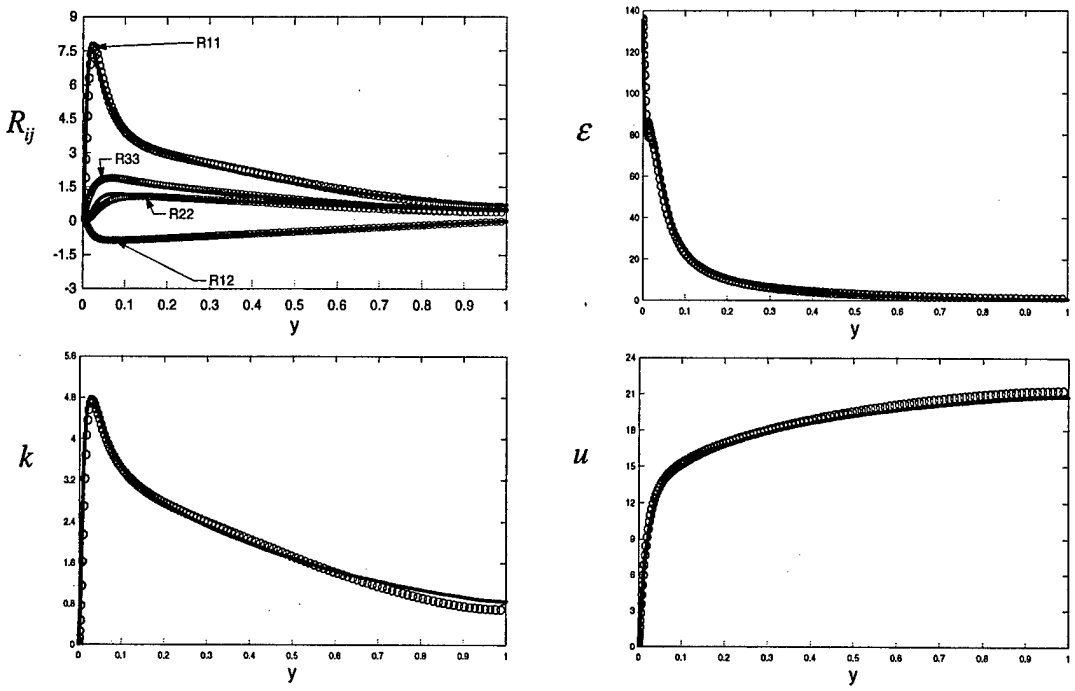

Figure 13. Channel flow (Re=590). Circles denote DNS data from Ref. 36 and thick line denotes full RST model predictions.

When attempting to add gradient information to a model, the variety of choices is so large that the traditional approach of expanding a quantity (such as the dissipation) in terms of all the possible unknowns becomes intractable. This paper has demonstrated a rational approach to deriving the gradient terms in the model. The resulting terms (Eqn E.7) do

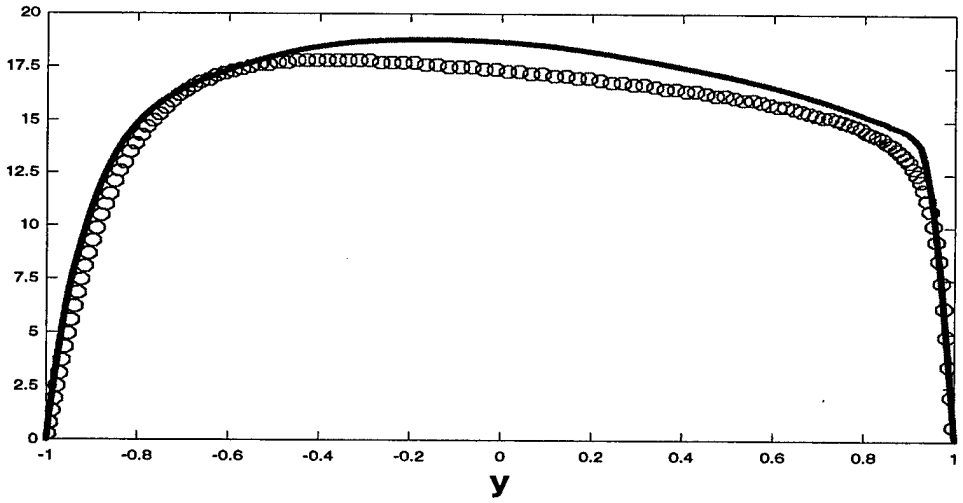

Figure 14. Full RST prediction of the mean velocity in rotating channel flow (Ro=0.15, Re=194). Circles denote DNS data from Ref. 38 and thick line denotes the model prediction.

not have any additional model constants, but do tend to greatly improve the model performance in regions where gradients are large.

It is interesting to note that the resulting gradient terms do have associations in other contexts. The term $2\nu(K^{1/2})_{,n}(K^{1/2})_{,n}$ is a common modification of the dissipation near a wall such that time scales at the wall remain finite, and the term $\nu K_{,n}(\frac{R_{ij}}{K})_{,n}$ appears in the Reynolds stress anisotropy transport equation.

The quasi-homogeneous term in Eqn E.7 is in many senses the harder part of the dissipation tensor to model. Our quasi-homogeneous model introduces a parameter to represent the affects of mean strain on the dissipation. In theory, this term should only be present in equilibrium situations (when production is roughly equal to dissipation). The near-wall 2C term does not introduce any addition model constants but is, like the strain dependent term, motivated rather than derived. Fortunately, these two modifications are not large in most flow situations. The bulk of the dissipation model is carried by the term $\tilde{\varepsilon}\frac{F}{1+F}\frac{2}{3}\delta_{ij}K + \tilde{\varepsilon}\frac{1}{1+F}R_{ij}$. This model satisfies an RDT limit and is realizable in the 2C limit. It agrees reasonably well with data from axisymmetric expansion at both small and large anisotropies. The key innovation in this term of the model is the functional form of the blending parameter *f*. It is suggested that the common practice of expanding parameters in simple polynomial series can be detrimental. Such expansions do not perform well when the expansion variable (such as F) is O(1).

References

1. S. B. Pope, *Turbulent Flows*, Cambridge University Press, 2000.
2. P. A. Durbin & B. A. Pettersson Reif , *Statistical Theory and Modeling for Turbulent Flows*. Wiley & Sons, 2001.
3. P. Bradshaw & J. B. Perot, A Note on the Turbulent Dissipation Rate in the Viscous Wall Region, Physics of Fluids A, **5** (12), 1993.
4. B. E. Launder, G. J. Reece & W. Rodi, "Progress in the development of a Reynolds stress turbulence closure", J. Fluid Mech. **68**, 537-566 (1975).
5. J. L. Lumley, "Computation modeling of turbulent flows", Adv. Appl. Mech. **18**, 126-176. (1978)
6. A. N. Kolmogoroff, "The local structure of turbulence in incompressible viscous fluid for very large Reynolds number," Dokl. Akad. Nauk SSSR, **30**, 301-305 (1941).
7. S. G. Saddoughi and S. V. Veeravalli, "Local isotropy in turbulent boundary layers at high Reynolds number," J. Fluid Mech. **268**, 333 -372 (1994).
8. S. Tavoularis and S. Corrsin, "Analytical methods for the development of Reynolds-stress closure in turbulence," J. Fluid Mech. **104**, 311-347 (1984).
9. W. K. George & H. J. Hussein, "Locally axisymmetric turbulence", J. Fluid Mech. **233**, 1-23 (1991).
10. M. Hallbäck, J. Groth & A. V. Johansson, "A Reynolds stress closures for the dissipation in anisotropic turbulent flows," 7th Symposium on Turbulent Shear Flows, Stanford University, August. (1989).

11. M. Hallbäck, J. Groth & A. V. Johansson, "An algebraic model for nonisotropic turbulent dissipation rate in Reynolds stress closures," Phys. Fluids, **2** (10, 1859-1866, (1990).
12. P. A. Durbin and C. G. Speziale, "Local anisotropy in strained turbulence at high Reynolds numbers", ASME J. Fluids Eng. **113**, 707-709 (1991).
13. J.G. Brasseur, "Comments on the Kolmogorov hypothesis of isotropy in the small scales," *AIAA* Paper 91-0230 (1991).
14. J. L. Lumly and G. R. Newman, "The return to isotropy of homogeneous turbulence," J. Fluid Mech. **82**, 161-178 (1977).
15. J. Rotta, "Stastische theorie nichthomegener turbulenz I," Z. für Physik **129**, 547-572 (1951).
16. D. Naot, A. Shavit & M. Wolfstein, "Two-point correlation model and the redistribution of Reynolds stresses," Phys. Fluids **16**, 738-743, (1973).
17. K. Hanjalic & B. E. Launder, "Contribution towards a Reynolds-stress turbulence closure for low-Reynolds-number turbulence," J. Fluid Mech. **74**, 593-610 (1976).
18. N. N. Mansour, J. Kim & P. Moin, "Reynolds-stress and dissipation-rate budgets in a turbulent channel flow," J. Fluid Mech. **194**, 15-44 (1988).
19. M. Hallbäck, A. V. Johansson and A. D. Burden, "Transition and turbulence modeling," Hallbäck, Johansson, Henningson & Alfredsson, eds., Kluwer Academic Publishers, 81-154, (1996).
20. Y. G. Lai & R. M. C. So, "On near-wall turbulent flow," J. Fluid Mech. **221**, 641-673, (1990).
21. B. E. Launder and B. L. Li, "On the elimination of wall topography parameters from second moment closure," Phys. Fluids **6**, 537-566 (1994).
22. C. G. Speziale and T. B. Gatski, "Analysis and modeling of anisotropies in the dissipation rate of turbulence," J. Fluid Mech. **344**, 155-180 (1997).
23. J. B. Perot "Shear-Free Turbulent Boundary Layers: Physics and Modeling," Ph.D Thesis, Stanford University Tech. Report TF60 (1993).
24. T. Sjögren and A. V. Johansson, "Development and calibration of algebraic nonlinear models for terms in the Reynolds stress transport equation," Phys. Fluids **12**, 1554-1572 (2000).
25. W. C. Reynolds, "Physical and analytical foundations, concepts, and new directions in turbulence modeling and simulation," In *Turbulence Models and their Applications*. Editions Eyrolles, 61 Bd Saint-Germain Paris 2 (1984).
26. M. Tagawa, Y. Nagano and T. Tsuji, "Turbulence model for dissipation components of Reynolds stresses," In *Eighth Sym. Turbulence Shear Flows*, Munich, Germany 29-3-1 (1991).
27. M. Oberlack, "Non-isotropic dissipation in non-homogeneous turbulence", J. Fluid Mech **350**, 351-374 (1997)
28. J. B. Perot & P. Moin, "Shear-Free Turbulent Boundary Layers, Part 2: New concepts for Reynolds stress transport equation modelling of inhomogeneous flows," J. Fluid Mech. **295**, 229-245 (1995).
29. J. B. Perot and P. Moin, "A Near Wall Model for the Dissipation Tensor," Eleventh Australasian Fluid Mechanics Conference, Hobart, Tasmania, Australia, 13-18 (1992).

30. B. Launder and W. C. Reynolds, "Asymptotic near-wall stress dissipation rates in a turbulent flow," Phys. Fluids, **26**, 1157-1158 (1983).
31. S. G. Speziale, "Analytical methods for the development of Reynolds stress closure in turbulence," Annual Review of Fluid Mechanics **23**, 107-157 (1991)
32. S. C. Crow, "Viscoelastic properties of fine grained incompressible turbulence," J. Fluid Mech. **33**, 1-20 (1968).
33. M. J. Lee and W. C. Reynolds, "Numerical experiments on the structure of homogeneous turbulence," Standford University Tech. Rep TF-24 (1985).
34. B. E. Launder and B. I.Sharma, "Application of the Energy-Dissipation Model of Turbulence to the Calcualtion of Flow Near a Spinning Disc", Letters in Heat and Mass Transfer, **1**, 131-138 (1974).
35. J. B. Perot and P. Moin, "Shear-Free Turbulent Boundary Layers, Part I: Physical Insights into Near Wall Turbulence," J. Fluid Mech. **295**, 199-227 (1995).
36. R. D. Moser, J. Kim and N. Mansour, "Direct numerical simulation of turbulent channel flow up to Re=590" Phys. Fluids. **11**, 943-945, (1999)
37. Kristoffersen, R., Andersson, H.I. 1993 "Direct simulations of low-Reynolds-number turbulent flow in a rotating channel" *J. Fluid Mech.*, **256**, 163-197.
38. H. Le, P. Moin, and J.Kim, "Direct numerical simulation of turbulent flow over a backward-facing step," J. Fluid Mech. **330**, 349-374, (1997).
39. S. Natu, " A Reynolds stress transport model for the near wall region," Masters Thesis, University of Massachusetts, Amherst, (2003).

Appendix F: Determination of Model Constants

To callibrate other model constants like , C_{p2}^{s}, C_{p2}^{w} and C_{p2}^{*} ,we used steady state DNS data for channel flow (Re = 590). First we backed out the constants using the equation (14) of the report for each Reynold stress assuming C_{p1}.

Using the equation (14) for R_{33}, we get,

$$0 = C_{p2}^{S}\left(\frac{P}{k}\overline{R_{33}}\right) + C_{p1}\left(\frac{2}{3}Ti\,\delta_{33} - Ti\,\overline{R_{33}}\right) + \overline{P_{33}} - \overline{R_{33}P} + \frac{\partial}{\partial x_j}\left[(\nu + \nu_T)\frac{\partial \overline{R_{33}}}{\partial x_j}\right] - 2\upsilon\frac{1}{K}\frac{\partial K}{\partial x_k}\frac{\partial(\overline{R_{33}})}{\partial x_k} - 2\nu\left[\frac{(\frac{\partial\sqrt{F}}{\partial x_s})(\frac{\partial\sqrt{F}}{\partial x_t})\overline{R_{st}}}{F}\right]\left[\delta_{33} - \frac{3}{2}\overline{R_{33}}\right]\} \quad \text{(F.1)}$$

Using equation (F.1), we can get the expected value of C_{p2}^{s}. After that if we put this calculated value of C_{p2}^{s} in equation (14) and solve the equation for R_{11} we will get the expected value for C_{p2}^{w}.

$$0 = C_{P2}^{S\ \text{calculated}}\left(2S_{12}\overline{R_{12}} + \frac{P}{k}\overline{R_{11}}\right) + C_{P2}^{W}\left(2W_{12}\overline{R_{12}}\right) + C_{P1}\left(\frac{2}{3}Ti\,\delta_{11} - Ti\,\overline{R_{11}}\right) + \overline{P_{11}} - \overline{R_{11}P} + \frac{\partial}{\partial x_j}\left[(\nu + \nu_T)\frac{\partial \overline{R_{11}}}{\partial x_j}\right] - 2\upsilon\frac{1}{K}\frac{\partial K}{\partial x_k}\frac{\partial(\overline{R_{11}})}{\partial x_k} - 2\nu\left[\frac{(\frac{\partial\sqrt{F}}{\partial x_s})(\frac{\partial\sqrt{F}}{\partial x_t})\overline{R_{st}}}{F}\right]\left[\delta_{11} - \frac{3}{2}\overline{R_{11}}\right]\} \quad \text{(F.2)}$$

Using calculated values C_{p2}^{s} and C_{p2}^{w} from equation (F.1) and (F.2) and then solving for R_{12}, we get expected value of C_{p2}^{*}, given by the equation (F.3),

$$0 = C_{P2}^{S\ calculated}\left(\frac{\partial U}{\partial x_2}(\overline{R_{22}}+\overline{R_{11}})+\frac{\mathrm{P}}{\mathrm{k}}\overline{R_{12}}\right)+C_{P2}^{W\ calculated}\frac{\partial U}{\partial x_2}(\overline{R_{22}}-\overline{R_{11}})$$
$$+C_{P1}\left(0\text{-Ti}\ \overline{R_{mn}}\right)+\overline{P_{12}}-\overline{R_{12}P}$$
$$+C_{P2}^{*}\ \mathrm{S}_{12}+\frac{\partial}{\partial x_j}\left[(\nu+\nu_T)\frac{\partial\overline{R_{12}}}{\partial x_j}\right] \qquad \text{(F.3)}$$
$$-2\upsilon\frac{1}{K}\frac{\partial K}{\partial x_k}\frac{\partial(\overline{R_{12}})}{\partial x_k}-2\nu[\frac{(\frac{\partial\sqrt{F}}{\partial x_s})(\frac{\partial\sqrt{F}}{\partial x_t})\overline{R_{st}}}{F}][0\ -\ \frac{3}{2}\overline{R_{12}}]\}$$

Then we tried to model these constants using different scalar quantities like F and α. First we matched the values from different combination of these scalar varients with the expected values and then tryied to use them to run the model. After doing this excercise for number combinations, the best results we got for the match and for the simulation of channel flow (Re=590) using these constant in the model are shown in Figures 1, 2 and 3.

The modeled constants are,

$$C_{p2}^{s}=\frac{\nu_T}{\nu+\nu_T}-0.2\mathrm{F} \qquad C_{p2}^{w}=\frac{\nu_T}{\nu+\nu_T}-0.4\mathrm{F} \qquad \text{(F.4)}$$
$$C_{p2}^{*}=0.2F^2-0.006\frac{P}{\hat{\varepsilon}}$$

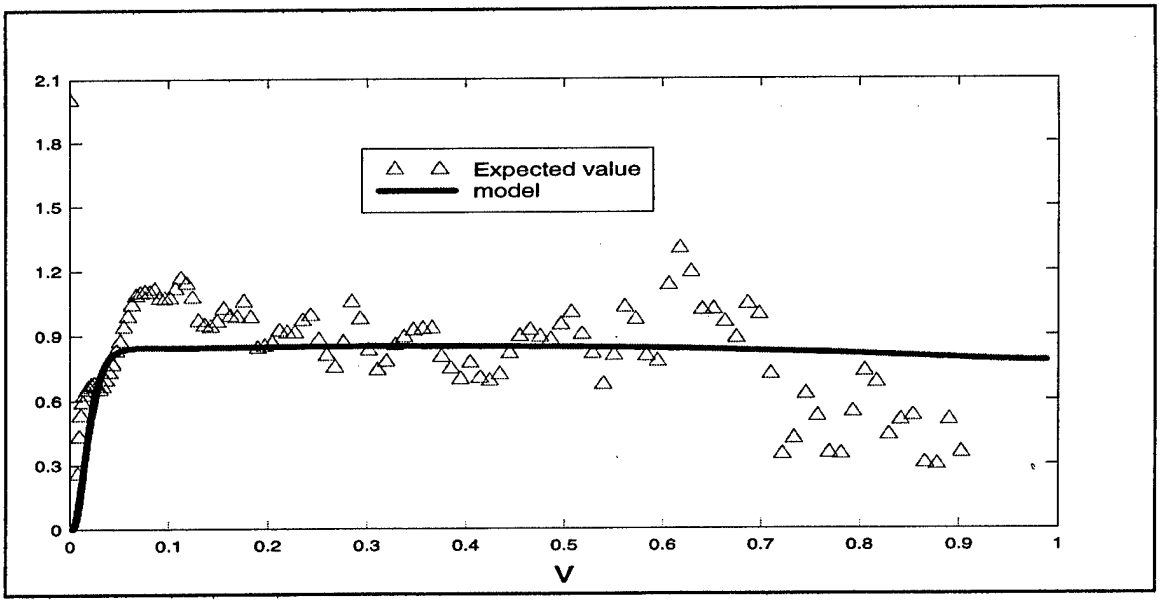

Figure 1: Backed out value of C_{p2}^{s} from DNS data(channel flow 590) compared with modeled value

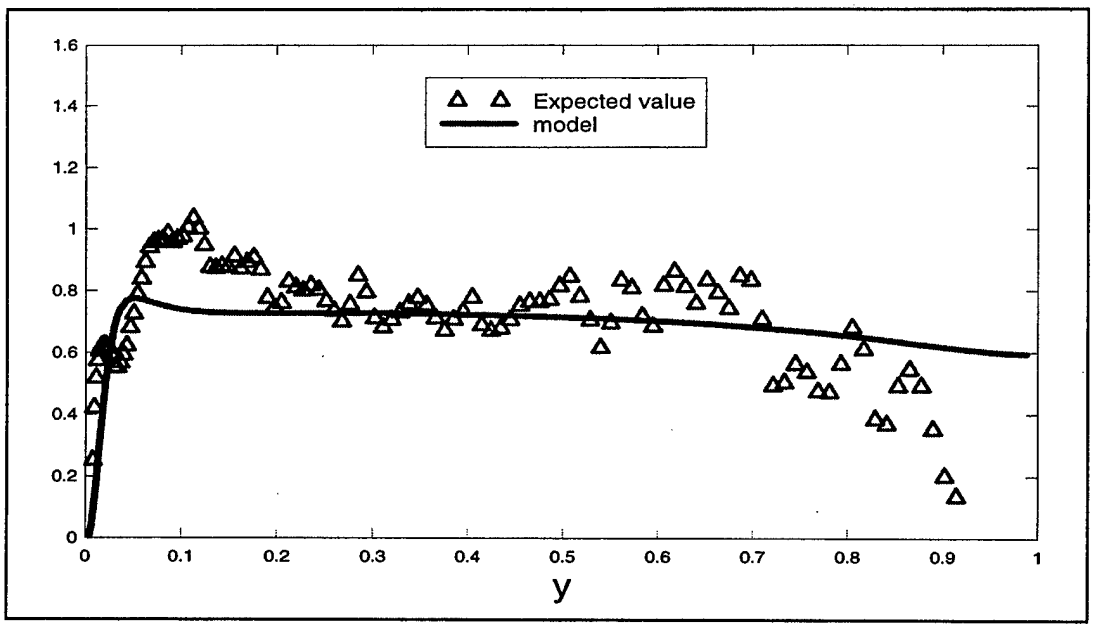

Figure 2: Backed out value of C_{p2}^{w} from DNS data(channel flow 590) compared with modeled value

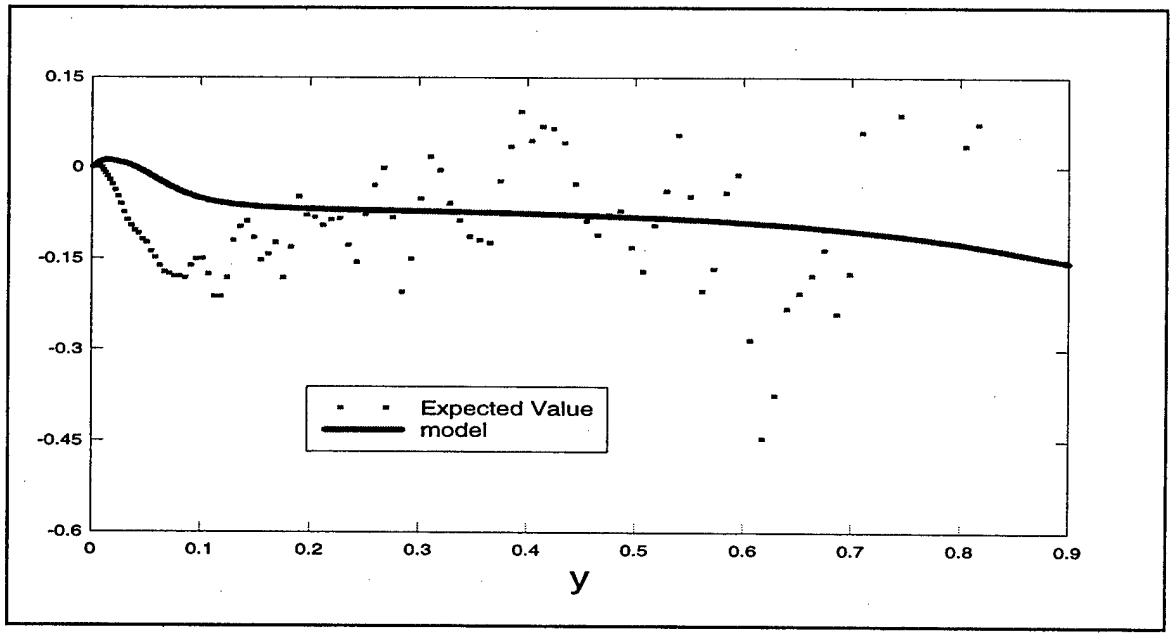

Figure 3: Backed out value of C_{p2}^{*} from DNS data(channel flow 590) compared with modeled value

Appendix G: PDF Model Results in Channel Flow

The simulation of the proposed RST model has been done for channel flow at different Reynolds numbers, to check the validity of the proposed model for dissipation tensor and pressure strain. The following figures 1 and 2 show the resulting Reynold stresses from the simulation using the proposed RST model till we get a steady state answer for the channel flow (Re = 590)

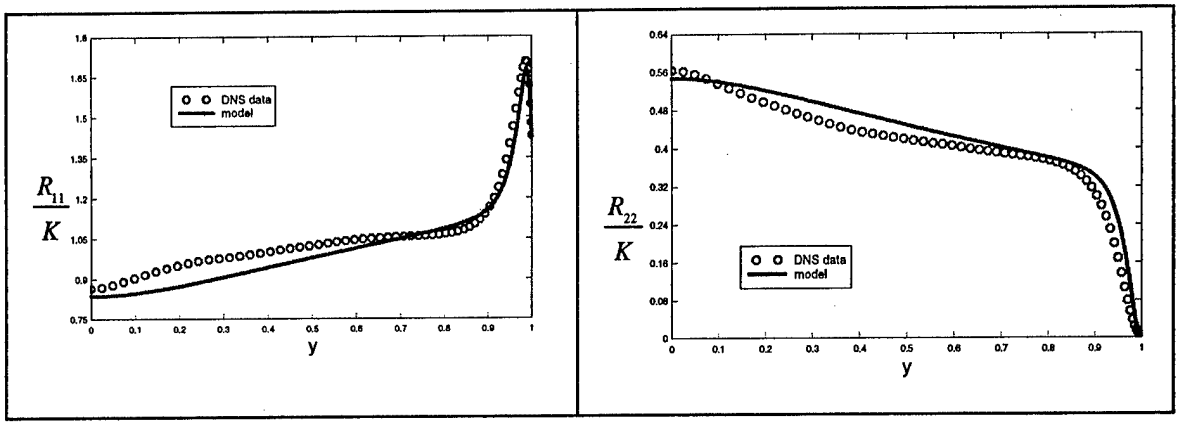

Figure 1 (a)Channel Flow(Re = 590) Figure 1(b)Channel Flow(Re = 590)

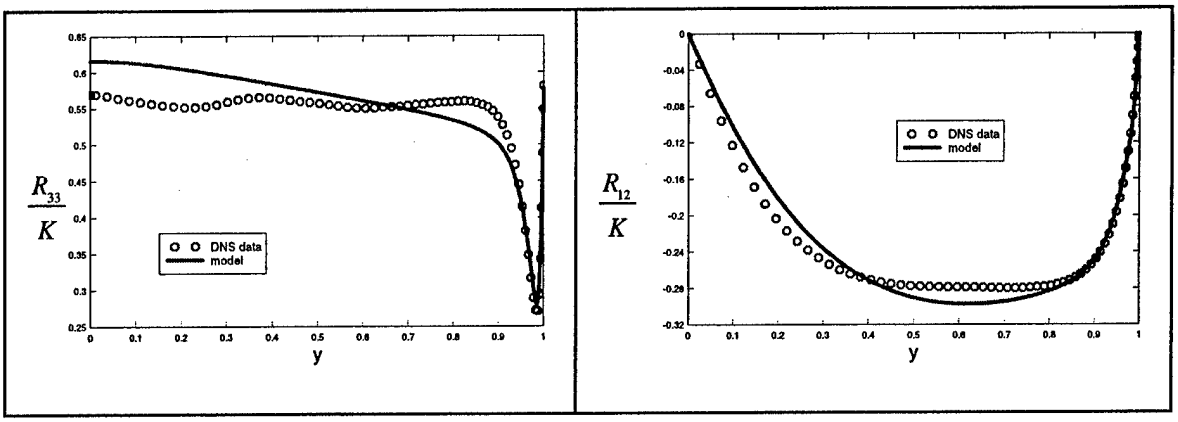

Figure 2 (a)Channel Flow(Re = 590) Figure 2(b)Channel Flow(Re = 590)

After getting R_{ij}/K, we simlply multiplied it by K to get only R_{ij} and then compared it with DNS data. Following figures 3(a), 3(b), 4(a) and 4(b) show the prediction.

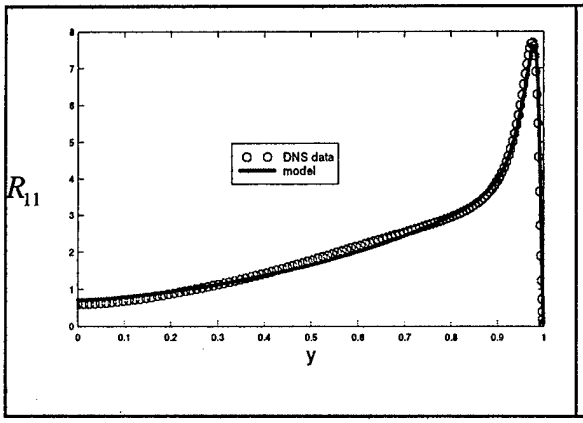

Figure 3 (a)Channel Flow(Re = 590)

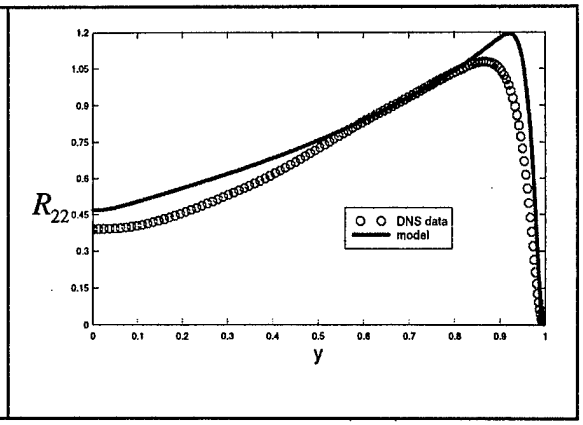

Figure 3 (b)Channel Flow(Re = 590)

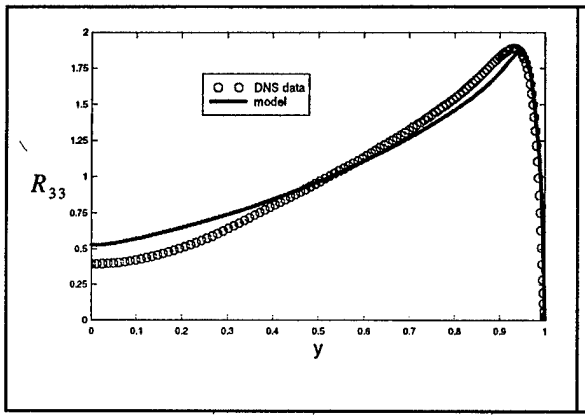

Figure 4 (a)Channel Flow(Re = 590)

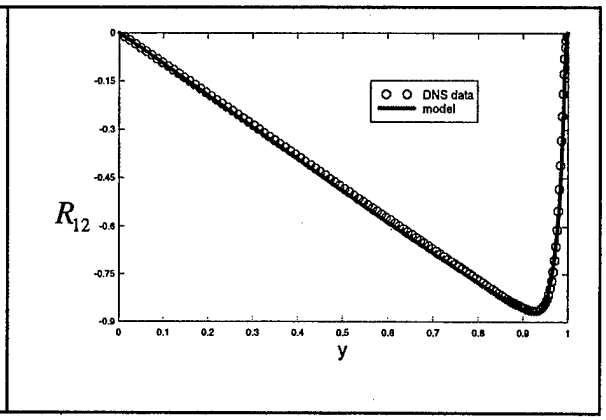

Figure 4(b)Channel Flow(Re = 590)

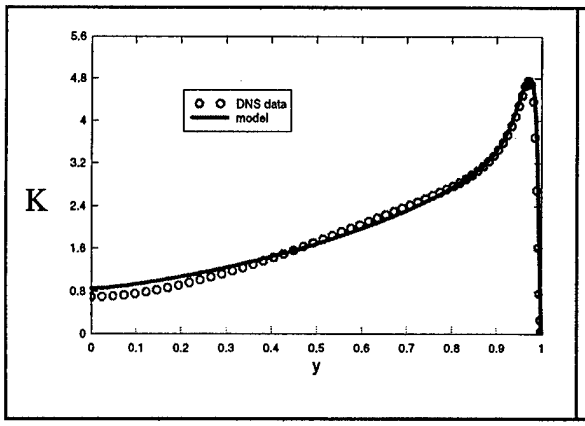

Figure 5 (a)Channel Flow(Re = 590)

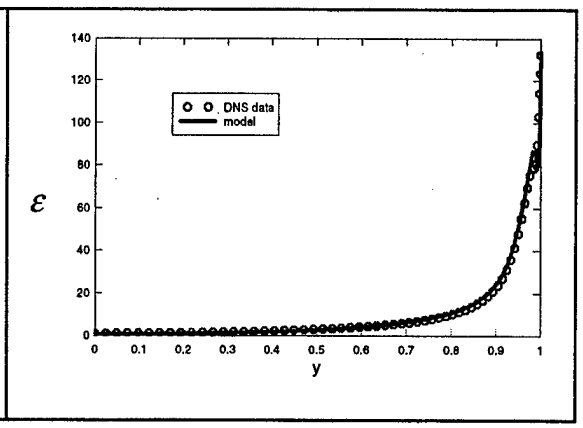

Figure 5(b)Channel Flow(Re = 590)

As can be seen from above figures, the predictions from the model match quite accurately with the DNS data. All the Reynolds stresses are modeled very well. The most important prediction for a turbulence model is the average velocity. Figure 6 shows model predictions of horizontal velocity with DNS data.

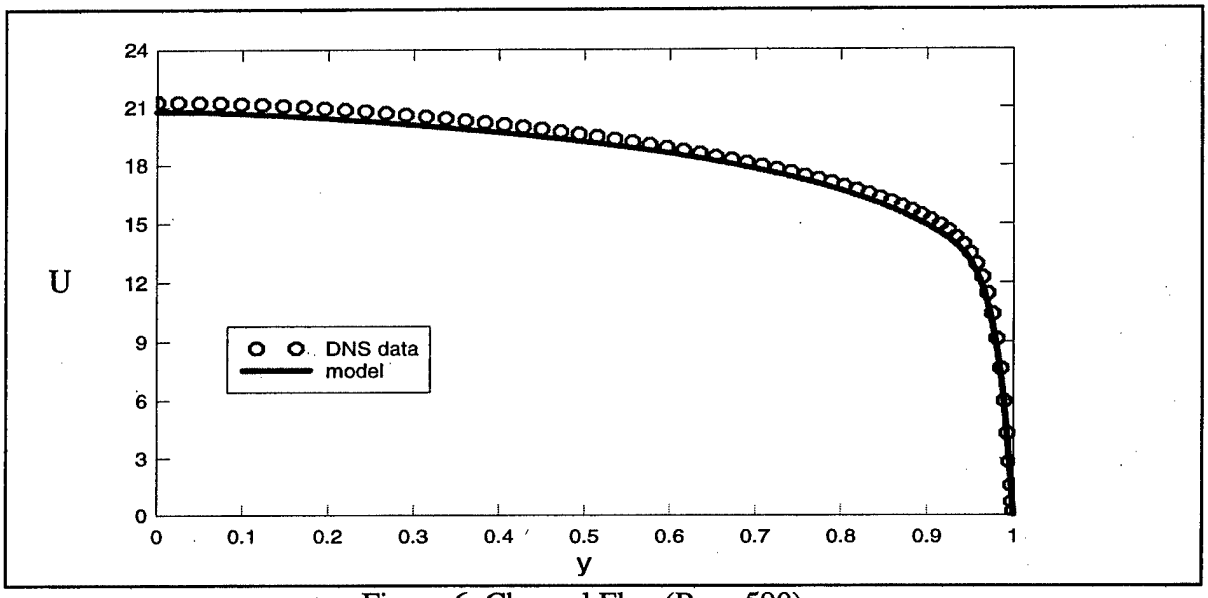

Figure 6 Channel Flow(Re = 590)

We also tried to simulate channel flow (Re= 395) using the model, to check the model predictions. Results are shown below.

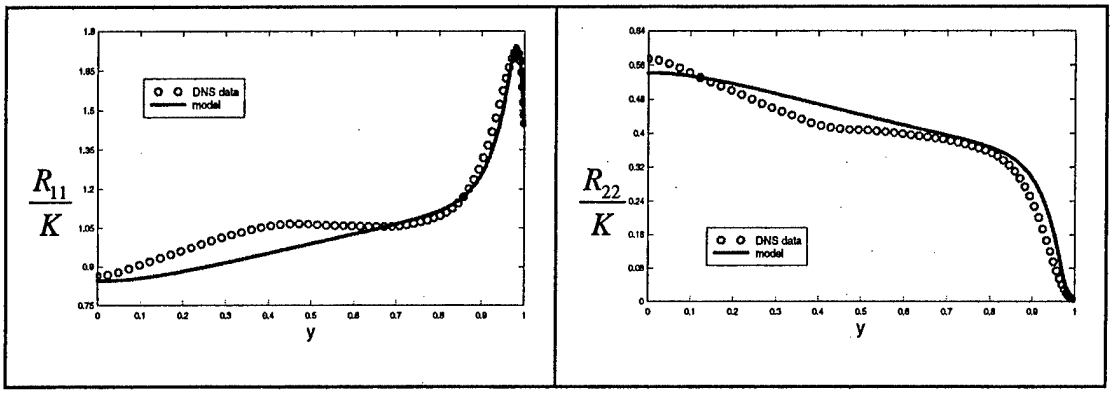

Figure 7 (a)Channel Flow(Re = 395) Figure 7(b)Channel Flow(Re = 395)

$\frac{R_{33}}{K}$ $\frac{R_{12}}{K}$

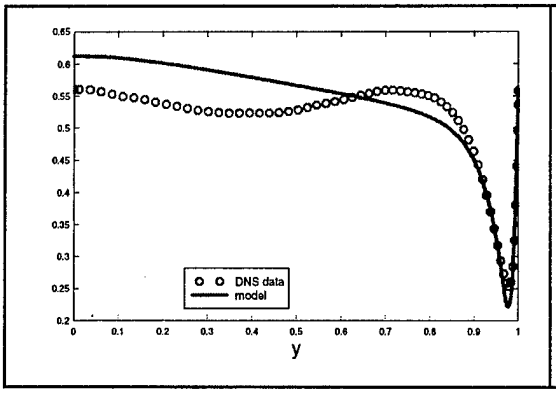

Figure 8 (a)Channel Flow(Re = 395)

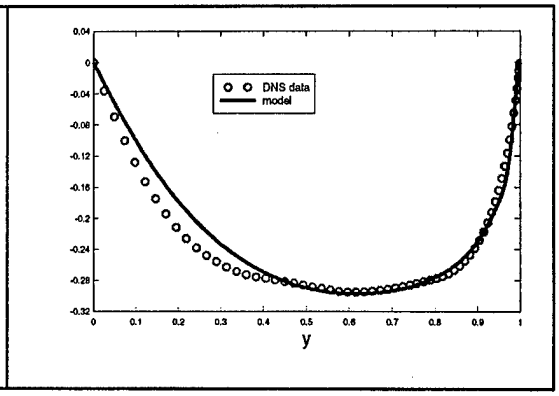

Figure 8(b)Channel Flow(Re= 395)

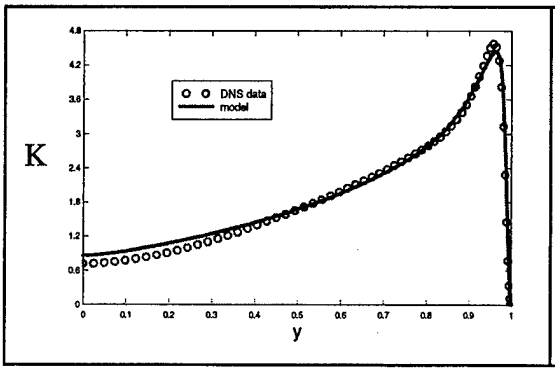

Figure 9 (a)Channel Flow(Re = 395)

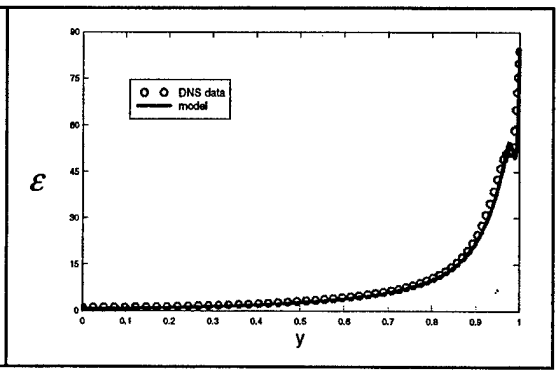

Figure 9(b)Channel Flow(Re = 395)

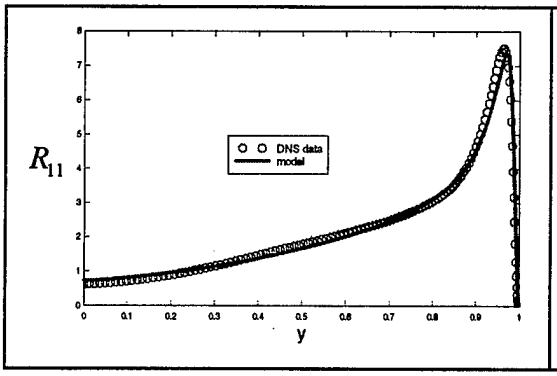

Figure 10 (a)Channel Flow(Re = 395)

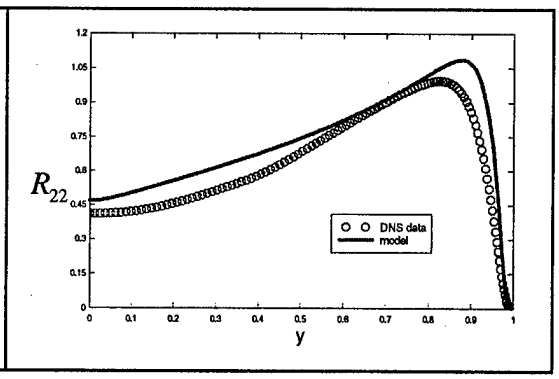

Figure 10(b)Channel Flow(Re = 395)

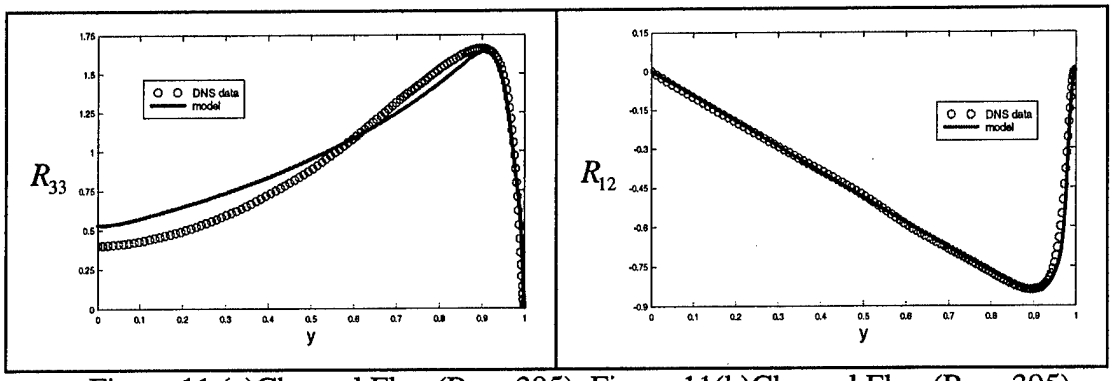

Figure 11 (a)Channel Flow(Re = 395) Figure 11(b)Channel Flow(Re = 395)

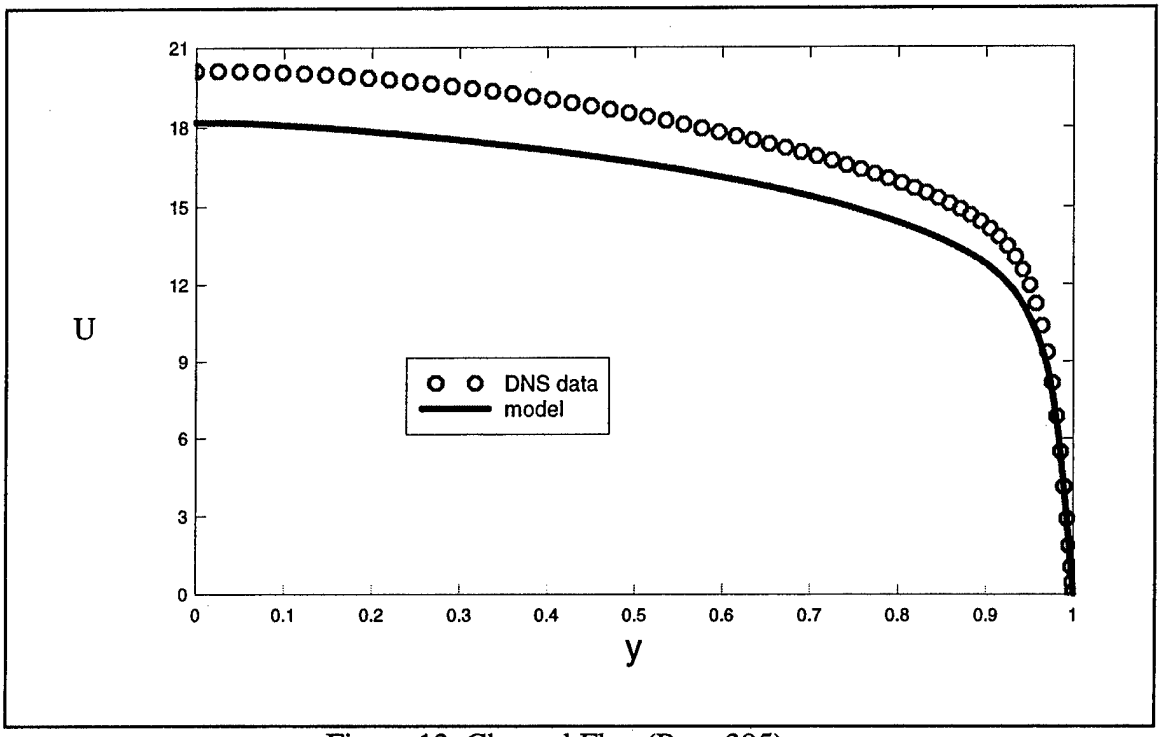

Figure 12 Channel Flow(Re = 395)

Appendix H: PDF Model Results for Homogeneous Shear

The eddy collision model has been applied to a number of homogeneous shear flows. These are experimental or DNS cases. The model given by equation 1 predicts all but the rotating cases reasonably well.

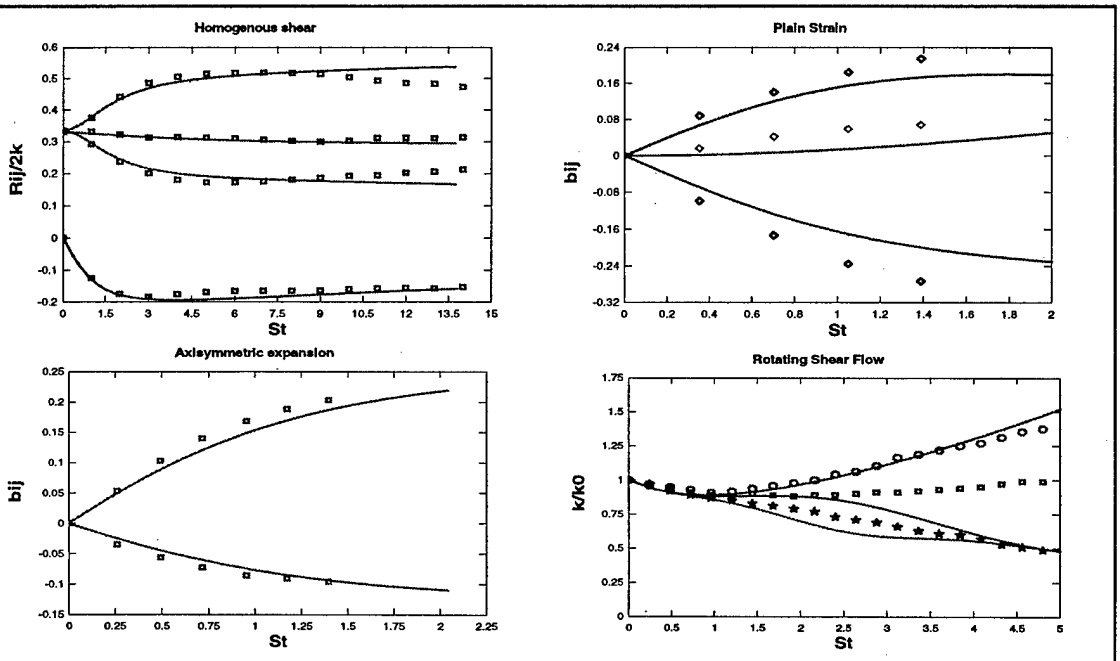

Figure 4: Eddy collision model applied to homogeneous shear flows. Symbols are experimental or DNS data. Lines are the model predictions.

The model has also been applied to turbulent channel flow at a shear stress Reynolds number of 590. The Reynolds stresses and mean flow are given in figure 5.

The fast pressure-strain constants in the current eddy collision model are given by,

$$C_{p2s} = \frac{\nu_T}{\nu + \nu_T} - 0.2\mathrm{F} \quad C_{p2w} = \frac{\nu_T}{\nu + \nu_T} - 0.4\mathrm{F} \quad C_{p2*} = 0.2F^2 - 0.006\frac{P}{\hat{\varepsilon}}$$

where $\nu_T = C_\mu \frac{Fk^2}{\hat{\varepsilon}}$ and $F = \text{determinant}(R_{ij}/k)$ where the Reynolds stress tensor is exactly given by $R_{ij} = \int v_i' v_j' f$ and the modified dissipation is given by $\hat{\varepsilon} = \varepsilon - 2\upsilon \frac{\partial(K^{1/2})}{\partial x_k} \frac{\partial(K^{1/2})}{\partial x_k}$. The transport constant is $C_\mu = 0.15$.

The dissipation constants are standard values with modifications for low Reynolds numbers and high rotation rates.

$$C_{\varepsilon 1} = 1.45\, C_r \quad C_{\varepsilon 2} = C_r(1.83 - 0.166 e^{-\frac{K^2}{4\nu\varepsilon}})$$

$$C_r = \frac{1 + 0.21\,Ro}{1 + 0.12\,Ro} \quad Ro = \frac{\varepsilon}{K}(W_{ij}W_{ij})^2$$

$$C_{\varepsilon 3} = C_\mu(0.33 + 0.5\frac{P}{\varepsilon})$$

In the oriented model, the dissipation transport equation is not necessary ($\varepsilon = \nu k / z^2$).

Appendix I: BGK moments

Conservation of mass (or probability) requires that the integral of the PDF be equivalent to one for all time. This means that the integral of its time derivative must be zero. Starting from the BGK model for the time derivative of distribution gives the following expression.

$$\int \frac{\partial f}{\partial t} \partial v = -\frac{\varepsilon}{(K-\hat{K})} \int \left(f - (\tfrac{4}{3}\pi\hat{K})^{-3/2} e^{-\frac{3v'_n v'_n}{4\hat{K}}} \right) \partial v \tag{I.1}$$

Since both distributions integrate to 1, we can see that

$$\frac{\partial}{\partial t} \int f \partial v = 0 \tag{I.2}$$

Conservation of momentum requires that no mean flow be created by the relaxation process. The mean velocity of the flow is equivalent to the first moment of the PDF. By taking the integral over all velocity space, we can show that.

$$\int v_i \frac{\partial f}{\partial t} \partial v = -\frac{\varepsilon}{(K-\hat{K})} \int v_i \left(f - (\tfrac{4}{3}\pi\hat{K})^{-3/2} e^{-\frac{3v'_n v'_n}{4\hat{K}}} \right) \partial v \tag{I.3}$$

Using the fact that the velocity is an independent variable (from time) and splitting the velocity into its mean and fluctuating parts gives.

$$\frac{\partial}{\partial t} \int v_i f \partial v = -\frac{\varepsilon}{(K-\hat{K})} \left\{ \int v_i f \partial v - u_i \int (\tfrac{4}{3}\pi\hat{K})^{-3/2} e^{-\frac{3v'_n v'_n}{4\hat{K}}} \partial v - \int v'_i (\tfrac{4}{3}\pi\hat{K})^{-3/2} e^{-\frac{3v'_n v'_n}{4\hat{K}}} \partial v \right\} \tag{I.4}$$

By definition $\int v_i f \partial v = u_i$. The second integral on the right hand side is equal to 1 and the last integral is zero since it has an odd integrand, so finally

$$\frac{\partial}{\partial t} u_i = -\frac{\varepsilon}{(K-\hat{K})} \{ u_i - u_i - 0 \} = 0 \tag{I.5}$$

The Reynolds transport equation is obtained by multiplying the PDF relation equation by $v'_i v'_j$ and then integrating over all velocity space.

$$\int v'_i v'_j \frac{\partial f}{\partial t} \partial v = \frac{\partial R_{ij}}{\partial t} = -\frac{\varepsilon}{(K-\hat{K})} \int v'_i v'_j \left(f - (\tfrac{4}{3}\pi\hat{K})^{-3/2} e^{-\frac{3v'_n v'_n}{4\hat{K}}} \right) \partial v \tag{I.6}$$

This then becomes

$$\frac{\partial}{\partial t} \int v'_i v'_j f \partial v = -\frac{\varepsilon}{(K-\hat{K})} \left\{ \int v'_i v'_j f \partial v - (\tfrac{4}{3}\pi\hat{K})^{-3/2} \int v'_i v'_j e^{-\frac{3v'_n v'_n}{4\hat{K}}} \partial v \right\} \tag{I.7}$$

Since $\int v'_i v'_j f \partial v = R_{ij}$ by definition, and the last integral must be isotropic

$$\frac{\partial R_{ij}}{\partial t} = -\frac{\varepsilon}{(K-\hat{K})} \left\{ R_{ij} - \tfrac{2}{3}\hat{K}\delta_{ij} \right\} \tag{I.8}$$

Appendix J: Relaxation Model Moments:

Here we verify conservation of mass for the relaxation models derived in Section 4 of Appendix C. The method is the same as before starting from the relaxation model for the PDF.

$$\int\frac{\partial f}{\partial t}\partial v=\int C_M\left(\frac{3\varepsilon}{2K}\left(\frac{4}{3}\pi\hat{K}\right)^{-3/2}e^{-\frac{3\hat{v}'_n\hat{v}'_n}{4\hat{K}}}-\frac{3\varepsilon}{2K}\frac{\tilde{v}'_n\tilde{v}'_n}{2K+(u-\tilde{u})^2}f\right)\partial v \tag{J.1}$$

with $\hat{v}'_i=v_i-\hat{u}_i$, $\tilde{v}'_i=v_i-\tilde{u}_i$.

$$\int\frac{\partial f}{\partial t}\partial v=C_M\frac{3\varepsilon}{2K}-C_M\frac{3\varepsilon}{2K}\int\frac{(v'_n+u_n-\tilde{u}_n)(v'_n+u_n-\tilde{u}_n)}{2K+(u-\tilde{u})^2}f\partial v=0 \tag{J.2}$$

Since $\int v'_n f\partial v=0$ we get

$$\int\frac{\partial f}{\partial t}\partial v=C_M\frac{3\varepsilon}{2K}-C_M\frac{3\varepsilon}{2K}\frac{1}{2K+(u-\tilde{u})^2}\int\left((u_n-\tilde{u}_n)(u_n-\tilde{u}_n)+v'_n v'_n\right)f\partial v=0\,. \tag{J.3}$$

The integrals can be evaluated to give

$$\int\frac{\partial f}{\partial t}\partial v=C_M\frac{3\varepsilon}{2K}-C_M\frac{3\varepsilon}{2K}\frac{(u-\tilde{u})^2}{2K+(u-\tilde{u})^2}-C_M\frac{3\varepsilon}{2K}\frac{2K}{2K+(u-\tilde{u})^2}=0 \tag{J.4}$$

Similarly, to verify conservation of momentum we continue as follows.

$$\int v_i\frac{\partial f}{\partial t}\partial v=\frac{\partial u_i}{\partial t}=\int C_M v_i\left(\frac{3\varepsilon}{2K}\left(\frac{4}{3}\pi\hat{K}\right)^{-3/2}e^{-\frac{3\hat{v}'_n\hat{v}'_n}{4\hat{K}}}-\frac{3\varepsilon}{2K}\frac{\tilde{v}'_n\tilde{v}'_n}{2K+(u-\tilde{u})^2}f\right)\partial v \tag{J.5}$$

expanding $\tilde{v}'_n=(u_n-\tilde{u}_n)+v'_n$ and $v_i=u_i+v'_i$ gives

$$\frac{\partial u_i}{\partial t}=C_M\frac{3\varepsilon}{2K}\hat{u}_i-C_M\frac{3\varepsilon}{2K}\frac{1}{2K+(u-\tilde{u})^2}\left((u-\tilde{u})^2u_i+2(u_n-\tilde{u}_n)R_{in}+2Ku_i+\int v'_i v'_n v'_n f\partial v\right) \tag{J.6}$$

Conservation requires the above equation be equal to zero, this implies that

$$\left(2K+(u-\tilde{u})^2\right)\left(\hat{u}_i-u_i\right)=2R_{in}(u_n-\tilde{u}_n)+\int v'_i v'_n v'_n f\partial v \tag{J.7}$$

From Appendix I, we see that if f is Gaussian, the last term on the right goes to zero, and $u_i=\tilde{u}_i=\hat{u}_i$ confirming conservation of momentum for Gaussian PDFs. For non-Gaussian PDFs the above relation must be satisfied.

The Reynolds stress transport equation is also derived similarly

$$\int v'_i v'_j\frac{\partial f}{\partial t}\partial v=\frac{\partial R_{ij}}{\partial t}=\int C_M v'_i v'_j\left(\frac{3\varepsilon}{2K}\left(\frac{4}{3}\pi\hat{K}\right)^{-3/2}e^{-\frac{3\hat{v}'_n\hat{v}'_n}{4\hat{K}}}-\frac{3\varepsilon}{2K}\frac{\tilde{v}'_n\tilde{v}'_n}{2K+(u-\tilde{u})^2}f\right)\partial v \tag{J.8}$$

By substituting in the relations $\hat{v}'_i=v_i-\hat{u}_i$ and $\tilde{v}'_i=v_i-\tilde{u}_i$ the integrals can be reduced.

$$\begin{aligned}\frac{\partial R_{ij}}{\partial t}=&C_M\frac{3\varepsilon}{2K}\int\left(\hat{v}'_i+\left(\hat{u}_i-u_i\right)\right)\left(\hat{v}'_j+\left(\hat{u}_j-u_j\right)\right)\left(\frac{4}{3}\pi\hat{K}\right)^{-3/2}e^{-\frac{3\hat{v}'_n\hat{v}'_n}{4\hat{K}}}\partial v\\&-C_M\frac{3\varepsilon}{2K}\frac{1}{2K+(u-\tilde{u})^2}\int v'_i v'_j\left((u_n-\tilde{u}_n)(u_n-\tilde{u}_n)+2v'_n(u_n-\tilde{u}_n)+v'_n v'_n\right)f\partial v\end{aligned} \tag{J.9}$$

since $\int\hat{v}'_i\left(\frac{4}{3}\pi\hat{K}\right)^{-3/2}e^{-\frac{3\hat{v}'_n\hat{v}'_n}{4\hat{K}}}\partial v=0$ (due to the odd integrand), we get

$$\frac{\partial R_{ij}}{\partial t} = C_M \frac{3\varepsilon}{2K}\int\left(\hat{v}'_i\hat{v}'_j + \left(\hat{u}_i - u_i\right)\left(\hat{u}_j - u_j\right)\right)\left(\tfrac{4}{3}\pi\hat{K}\right)^{-3/2} e^{-\frac{3\hat{v}'_n\hat{v}'_n}{4\hat{K}}}\partial v$$
$$- C_M \frac{3\varepsilon}{2K}\frac{1}{2K+(u-\tilde{u})^2}\left((u-\tilde{u})^2 R_{ij} + 2(u_n-\tilde{u}_n)\int v'_i v'_j v'_n f\partial v + \int v'_i v'_j v'_n v'_n f\partial v\right) \quad \text{(J.10)}$$

The first integral is reduced in terms of 'hats'.

$$\frac{\partial R_{ij}}{\partial t} = C_M \frac{3\varepsilon}{2K}\left(\frac{2}{3}\hat{K}\delta_{ij} + \left(\hat{u}_i - u_i\right)\left(\hat{u}_j - u_j\right)\right)$$
$$- C_M \frac{3\varepsilon}{2K}\frac{1}{2K+(u-\tilde{u})^2}\left((u-\tilde{u})^2 R_{ij} + 2(u_n-\tilde{u}_n)\int v'_i v'_j v'_n f\partial v + \int v'_i v'_j v'_n v'_n f\partial v\right) \quad \text{(J.11)}$$

To ensure the correct dissipation of energy, we require that the model satisfies the equation $\frac{\partial K}{\partial t} = \frac{1}{2}\frac{\partial R_{ii}}{\partial t} = -\varepsilon$.

$$-\frac{1}{2}\frac{\partial R_{ii}}{\partial t} = \varepsilon = -C_M \frac{3\varepsilon}{2K}\left(\hat{K} + \frac{1}{2}\left(\hat{u}-u\right)^2\right)$$
$$+C_M \frac{3\varepsilon}{2K}\frac{1}{2K+(u-\tilde{u})^2}\left((u-\tilde{u})^2 K + (u_n-\tilde{u}_n)\int v'_i v'_i v'_n f\partial v + \frac{1}{2}\int v'_i v'_i v'_n v'_n f\partial v\right) \quad \text{(J.12)}$$

This can be simplified to

$$\hat{K} + \frac{1}{2}\left(\hat{u}-u\right)^2 + \frac{2K}{3C_M} =$$
$$\frac{1}{2K+(u-\tilde{u})^2}\left((u-\tilde{u})^2 K + (u_n-\tilde{u}_n)\int v'_i v'_i v'_n f\partial v + \frac{1}{2}\int v'_i v'_i v'_n v'_n f\partial v\right) \quad \text{(J.13)}$$

or finally

$$\left(\frac{\hat{K}}{K} + \frac{1}{2K}\left(\hat{u}-u\right)^2 + \frac{2}{3C_M}\right)\left(2K + (u-\tilde{u})^2\right) =$$
$$(u-\tilde{u})^2 + \frac{u_n-\tilde{u}_n}{K}\int v'_i v'_i v'_n f\partial v + \frac{1}{2K}\int v'_i v'_i v'_n v'_n f\partial v \quad \text{(J.14)}$$

For an elliptic Gaussian PDF the above equation reduces to

$$\frac{\hat{K}}{K} + \frac{2}{3C_M} = \frac{1}{4K^2}\int v'_i v'_i v'_n v'_n f\partial v = \frac{1}{4K^2}\left(R_{nn}R_{ii} + 2R_{ni}R_{ni}\right) \quad \text{(J.15)}$$

or alternatively

$$\frac{\hat{K}}{K} = 1 - \frac{2}{3C_M} + \frac{R_{ni}R_{ni}}{2K^2} \quad \text{(J.16)}$$

This can be rearranged to become

$$\frac{3}{2}C_M = \left(1 - \frac{\hat{K}}{K} + \frac{R_{ni}R_{ni}}{2K^2}\right)^{-1} \quad \text{(J.17)}$$

So if we assume Gaussian form for the PDF, the Reynolds transport equation can be written as follows.

$$\frac{\partial R_{ij}}{\partial t} = \frac{\varepsilon}{K}\left(1 - \frac{\hat{K}}{K} + \frac{R_{ni}R_{ni}}{2K^2}\right)^{-1}\left(\frac{2}{3}\hat{K}\delta_{ij}\right) - \frac{\varepsilon}{K}\left(1 - \frac{\hat{K}}{K} + \frac{R_{ni}R_{ni}}{2K^2}\right)^{-1}\frac{1}{2K}\left(R_{nn}R_{ij} + 2R_{ni}R_{nj}\right) \quad \text{(J.18)}$$

This simplifies to

$$\frac{\partial R_{ij}}{\partial t} = \frac{\varepsilon}{K}\frac{1}{1 - \frac{\hat{K}}{K} + \frac{R_{mn}R_{mn}}{2K^2}}\left(\frac{2}{3}\hat{K}\delta_{ij} - R_{ij} - \frac{R_{ni}R_{nj}}{K}\right) \quad \text{(J.19)}$$

Rearranging into the classic return model form gives

$$\frac{\partial R_{ij}}{\partial t} = -\frac{\varepsilon}{K}R_{ij} - \frac{\varepsilon}{K}\frac{\frac{\hat{K}}{K} - \frac{R_{mn}R_{mn}}{2K^2}}{1-\frac{\hat{K}}{K}+\frac{R_{mn}R_{mn}}{2K^2}}\left(R_{ij} - \frac{2}{3}K\delta_{ij}\right) + \frac{\varepsilon}{K^2}\frac{1}{1-\frac{\hat{K}}{K}+\frac{R_{mn}R_{mn}}{2K^2}}R_{mn}R_{mn}\frac{\delta_{ij}}{3} - \frac{\varepsilon}{K^2}\frac{1}{1-\frac{\hat{K}}{K}+\frac{R_{ni}R_{ni}}{2K^2}}R_{ni}R_{nj} \qquad \text{(J.20)}$$

And when written as follows, the values of C_R and C_N become apparent.

$$\frac{\partial R_{ij}}{\partial t} = -\frac{\varepsilon}{K}R_{ij} - \frac{\varepsilon}{K}\left(\frac{\frac{4}{3}+\frac{\hat{K}}{K} - \frac{R_{ni}R_{ni}}{2K^2}}{1-\frac{\hat{K}}{K}+\frac{R_{ni}R_{ni}}{2K^2}} + \frac{4}{3}\frac{-1}{1-\frac{\hat{K}}{K}+\frac{R_{ni}R_{ni}}{2K^2}}\right)\left(R_{ij} - \frac{2}{3}K\delta_{ij}\right) + \frac{\varepsilon}{K^2}\frac{-1}{1-\frac{\hat{K}}{K}+\frac{R_{ni}R_{ni}}{2K^2}}\left(R_{ni}R_{nj} - R_{ni}R_{ni}\frac{\delta_{ij}}{3}\right) \qquad \text{(J.21)}$$

Appendix K: Moments of a Gaussian PDF

If we have a PDF, f, of elliptic Gaussian shape we can write the PDF as

$$f = [(2\pi)^3 \det(R_{nm})]^{-1/2} e^{-\frac{1}{2}R^{-1}_{nm} v'_n v'_m} \tag{K.1}$$

Since only R_{ij} is a function of space, this implies that the derivative satisfies

$$-R_{kl}\frac{\partial f}{\partial v_k} = v'_l f \tag{K.2}$$

This allows us to write the third moment as a second moment and then apply the chain rule.

$$\int v'_i v'_n v'_m f \partial v = -R_{km}\int v'_i v'_n \frac{\partial f}{\partial v_k}\partial v = -R_{km}\int\left(\frac{\partial v'_i v'_n f}{\partial v_k} - f\frac{\partial v'_i v'_n}{\partial v_k}\right)\partial v \tag{K.3}$$

By Gauss's divergence theorem the first integral term goes to zero, since $f \rightarrow 0$ at infinity. Differentiating the second term gives,

$$\int v'_i v'_n v'_m f \partial v = R_{km}\int f\left(v'_i \delta_{nk} + v'_n \delta_{ik}\right)\partial v = R_{nm}\int v'_i f \partial v + R_{im}\int v'_n f \partial v = 0 \tag{K.4}$$

which is what we would expect since the PDF is an even function and the integrand is an odd function (cubic).

The expression (K.2) and the chain rule is also useful for evaluating the fourth moment of an elliptic Gaussian.

$$\int v'_m v'_n v'_i v'_j f d\mathbf{v} = -R_{kj}\int v'_m v'_n v'_i \frac{\partial f}{\partial v_k} d\mathbf{v} = R_{kj}\int f \frac{\partial v'_m v'_n v'_i}{\partial v_k} d\mathbf{v} \tag{K.6}$$

Taking the derivative gives the fourth moment in terms of the second moments

$$= R_{kj}\int f\left(v'_m v'_n \delta_{ik} + v'_n v'_i \delta_{mk} + v'_m v'_i \delta_{nk}\right) d\mathbf{v} = R_{mn}R_{ij} + R_{ni}R_{mj} + R_{mi}R_{nj} \tag{K.7}$$

Appendix L: General relaxation moments:

Here we verify conservation of mass for the more general relaxation models derived in Section 6 of Appendix C. The method is the same as before starting from the general relaxation model for the PDF, Eq. (C.33). Conservation of mass then requires that the right hand side of the zeroth moment be equal to zero.

$$\int\frac{\partial f}{\partial t}\partial v = C_M\,\frac{\varepsilon}{2K}\int\prod_{ii}[(2\pi)^3\det(\hat{R}_{nm})]^{-1/2}e^{-\frac{1}{2}\hat{R}^{-1}_{nm}\hat{v}'_n\,\hat{v}'_m}\partial v - C_M\,\frac{\varepsilon}{2K}\int\frac{\Pi_{in}\,R^{-1}_{im}\tilde{v}'_m\,\tilde{v}'_n}{1+(u_n-\tilde{u}_n)(u_m-\tilde{u}_m)\frac{\Pi_{in}}{\Pi_{pp}}R^{-1}_{im}}f\partial v \qquad \text{(L.1)}$$

$$\int\frac{\partial f}{\partial t}\partial v = C_M\,\frac{\varepsilon}{2K}\prod_{ii} - C_M\,\frac{\varepsilon}{2K}\frac{\Pi_{in}\,R^{-1}_{im}}{1+(u_n-\tilde{u}_n)(u_m-\tilde{u}_m)\frac{\Pi_{in}}{\Pi_{pp}}R^{-1}_{im}}\int\tilde{v}'_m\,\tilde{v}'_n\,f\partial v \qquad \text{(L.2)}$$

Substituting with $\tilde{v}'_i = v'_i + u_i - \tilde{u}_i$, and recalling that $\int v'_m f\partial v = 0$ gives

$$\int\frac{\partial f}{\partial t}\partial v = C_M\,\frac{\varepsilon}{2K}\prod_{ii} - C_M\,\frac{\varepsilon}{2K}\frac{\Pi_{in}\,R^{-1}_{im}}{1+(u_n-\tilde{u}_n)(u_m-\tilde{u}_m)\frac{\Pi_{in}}{\Pi_{pp}}R^{-1}_{im}}\int\left(v'_m v'_n+(u_m-\tilde{u}_m)(u_n-\tilde{u}_n)\right)f\partial v \qquad \text{(L.3)}$$

$$\int\frac{\partial f}{\partial t}\partial v = C_M\,\frac{\varepsilon}{2K}\prod_{ii} - C_M\,\frac{\varepsilon}{2K}\frac{\Pi_{in}\,R^{-1}_{im}}{1+(u_n-\tilde{u}_n)(u_m-\tilde{u}_m)\frac{\Pi_{in}}{\Pi_{pp}}R^{-1}_{im}}\left(R_{mn}+(u_m-\tilde{u}_m)(u_n-\tilde{u}_n)\right)=0 \qquad \text{(L.4)}$$

The momentum equation is the first moment

$$\frac{\partial u_p}{\partial t} = C_M\,\frac{\varepsilon}{2K}\prod_{ii}\int v_p[(2\pi)^3\det(\hat{R}_{nm})]^{-1/2}e^{-\frac{1}{2}\hat{R}^{-1}_{nm}\hat{v}'_n\,\hat{v}'_m}\partial v - C_M\,\frac{\varepsilon}{2K}\int\frac{\Pi_{in}\,R^{-1}_{im}\tilde{v}'_m\,\tilde{v}'_n}{1+(u_n-\tilde{u}_n)(u_m-\tilde{u}_m)\frac{\Pi_{in}}{\Pi_{pp}}R^{-1}_{im}}v_p f\partial v \qquad \text{(L.5)}$$

$$\frac{\partial u_p}{\partial t} = C_M\,\frac{\varepsilon}{2K}\prod_{ii}\hat{u}_p - C_M\,\frac{\varepsilon}{2K}\frac{\Pi_{in}\,R^{-1}_{im}}{1+(u_n-\tilde{u}_n)(u_m-\tilde{u}_m)\frac{\Pi_{in}}{\Pi_{pp}}R^{-1}_{im}}\int\left(v'_m+(u_m-\tilde{u}_m)\right)\left(v'_n+(u_n-\tilde{u}_n)\right)v_p f\partial v \qquad \text{(L.6)}$$

$$\begin{aligned}\frac{\partial u_p}{\partial t} = {} & C_M\,\frac{\varepsilon}{2K}\prod_{ii}\hat{u}_p - C_M\,\frac{\varepsilon}{2K}\frac{\Pi_{in}\,R^{-1}_{im}}{1+(u_n-\tilde{u}_n)(u_m-\tilde{u}_m)\frac{\Pi_{in}}{\Pi_{pp}}R^{-1}_{im}}\left(\int v'_m v'_n v'_p\,f\partial v + R_{mn}u_p\right)\\ & - C_M\,\frac{\varepsilon}{2K}\frac{\Pi_{in}\,R^{-1}_{im}}{1+(u_n-\tilde{u}_n)(u_m-\tilde{u}_m)\frac{\Pi_{in}}{\Pi_{pp}}R^{-1}_{im}}\left(R_{mp}(u_n-\tilde{u}_n)+R_{np}(u_m-\tilde{u}_m)+(u_m-\tilde{u}_m)(u_n-\tilde{u}_n)u_p\right)\end{aligned} \qquad \text{(L.7)}$$

Conservation of momentum therefore requires that

$$\begin{aligned}C_M\,\frac{\varepsilon}{2K}\prod_{ii}\hat{u}_p = {} & C_M\,\frac{\varepsilon}{2K}\frac{\Pi_{in}\,R^{-1}_{im}}{1+(u_n-\tilde{u}_n)(u_m-\tilde{u}_m)\frac{\Pi_{in}}{\Pi_{pp}}R^{-1}_{im}}\left\{\int v'_m v'_n v'_p\,f\partial v + R_{mn}u_p\right.\\ & \left.+\left(R_{mp}(u_n-\tilde{u}_n)+R_{np}(u_m-\tilde{u}_m)+(u_m-\tilde{u}_m)(u_n-\tilde{u}_n)u_p\right)\right\}\end{aligned} \qquad \text{(L.8)}$$

which simplifies to

$$\begin{aligned}\hat{u}_p\left[1+(u_n-\tilde{u}_n)(u_m-\tilde{u}_m)\frac{\Pi_{in}}{\Pi_{pp}}R^{-1}_{im}\right] = {} & \frac{\Pi_{in}\,R^{-1}_{im}}{\Pi_{ii}}\int v'_m v'_n v'_p\,f\partial v + u_p\\ & +\frac{\Pi_{in}}{\Pi_{ii}}R^{-1}_{im}\left(R_{mp}(u_n-\tilde{u}_n)+R_{np}(u_m-\tilde{u}_m)\right)+\frac{\Pi_{in}}{\Pi_{ii}}R^{-1}_{im}(u_m-\tilde{u}_m)(u_n-\tilde{u}_n)u_p\end{aligned} \qquad \text{(L.9)}$$

and

$$\begin{aligned}\left(\hat{u}_p-u_p\right)\left[1+(u_n-\tilde{u}_n)(u_m-\tilde{u}_m)\frac{\Pi_{in}}{\Pi_{pp}}R^{-1}_{im}\right] = {} & \\ \frac{\Pi_{in}}{\Pi_{ii}}R^{-1}_{im}\left(\int v'_m v'_n v'_p\,f\partial v + R_{mp}(u_n-\tilde{u}_n)+R_{np}(u_m-\tilde{u}_m)\right) & \end{aligned} \qquad \text{(L.10)}$$

Appendix M: General Reynolds transport Equation

Below, the Reynolds transport equation is derived for the general relaxation model.

$$\frac{\partial R_{lp}}{\partial t} = C_M \frac{\varepsilon}{2K}\left(\Pi_{ii} \int v'_l v'_p [(2\pi)^3 \det(\hat{R}_{nm})]^{-1/2} e^{-\frac{1}{2}\hat{R}^{-1}_{nm}\hat{v}'_n \hat{v}'_m} \partial v - \int \frac{\Pi_{in} R^{-1}_{im} \tilde{v}'_m \tilde{v}'_n}{1+(u_n-\tilde{u}_n)(u_m-\tilde{u}_m)\frac{\Pi_{in}}{\Pi_{pp}} R^{-1}_{im}} v'_l v'_p f \partial v \right) \tag{M.1}$$

Substitution gives

$$\frac{\partial R_{lj}}{\partial t} = C_M \frac{\varepsilon}{2\hat{K}} \Pi_{ii} \int \left(\hat{v}'_l \hat{v}'_j + (\hat{u}_l - u_l)(\hat{u}_j - u_j) \right) [(2\pi)^3 \det(\hat{R}_{nm})]^{-1/2} e^{-\frac{1}{2}\hat{R}^{-1}_{nm}\hat{v}'_n \hat{v}'_m} \partial v$$

$$- C_M \frac{\varepsilon}{2\hat{K}} \frac{\Pi_{in} R^{-1}_{im}}{1+(u_n-\tilde{u}_n)(u_m-\tilde{u}_m)\frac{\Pi_{in}}{\Pi_{pp}} R^{-1}_{im}} \int v'_l v'_j \tilde{v}'_m \tilde{v}'_n f \partial v \tag{M.2}$$

$$\frac{\partial R_{lj}}{\partial t} = C_M \frac{\varepsilon}{2\hat{K}} \left(\Pi_{ii} \hat{R}_{lj} + \Pi_{ii} (\hat{u}_l - u_l)(\hat{u}_j - u_j) - \frac{\Pi_{in} R^{-1}_{im}}{1+(u_n-\tilde{u}_n)(u_m-\tilde{u}_m)\frac{\Pi_{in}}{\Pi_{pp}} R^{-1}_{im}} \int v'_l v'_j \tilde{v}'_m \tilde{v}'_n f \partial v \right) \tag{M.3}$$

If we choose $u_n = \tilde{u}_n$ and use the general form of the Reynolds stress model, $\frac{\partial R_{ij}}{\partial t} = -\frac{\varepsilon}{2K}\left(\Pi_{im} R_{mj} + \Pi_{jm} R_{mi} \right)$, we arrive at the following equation.

$$-\left(\Pi_{im} R_{mj} + \Pi_{jm} R_{mi} \right) = C_M \Pi_{ii} \left(\hat{R}_{lj} + (\hat{u}_l - u_l)(\hat{u}_j - u_j) - \frac{\Pi_{in} R^{-1}_{im}}{\Pi_{ii}} \int v'_l v'_j v'_m v'_n f \partial v \right) \tag{M.4}$$

Which gives us the definition of $\hat{R}$.

$$\hat{R}_{lj} = \frac{-1}{C_M \Pi_{ii}} \left(\Pi_{im} R_{mj} + \Pi_{jm} R_{mi} \right) - (\hat{u}_l - u_l)(\hat{u}_j - u_j) + \frac{\Pi_{in} R^{-1}_{im}}{\Pi_{ii}} \int v'_l v'_j v'_m v'_n f \partial v \tag{M.5}$$